Tracing water masses and continental weathering by neodymium and hafnium isotopes in the Atlantic sector of the Southern Ocean

Dissertation
zur Erlangung des Doktorgrades

Dr. rer. nat.

der Mathematisch-Naturwissenschaftlichen Fakultät
der Christian-Albrechts-Universität zu Kiel

vorgelegt von
Torben Stichel

Dipl.-Geol., Universität Kiel
Kiel, 2010

1. Gutacher und Betreuer:	Prof. Dr. Martin Frank
2. Gutachter:	Prof. Dr. Anton Eisenhauer
Eingereicht am:	14. Dezember 2010
Datum der Disputation:	
Zum Druck genehmigt:	

gez. (Titel, Vor- und Zuname), Dekan

Erklärung

Hiermit versichere ich an Eides statt, dass ich diese Dissertation selbständig und nur mit Hilfe der angegebenen Quellen und Hilfsmittel erstellt habe. Ferner versichere ich, dass der Inhalt dieses Dokumentes weder in dieser, noch in veränderter Form, einer weiteren Prüfungsbehörde vorliegt. Die Arbeit ist unter Einhaltung der Regeln guter wissenschaftlicher Praxis der Deutschen Forschungsgemeinschaft entstanden.

Kiel, den

(Torben Stichel, Dipl.-Geol.)

...to Luisa

Contents

Abstract

Radiogenic isotopes, such as the ones of hafnium (Hf) and neodymium (Nd), have been used to investigate present and past ocean circulation patterns, hydrothermal inputs and continental weathering regimes. This thesis presents a detailed study of the dissolved Hf and Nd isotope composition and concentration of seawater in the Atlantic sector of the Southern Ocean. The goal is to better understand their controlling factors, mainly weathering inputs, biogeochemical cycling, and water mass mixing. The samples were collected along the Zero Meridian, in the Weddell Sea and in the Drake Passage during expedition ANTXXIV/3 with R/V *Polarstern* in 2008 in the frame of the International Polar Year (IPY) and the GEOTRACES program. Volumes of seawater between 60 L (deeper than 200 m) and 130 L (surface) were collected for Hf, and a volume of 20 L for Nd isotopes following GEOTRACES protocols. For isotopic analysis, the samples were chemically and ion chromatographically purified, for which existing methods had to be significantly modified, as described in detail in Chapter 2. Hafnium and Nd concentrations were determined on aliquots of the same samples by isotope dilution. The isotope compositions and concentrations were measured by Thermal Ionisation Mass Spectrometry (TIMS) or Multi-Collector Inductively Coupled Plasma Mass Spectrometry (MC-ICPMS).

The distribution of Hf and Nd concentrations in the surface water (Chapter 3) is generally similar with essentially constant values south of the Polar Front (~0.3 pmol/kg and ~18 pmol/kg, respectively). Minimum Hf (~0.12 pmol/kg) and Nd (~7 pmol/kg) concentrations are observed between the Subtropical Front and the Polar Front, most probably due to the limited terrigenous flux in this area, but may also result from scavenging by biogenic opal. In contrast, at the northernmost station, 200 km southwest of Cape Town, a pronounced increase of the Nd concentration is observed, while the Hf concentration is at its minimum. This indicates a lower amount of Hf than of Nd released by weathering of the Archean cratonic rocks of South Africa.

In the vicinity of landmasses the Hf and Nd isotope composition is clearly affected by terrigenous inputs, whereas most of the open surface waters are characterized by the same isotope composition as the deep waters (presented in Chapter 4). Only in the area of the Agulhas retroflection low Nd isotope values (ε_{Nd} = -18.9) are

observed implying that unradiogenic inputs originating from South Africa are supplied via the Agulhas Current. The Nd isotope compositions are more radiogenic ($\varepsilon_{Nd} \sim -8$) towards the Subtropical Front and within the Antarctic Circumpolar Current and slightly decrease to $\varepsilon_{Nd} \sim -8.5$ in the Weddell Gyre (WG). Near the volcanic King George Island (KGI) the isotopic data show significant increases to $\varepsilon_{Hf} = 6.1$ and $\varepsilon_{Nd} = -4.0$. The Hf and Nd concentrations show peak values (0.38 pmol/kg and 22.6 pmol/kg, respectively), suggesting an enhanced release from mafic rocks of the Antarctic Peninsula. The overall Hf isotope composition varies within a small range (between $\varepsilon_{Hf} = 6.1$ at KGI and $\varepsilon_{Hf} = 2.8$ in the WG). Near the Antarctic continent the isotope composition drops from $\varepsilon_{Hf} \sim 5$ to $\varepsilon_{Hf} \sim 3$, indicating a release of unradiogenic Hf by glacial grinding and destruction of weathering resistant minerals such as zircons. The Hf isotope composition and concentration data show that it is a sensitive tracer for physical weathering conditions on the adjacent continental landmass. The range of Nd isotopes is a factor of five larger than of Hf isotopes, which confirms that Nd isotopes are a highly sensitive tracer for the provenance of weathering inputs to marine surface waters.

In Chapter 4 the first combined deepwater profiles of dissolved Hf and Nd concentrations and isotope compositions from the Atlantic sector of the Southern Ocean are presented. Eight full-depth profiles were analyzed for both Hf and Nd, whereas four additional profiles were analyzed for Nd only. In the upper few hundred meters Hf concentrations are low (0.2 pmol/kg to 0.4 pmol/kg) and increase to relatively constant values (0.6 pmol/kg) in the deeper water column. North of the Polar Front, Nd concentrations increase linearly towards the bottom indicating uptake and release by biogenic opal, whereas in the WG the Nd concentrations are essentially constant (25 pmol/kg) at depths greater than ~ 1000 m. Hafnium shows homogenous isotope compositions (average value $\varepsilon Hf = 4.6$), whereas Nd isotopes mark distinct differences between water masses, such as modified North Atlantic Deep Water ($\varepsilon Nd = -11$ to $\varepsilon Nd = -10$) and Antarctic Bottom Water ($\varepsilon Nd = -8.6$ to $\varepsilon Nd = -9.6$). Waters locally advected via the Agulhas Current can also be identified by their unradiogenic Nd isotope compositions. Mixing calculations suggest that a small fraction of Nd is removed by particle scavenging during mixing of water masses north of the Polar Front. The calculation of the mixture of a North Pacific and a North Atlantic end-member shows that Nd isotope and concentration patterns in the Lower Circumpolar Deep Water can be explained by ~ 30:70 contributions of these end-members.

In conclusion, Hf and Nd isotopes and their concentration patterns provide valuable insights into the weathering inputs and their provenance in the Atlantic sector of the Southern Ocean. The Hf isotopes largely reflect local imprints in the surface layer, whereas the deeper parts are isotopically invariant. The enhanced release of Hf from volcanic rocks implies that those rock types are an important source for radiogenic Hf into the ocean. Both elements readily adsorb onto siliceous frustules of diatoms, whereas scavenged Nd is released easier during reminerlization than Hf. Mixing calculation reveals that Nd is removed by 10 % to 20 % during mixing between northern and southern sourced waters. However the entire Nd budget in the Atlantic sector of the Southern Ocean is governed by Pacific (~ 30 %) and Atlantic (~ 70%) contributions, implying that local contributions from Antarctica are inferior. The Nd isotopes reflect the modification of CDW during AABW formation. This information can be used to evaluate paleo-AABW production and distribution.

Zusammenfassung

Die Anwendung radiogener Isotope von Hafnium (Hf) oder Neodym (Nd) erlaubt wertvolle Einsichten in Ozeanzirkulation, hydrothermale Einträge sowie Verwitterungseinträge von Land. Diese Dissertation beschäftigt sich mit einer detaillierten Untersuchung der Verteilung der gelösten Isotopie und Konzentration von Hf und Nd im atlantischen Sektor des Zirkumantarktischen Ozeans. Das Ziel war dabei, die steuernden Faktoren der Verteilungen, hauptsächlich Verwitterungseintrag Zirkulation und die biogeochemischen Kreisläufe, besser zu verstehen. Die Proben wurden entlang des Nullmeridians, im Weddellmeer und in der Drake-Passage während der Expedition (ANTXXIV/3) auf dem deutschen Forschungsschiff *Polarstern* genommen. Diese Ausfahrt fand im Rahmen des Internationalen Polarjahres sowie dem GEOTRACES Programm im Frühjahr 2008 statt. Das Probenvolumen für die Hf-Proben reichte von 60 L (tiefer als 200 m) bis 130 L (Oberflächenproben). Für Nd wurden Proben im Volumen von 20 L gesammelt. Neben der isotopischen Zusammensetzung wurden auch Hf und Nd Konzentrationen mit Hilfe der Isotopenverdünnungsmethode ermittelt. Die großvolumigen Proben wurden an Bord mit einer Eisenhydroxyd-Fällung aufkonzentriert worden. Die weitere chemische Aufbereitung fand dann am Land im Labor statt und folgte den Vorgaben des GEOTRACES Programm. Die detaillierte Beschreibung der Methode, die für diese Studie modifiziert wurde, ist in Kapitel 2 dargestellt. Die isotopische Zusammensetzungen sowie Konzentrationen sind an Multikollektor Massenspektrometern mit entweder einer thermischen Ionenquelle (TIMS) oder einer Ionenquelle mit induktiv gekoppeltem Plasma (MC-ICPMS) gemessen worden.

Die Verteilungsmuster der Hf- und Nd-Konzentrationen im Oberflächenwasser (Kapitel 3) ähneln sich und zeigen relativ konstante Werte von ~ 0.3 pmol/kg (Hf) und ~ 18 pmol/kg (Nd) südlich der Polarfront und im Weddellmeer. Die niedrigsten Hf und Nd Konzentrationen wurden zwischen der Subtropischen Front und der Polafront gemessen. Der Grund hierfür liegt vermutlich an einem geringen externen Eintrag, aber auch in der Adsorption an silikatische Primärproduzenten. Diese Beobachtung steht im Kontrast zu den nördlichsten Hf und Nd Konzentrationen etwa 200 km südwestlich von Kapstadt, wo die Hf- Konzentration eine der niedrigsten im gesamten Datensatz ist, während die von Nd mit 24 pmol/kg eine der höchsten ist. Das bedeutet, dass weniger

Hf im Vergleich zu Nd durch Verwitterung aus den Gesteinen des alten südafrikanischen Kratons mobilisiert wird.

In der Nähe von Landmassen sind die Hf und Nd Isotopensignaturen des Oberflächenwassers deutlich von terrigenen Einträgen beeinflusst. Im Gegensatz hierzu sind die meisten Oberlächendaten im offenen Ozean nahezu konstant und vergleichbar mit der Zusammensetzung des Tiefenwassers (Kapitel 4). Im Einflussbereich des Agulhasstroms werden die niedrigsten Nd-Isotopiewerte von bis zu $\varepsilon_{Nd} = -18.9$ gemessen, was durch erhöhten terrigenen Eintrag von Südafrika in den Agulhasstrom begründet liegt. In Richtung der Subtropischen Front werden die Werte radiogener und liegen bei $\varepsilon_{Nd} \approx -8$ innerhalb des Antarktischen Zirkumpolarstroms. Im Weddellmeer, sowie im gesamten im Weddellwirbel sind die Werte wieder etwas niedriger bei $\varepsilon_{Nd} \approx -8.5$. In der Nähe der vulkanischen Insel *King George Island* wurden die radiogensten Isotopenwerte für Hf ($\varepsilon_{Hf} = 6.1$) und Nd ($\varepsilon_{Nd} = -4.0$) gemessen. Die Hf-Konzentration ist hier mit 0.38 pmol/kg am höchsten, was eine erhöhte Freisetzung von Hf aus den vulkanischen Gesteine anzeigt. Die Variation der Hf Isotopie liegt gesamten Datensatz zwischen $\varepsilon_{Hf} = 6.1$ und $\varepsilon_{Hf} = 2.8$. In der Nähe des antarktischen Kontinents fällt die Isotopie von $\varepsilon_{Hf} \approx 5$ auf $\varepsilon_{Hf} \approx 3$, was für eine Freisetzung von unradiogenem Hf durch Zerreibung verwitterungsresistenter Minerale wie Zirkon spricht. Die kombinierten Isotopien und Konzentrationen von Hf und Nd zeigen also, dass Hf ein sensitiver Anzeiger für vorherrschende physikalische Verwitterung ist. Die gemessenen Isotopien für Nd decken einen Bereich von etwa 15 ε_{Nd}-Einheiten ab und zeigen somit, dass Nd sensitiver Anzeiger ist, um die Herkunftsgebiete der jeweiligen Einträge zu identifizieren.

Im vierten Kapitel werden die ersten kombinierten Profile von gelösten Hf- und Nd-Konzentrationen und Isotopensignaturen der Wassermassen aus dem Untersuchungsgebiet präsentiert. Der Datensatz besteht aus acht Profilen für Hf und Nd, sowie aus vier weiteren, an denen nur Nd untersucht wurde. Die Konzentrationen zeigen für beide Elemente ein für partikelreaktive Metalle typisches Profil, indem die flacheren Tiefen geringe und größere Tiefen höhere Konzentrationen aufweisen. Nördlich der Polarfront steigen die Nd-Konzentrationen linear von etwa 10 pmol/kg bei ~ 200 m auf bis zu 31 pmol/kg am Boden an, was vermutlich auf Adsorption/Desorptionsprozesse an biogenem Opal zurückzuführen ist. Im

Weddellwirbel hingegen sind die Konzentrationen in Wassertiefen unterhalb ~ 1000 m relativ konstant bei 25 pmol/kg.

Die isotopische Zusammensetzung von Hf ist im gesamten Gebiet innerhalb des analytischen Fehlers unverändert bei $\varepsilon_{Hf} \approx 4.6$, wohingegen sich die Nd-Isotopie von Wassermassen wie modifiziertem Nordatlantischen Tiefenwasser ($\varepsilon_{Nd} = -11$ bis -10) und Antarktischem Bodenwasser ($\varepsilon_{Nd} = -8.6$ bis -9.6) eindeutig vom durchschnittlichen Zirkumpolaren Tiefenwasser (CDW, $\varepsilon_{Nd} \approx -8.5$) unterscheiden lässt. Zusätzlich ist einströmendes Wasser des Agulhasstroms durch seine unradiogene Nd-Isotopensignatur im Gebiet der sich nach Westen bewegenden Agulhas-Ringe nachweisbar. Mischungsrechnungen lassen eine Erniedrigung der Nd Konzentration durch Adsorption an Partikel im Gebiet der Polarfront vermuten. Berechnungen anhand zweier Endglieder, dem Nordpazifik und dem Nordatlantik, zeigen jedoch, dass die Nd Isotopie und Konzentration im tiefen CDW vollständig durch Wassermassenmischung mit einem Verhältnis von ungefähr 30:70 dieser Endglieder erklärt werden kann.

Die generellen Schlussfolgerungen (Kapitel 5) aus dieser Arbeit zeigen, dass Hf und Nd Isotope und Konzentrationen wertvolle Einsichten in Verwitterungseinträge und deren Herkünfte geben. Hafnium Isotope spiegeln eher lokale Einflüsse im Oberflächenwasser wieder, während in größeren Tiefen die Isotopie konstant bleibt. Es konnte gezeigt werden, dass aus vulkanischen Gesteinen im erhöhten Maße Hf freigesetzt wird, was global gesehen vermutlich einen nicht unerheblichen Effekt auf das Hf-Budget im Ozean hat. Die unradiogenen Hf-Isotopenwerte im Vergleich zu Nd in der Nähe der Antarktis deuten stark auf erhöhte physikalische Verwitterung hin. Die Kombination aus Hf- und Nd-Isotopen ist folglich ein sensitiver Anzeiger für Änderungen im Verwitterungsregime. Beide Elemente sind sehr partikelreaktiv, indem sie gern an Silikatschaler wir Diatomen adsorbieren. Es konnte ferner gezeigt werden, dass Nd ein sensibler Anzeiger für Wassermassenmischung ist und das in einem Gebiet, wie der Südatlantik, der stark durchmischt wird. Trotz einer Partikel-Adsorption von etwa 10 % bis 20 % im Bereich der Subantarktischen und der Polarfront konnte anhand von Mischungsrechnungen gezeigt werden, dass das Nd-Budget im Untersuchungsgebiet aus reiner Wassermassenmischung von Pazifischen (~ 30 %) und Nordatlantischen (~ 70 %) Ursprungs zu erklären ist. Es konnte außerdem gezeigt werden, dass sich CDW und AABW isotopisch unterscheiden lassen. Diese Information

ist sehr relevant, um Produktion und Verbreitung des AABW in der Vergangenheit zu rekonstruieren.

Chapter 1

Introduction

1.1 The global thermohaline circulation and water masses in the Southern Ocean

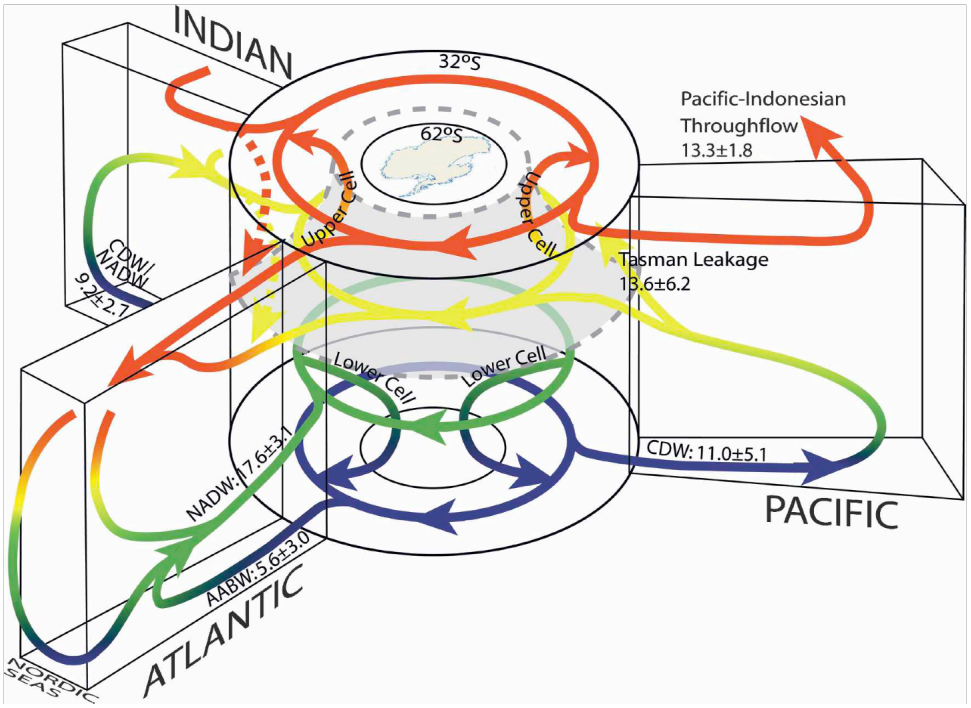

Figure 1.1: A generalized ocean circulation scheme around Antarctica adapted from Lumpkin and Speer (2007). North Atlantic Deep Water (NADW) joins the Antarctic Circumpolar Current (ACC) to form the lower cell of the Circumpolar Deep Water (LCDW). LCDW is partly transferred into Antarctic Bottom Water (AABW) by admixture of dense shelf waters near Antarctica. LCDW and AABW permeate the world ocean as bottom waters. After upwelling in the Pacific or Indian Oceans, these waters return to the ACC at intermediate depths as Upper Circumpolar Deep Water (UCDW) to form northward flowing Antarctic Intermediate Water (AAIW; "cold route"). Northward flowing AAIW in the Pacific sector flows into Indian Ocean via the Indonesian Throughflow. From the Indian sector of the Southern Ocean these intermediate waters return to the Atlantic Ocean via the Agulhas Current ("warm route").

The global circulation of heat and water masses by ocean currents is referred to as the "global conveyor belt" (Broecker, 1991). The deep ocean circulation is mainly governed by differences in temperature and salinity (thermohaline circulation), whereas the surface ocean is driven by atmospheric exchange, such as moisture transport and wind stress. In particular by heat and moisture fluxes the ocean circulation has crucial impact to the global climate.

Deepwater formation occurs at high latitudes by sinking of the North Atlantic Deep Water (NADW) or around the Antarctic continent (Stommel, 1958). NADW is produced from highly saline waters originating from the Caribbean warm-pool, which

flow north as part of the Gulf Stream until thy reach the Greenland-Norwegian Seas, where they are cooled and thereby increase their density. These waters are mixed with various other water masses, such as colder and fresher Arctic waters via the Denmark Strait, but also receive significant contributions from deep waters formed in the Labrador Sea. NADW then flows southward along the western boundary of the Atlantic Ocean into the Southern Ocean, where it is eventually advected into the Antarctic Circumpolar Current (ACC) to form Circumpolar Deep Water (CDW; e.g. Rhein et al., 1995; Stramma and England, 1999). The ACC is the largest current system in the world ocean, flowing eastward without interruptions around the Antarctic continent. The ACC is bounded to the north by the Subtropical Front (STF), reaches from the surface to abyssal depths and is divided into Upper (UCDW) and Lower Circumpolar Deep Water (LCDW). The southern boundary (BDY) of the ACC is marked by several cyclonically circulating current systems, such as the Weddell Gyre (WG) or the Ross Sea Gyre. These gyres are mainly fed by LCDW from the ACC and are the most important areas for the deepwater formation of northward flowing Antarctic Bottom Water (AABW; e.g. Gordon, 1971; Orsi et al., 1999; Stramma and England, 1999). The formation process of AABW is governed by the loss of heat near the Antarctic continent, which induces the formation of sea ice. Sea ice development leads to brine formation, and thus increased density of Antarctic Surface Water (AASW), which sinks down and mixes with underlying water masses such as Warm Deep Water (WDW) in the Weddell Sea. Those fractions, which are dense enough to reach the bottom of the ocean, form AABW. Due to its high density ($\gamma^n \geq 28.27$ kg/m3), the distribution of pure AABW is strongly restricted by topography and is thus only found in closely defined parts of the world ocean, such as the Argentine or the Mozambique Basin (Orsi et al., 1999). The bottom water of Southern Ocean origin that penetrates the remainder of the global deep ocean is less dense LCDW and is often named ACC bottom water (Orsi et al., 1999).

The ACC works as a distributor of global water masses (Fig. 1.1). NADW joins the ACC in the Atlantic sector and water masses originating from the ACC fill the abyssal Indian and Pacific Oceans as AABW or LCDW. These waters are either recirculated into the ACC or, after modification, reach the surface of the respective basins via upwelling. Upwelling in the North Pacific forms North Pacific Deep Water (NPDW), which partly forms a shallow water mass flowing through the Indonesian Gateway into the Indian Ocean to circulate back into the Atlantic via the Agulhas

Current ("warm route"). The warm route is joined by Antarctic Intermediate Water (AAIW), which enters the Pacific from the south at intermediate depth. The remainder of NPDW follows the "cold route" back into the Southern Ocean to join the ACC through the Drake Passage as UCDW. Through upwelling at the Polar Front this water mass is transferred into northward flowing Antarctic Intermediate Water (AAIW).

1.2 Radiogenic isotopes as proxies for past ocean circulation

As outlined above, modern ocean circulation is derived from conservative seawater properties, such as salinity or temperature. Since such properties are not preserved in paleo records, the only way to reconstruct past ocean circulation patterns is the usage of suitable proxies. The first geochemical proxies applied in this field of research were stable carbon isotopes ($\delta^{13}C$) and cadmium/calcium ratios recorded in benthic foraminifera (e.g. Curry and Lohmann, 1983; Boyle, 1988). These proxies are thought to mirror the nutrient supply of distinct water masses, and therefore to allow separating nutrient-rich from depleted waters. However, such proxies exhibit problems in their applicability in that non-conservative effects, such as carbonate ion availability and thermodynamic effects, are superimposed (Frank, 2002). In his review, Frank (2002) describes that the alternative application of radiogenic isotopes is a promising tool to reconstruct past ocean circulation. In the search for tracers to reconstruct or monitor ocean circulation on the basis of radiogenic isotopes, their residence time in seawater is of a crucial role. The global ocean has a turnover time of about 1500 years (Broecker and Peng, 1982), therefore the residence time of an oceanic tracer must be short enough to prevent homogenization within the world ocean. On the other hand it must also be long enough to preserve and transport isotopic signatures of water masses. This is the case for hafnium (Hf) and neodymium (Nd), which have residence times in the order of a couple of hundred to 2000 years (e.g. Frank, 2002) and are the subject of this study. In order to better understand the behavior of Hf and Nd in seawater and to interpret paleo-records, it is of great importance to investigate their modern characteristics. During the last years national and international collaborations on trace metals and their isotopes (TEI) have been carried out within the GEOTRACES program (see science plan on http://www.geotraces.org). The primary goals of GEOTRACES are: (1) to determine the global distribution of selected TEI (including Hf and Nd); (2) to understand the processes governing their cycles and (3) to validate TEI used as

proxies of past environment. In the frame of GEOTRACES and the International Polar Year (IPY) 2007/2008 the expedition ANTXXIV/3 on the German R/V *Polarstern* from Cape Town (South Africa) to Punta Arenas (Chile) has been realized to combine the investigation of physical oceanography and TEI in the Atlantic sector of the Southern Ocean. During this expedition over 120 samples for Hf and Nd analysis have been collected and the results are presented in this study.

1.3 Hafnium and neodymium isotope evolution

The radiogenic Hf and Nd isotope compositions of rocks and minerals are highly variable. They can be used as tracer for high and low temperature geochemical studies to reconstruct igneous processes or weathering regimes, as well as the provenance of rocks and their weathering products. In contrast to stable isotope systems such as oxygen or carbon, Hf and Nd isotopes are governed by the decay of their respective parent isotope. The β-decay of ^{176}Lu (lutetium) results in the radiogenic ^{176}Hf isotope, which is given as a ratio to primordial ^{177}Hf. In the case of Nd, the α-decay of ^{147}Sm (samarium) produces radiogenic ^{143}Nd, which is given as a ratio to primordial ^{144}Nd. Radioactive decay thus leads to ingrowth of the abundance of the respective daughter isotopes in the radiogenic isotope ratios (^{176}Hf/^{177}Hf, ^{143}Nd/^{144}Nd) over time. The radiogenic isotope composition of any geological sample is thus governed by the abundance of parent/daughter isotope ratios, which varies as a function of mineralogical processes, such as crystallization or weathering. For example, minerals with low Lu/Hf ratios will consequently lead to a low ^{176}Hf/^{177}Hf of the bulk rocks over time. Both isotope systems are expressed in the ε-notation, which in the case of Hf is calculated as:

$$\varepsilon_{\mathrm{Hf}} = \left[\frac{\left(\frac{^{176}\mathrm{Hf}}{^{177}\mathrm{Hf}} \right)_{\mathrm{sample}}}{\left(\frac{^{176}\mathrm{Hf}}{^{177}\mathrm{Hf}} \right)_{\mathrm{CHUR}}} - 1 \right] \times 10^4 \qquad (1.1)$$

and the $\varepsilon_{\mathrm{Nd}}$ is calculated as:

$$\varepsilon_{\mathrm{Nd}} = \left[\frac{\left(\frac{^{143}\mathrm{Nd}}{^{144}\mathrm{Nd}} \right)_{\mathrm{sample}}}{\left(\frac{^{143}\mathrm{Nd}}{^{144}\mathrm{Nd}} \right)_{\mathrm{CHUR}}} - 1 \right] \times 10^4 \qquad (1.2)$$

where CHUR represents the CHondritic Uniform Reservoir (0.282769 for $^{176}Hf/^{177}Hf$ (Nowell et al., 1998) and 0.512638 for $^{143}Nd/^{144}Nd$ (Jacobsen and Wasserburg, 1980) for present day. The isotopic evolution of CHUR over Earth's history is schematically shown in fig. 1.2 and illustrates that for any given time of the past 4.6 Gyr a precise value for CHUR can be calculated. The ε-notation can thus be expressed for the present day isotope composition (ε(0)) or as the composition at the time of rock formation (ε(t)). During igneous processes, elemental fractionation, especially between elements such as Rare Earth Elements (REE, including Lu, Sm and Nd) or High Field Strength Elements (HFSE, including Hf), commonly occurs. These fractionation processes result in a different incorporation of such elements into minerals during rock formation. For example, Nd is slightly less compatible than Sm, resulting in a relative enrichment of Nd in crustal melts. The continental crust is to a large part built of highly fractionated melt and thus has relatively low Sm/Nd ratio, resulting in a low $^{143}Nd/^{144}Nd$ ratio. This is analogous to the Lu/Hf system, resulting in low $^{176}Hf/^{177}Hf$. Continental rocks therefore, have an unradiogenic Hf and Nd isotope composition, expressed by low ε values (Fig. 1.2), whereas less fractionated mantle-derived rocks have a more radiogenic composition (high ε values). Old continental rocks with low initial Sm/Nd and Lu/Hf ratios thus evolve an unradiogenic bulk composition over time.

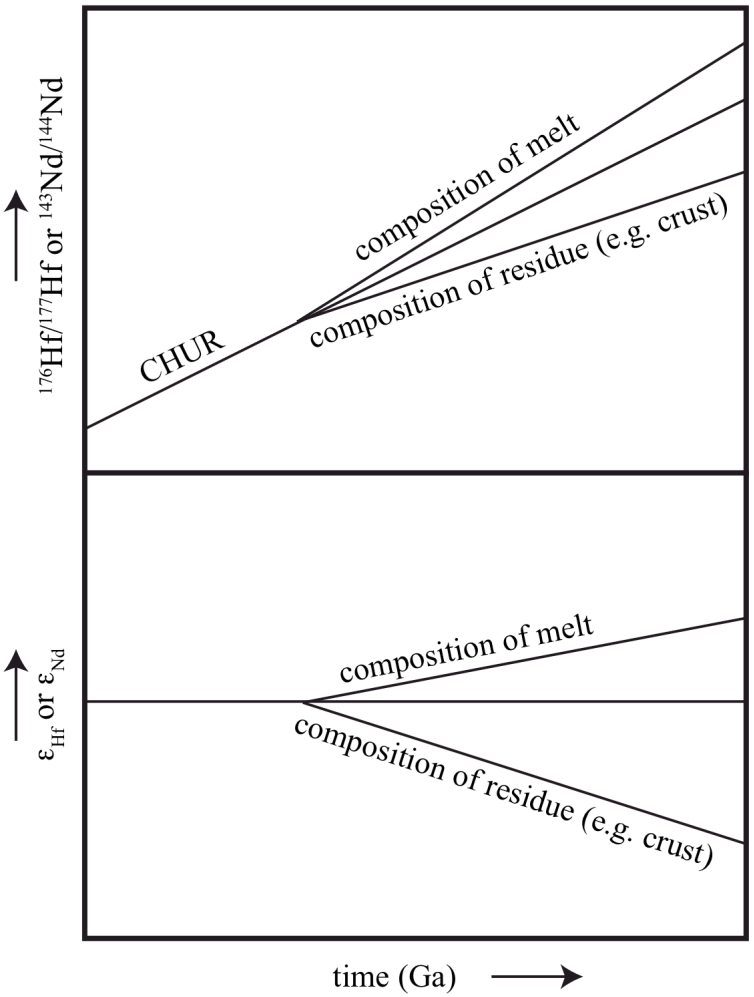

Figure 1.2: The Hf and Nd isotope evolution over time. During igneous processes the elemental fractionation of Sm/Nd and Lu/Hf leads different isotopic evolution of the residue (e.g. crust) and the melt over time.

1.4 Low temperature geochemical processes governing the radiogenic isotope composition of Hf and Nd

The Hf and Nd isotope distribution in weathered material, such as sediments or weathering solutions ultimately controlling the radiogenic isotope composition of seawater, provides a powerful tool to constraining the provenance of weathering products. The elemental variability of Lu/Hf and Sm/Nd in rock forming minerals results in a heterogeneity in the radiogenic isotope composition of rocks over time. During weathering more resistant minerals retain their elemental composition, whereas other minerals are more easily destroyed and release their components and isotopic compositions during alteration. This process is often referred to as *incongruent weathering*. The majority of rock-forming minerals possesses a rather homogenous

Sm/Nd ratio, because Sm and Nd are elements of similar chemical characteristics and ionic radii within the group of REEs (McCulloch and Wasserburg, 1978). Thus, the resulting Nd isotope composition of the weathered material does not differ significantly from the bulk composition of the source rock. The Nd isotope composition is therefore largely governed by *congruent weathering* during low temperature alteration. The Hf isotope composition on the other hand, is the result of the decay of Lu, which is chemically different from Hf, leading to largely variable Lu/Hf of different minerals. During weathering processes, sorting occurs so that mineral phases, such as zircons with low Lu/Hf, are deposited in the sandy fraction close to the shelf, whereas clay minerals, which are characterized by high Lu/Hf, are transported further (Patchett et al., 1984). Additionally, zircons are highly resistant to chemical disaggregation, and therefore retain their low Lu/Hf (~ 0.002, Kinny and Maas (2003)) during weathering. Hafnium is to a large extent stored in zircons, which have relatively high Hf concentrations (~ 2 wt.%, Hoskin and Schaltegger (2003) and references therein) compared to the average crustal abundance of Hf (~ 3 ppm, Taylor and McLennan (1985)). Recent studies of rivers and surface seawater have shown that their Hf isotope compositions are shifted to more radiogenic values compared to the weathered lithology (Bayon et al., 2006; Rickli et al., 2010). This implies that the dissolved Hf isotope composition is most likely a result of retention by such resistant minerals. Additionally it has been shown that trace minerals in granites, such as apatites with high Lu/Hf, are readily altered during early stages of weathering (Bayon et al., 2006). This implies a temporal evolution of the Hf isotope composition in the weathering solutions with increasing degree of weathering. Data obtained from ferromanganese crusts, which incorporate the ambient seawater radiogenic isotope composition, have shown that during periods with enhanced physical weathering, such as glaciations, a less radiogenic Hf isotope composition is released compared to regimes and times when weathering was dominated by chemical weathering (Piotrowski et al., 2000; van de Flierdt et al., 2002).

1.5 Hafnium and neodymium isotopes in seawater

1.5.1 Sources of hafnium and neodymium in the ocean

The Hf and Nd isotope composition of rocks largely depends on the lithology and the crustal age, as outlined above. The distinct radiogenic isotope composition of the

source rocks is delivered into the adjacent ocean basins. This occurs essentially in dissolved form via rivers, by eolian input, hydrothermal vent fluids or by interaction of seawater with shelf sediments. The relative importance of each source, however, is different for each element, which will be discussed below.

The exact sources of both elements are not equally well constrained due to the fact that more than three decades of studies on seawater Nd have been carried out compared to only a handful of mainly recent studies on Hf. Neodymium is largely delivered into the ocean by fluvial and eolian dust inputs (e.g. Goldstein et al., 1984). However, the exchange of seawater with continental deposits on the shelves, often referred to as "boundary exchange", is also believed to be a major contributor to the global seawater Nd budget (Lacan and Jeandel, 2005). Hydrothermal inputs of Nd have been proven to be negligible, due to efficient scavenging at these sites (German et al., 1990; Halliday et al., 1992).

The input mechanisms of Hf into the ocean are still largely under debate. This lack of information is caused by the analytically challenging acquisition of Hf data from sea- or river water. Hafnium is thought to be transported to the ocean by riverine inputs (e.g. Bayon et al., 2006), whereas some authors propose a significant contribution by hydrothermal fluids from submarine spreading centers (White et al., 1986; Bau and Koschinsky, 2006).

1.5.2 Residence time of hafnium and neodymium in seawater

The oceanic residence time of TEI is of great importance to investigate ocean circulation patterns. Neodymium and Hf have oceanic residence times that potentially allow them to be used as tracers for water masses and their mixing, as well as changes in weathering regime (Piepgras and Wasserburg, 1982; Lacan and Jeandel, 2005; Godfrey et al., 2008; Rickli et al., 2009; Zimmermann et al., 2009a). The global average residence time of Nd is relatively well constrained at 500 to 2000 years (Jeandel et al., 1995; Tachikawa et al., 1999; Tachikawa et al., 2003), although more recent estimates point to a somewhat lower number of less than 500 years (Siddall et al., 2008; Arsouze et al., 2009). However, despite the fact there have been numerous studies on the Nd isotope distribution in seawater, large areas of the global ocean, including the Southern Ocean, still remain largely unexplored, resulting in persisting uncertainties concerning the residence time and the reflection of water mass distribution by Nd isotopes.

The global average residence time of Hf in seawater is much less certain with estimates ranging from 250 to 7500 years (Firdaus et al., 2008; Godfrey et al., 2008; Godfrey et al., 2009; Rickli et al., 2009; Zimmermann et al., 2009a). This uncertainty is mainly due to the lack of knowledge of the input sources of Hf in seawater, but also results from the sparse data available on dissolved Hf concentrations and isotope compositions of seawater. The very low Hf concentration of $\leq$ 1.2 pmol/kg, (e.g. Firdaus et al., 2008; Rickli et al., 2009) make clear that it is still challenging to analyze the Hf isotope composition of seawater reliably. Nevertheless, a number of recent studies combining dissolved Hf and Nd isotope distributions from different areas of the global ocean have revealed that the lower end of the above estimates of the seawater residence time of Hf is more plausible (Rickli et al., 2009; Zimmermann et al., 2009a;b; Rickli et al., 2010).

1.5.3 Hafnium and neodymium isotope systematics and the seawater array

Hafnium and Nd isotopes are closely coupled in mantle-derived and continental rocks (Patchett et al., 1984; Vervoort et al., 1999, Fig. 1.3). The global range of Hf isotopes is about a factor of 1.5 higher than of Nd suggesting Hf to be a sensitive tracer for continental inputs into the ocean. The large isotopic difference between the Atlantic basin, being surrounded by lithologies of continental origin, and the Pacific basin, surrounded by active volcanic margins, is a promising basis of a two end-member mixing model. Data from ferromanganese crusts and nodules (e.g. Godfrey et al., 1997; Albarède et al., 1998; Piotrowski et al., 2000; van de Flierdt et al., 2002; van de Flierdt et al., 2006) or, more recently, from Atlantic and Pacific seawater (Godfrey et al., 2009; Rickli et al., 2009; Zimmermann et al., 2009a;b; Rickli et al., 2010) have shown that the Hf isotope composition is shifted towards more radiogenic values for a given Nd value (Fig. 1.3). The reasons for this offset are most likely different input mechanisms and pathways, which are still largely under debate. The incongruent release of more radiogenic Hf during weathering is one valid hypothesis to explain the observed isotopic fractionation (Bayon et al., 2006; van de Flierdt et al., 2007; Rickli et al., 2010). Another plausible explanation is the potential input of radiogenic Hf from hydrothermal vents (e.g. Godfrey et al., 1997; Bau and Koschinsky, 2006), which is not accompanied by inputs of radiogenic Nd (German et al., 1990; Halliday et al., 1992). A third explanation could be a generally longer oceanic residence time of Hf and thus

stronger homogenization of the input signatures compared with Nd (White et al., 1986; Godfrey et al., 2008). The relative importance of each process controlling the Hf budget in the ocean is unclear and currently remains unresolved.

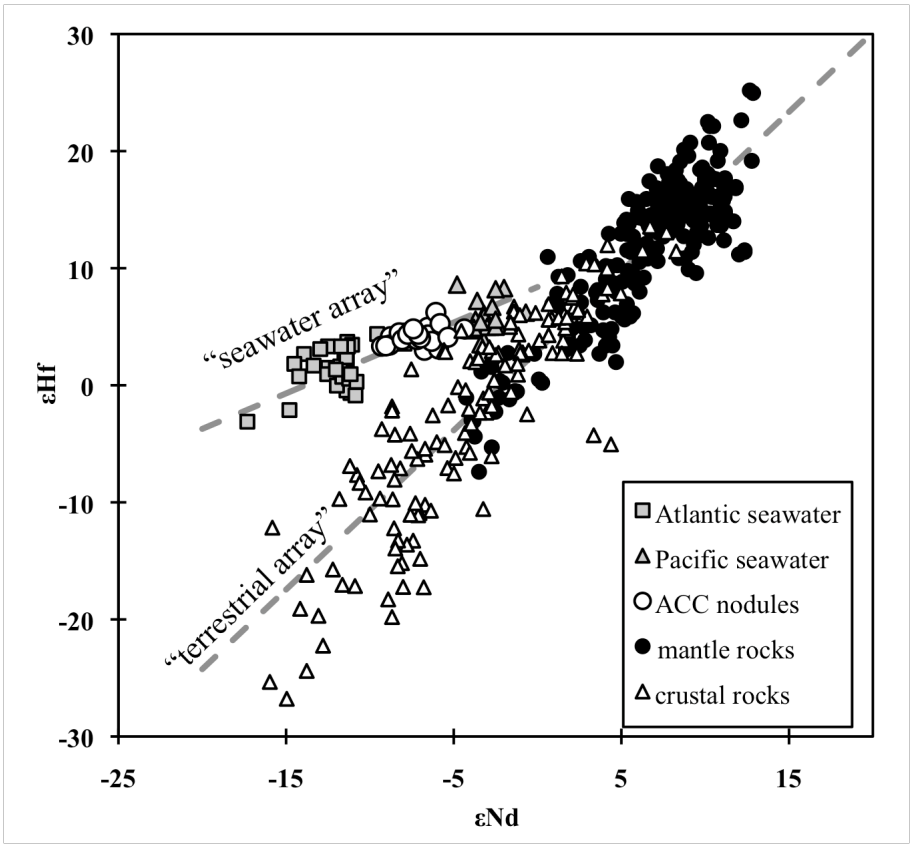

Figure 1.3: Hf and Nd isotope composition of terrestrial rocks ("terrestrial array") and combined seawater and ferromanganese data ("seawater array"). The combined Hf and Nd isotope composition of the terrestrial array (Vervoort et al., 1999) is characterized by a larger ε_{Hf} variability compared to that of ε_{Nd}. The seawater array displays more radiogenic ε_{Hf} for a given Nd value. Atlantic Hf isotope composition (Rickli et al., 2009) plots on the unradiogenic part of this array, whereas Pacific compositions (Zimmermann et al., 2009a) form the radiogenic part. The Hf and Nd isotope composition of Southern Ocean ferromanganese crusts and nodules (van de Flierdt et al., 2006) plot between Atlantic and Pacific compositions.

1.6 Previous work, motivation and research questions

1.6.1 Previous work

The hydrography of the Southern Ocean is relatively well known. In terms of marine Hf and Nd isotope distributions in the Southern Ocean, most information has been derived from analyses of ferromanganese (FeMn) crusts and nodules (Albarède and Goldstein, 1992; Albarède et al., 1997; Albarède et al., 1998; Piotrowski et al., 2000; van de Flierdt et al., 2006). The knowledge on dissolved seawater radiogenic isotope compositions in the Southern Ocean is currently only based on four full depth

profiles for Nd isotopes (Piepgras and Wasserburg, 1982; Jeandel, 1993), whereas for Hf only two data points exist (Rickli et al., 2009). The poor data-coverage of modern Hf and Nd is one the prime motivations for this study. Additionally, the Southern Ocean is a key area of the global thermohaline circulation and the knowledge of the present day isotopic distributions of deep water formation sites are essential for understanding the input parameters as well as for a reliable application of radiogenic Nd and Hf isotopes as proxies for past ocean circulation.

The first comprehensive study on the Hf isotope composition of seawater based on FeMn deposits was carried out by White et al. (1986). They suggested that the Hf budget in the ocean is governed by a relative dominance of mantle derived radiogenic Hf by reduced fluxes from land through the retention of unradiogenic Hf in weathering resistant zircons. As described in section 1.2, zircons have relatively high Hf concentrations and can thus be responsible for a low Hf flux from land because of their indestructibility. The retention of unradiogenic Hf in resistant minerals being one of the reasons for the observed Hf isotope composition in FeMn-deposits, the idea arose that Hf isotopes, in combination with Nd isotopes, can be used as a potential weathering tracer (Piotrowski et al., 2000; van de Flierdt et al., 2002). These authors observed changes toward less radiogenic Hf isotope compositions recorded by FeMn deposits, which coincided with the onset of major glaciations. They concluded that enhanced physical weathering by glacial grinding has the potential to release unradiogenic Hf from resistant minerals. However, a reason for the observed general offset in the isotope composition obtained from available seawater data form FeMn deposits towards more radiogenic Hf values compared to the terrestrial array (see section 1.4, Fig. 1.3) has, so far, only been hypothesized. Bayon et al. (2006) showed for the first time in river water that preferential release of radiogenic Hf from readily weathered mineral phases, such as sphene or apatite, is a possible explanation for the Hf isotope composition of Atlantic seawater derived from FeMn crusts. This was largely confirmed by mass balance calculations, which revealed that if 65 % to 70 % of all Hf is sequestered in zircons, a weathering input of a “zircon-free” crust can fully explain the isotopic offset of the combined Hf-Nd isotope composition of seawater from terrestrial rocks (van de Flierdt et al., 2007). An obvious explanation for the offset in seawater Hf is also delivered by a potential longer oceanic residence time compared to Nd (White et al., 1986). Particulate scavenging of Hf in estuaries has been suggested to be the major reason of the observed

low concentration of Hf in seawater (Godfrey et al., 2008). According to these authors, if rivers were considered as the main contributor of Hf into the ocean, paradoxically, these sources would at the same time represent a major Hf sink and thus result in an estimated oceanic residence time of more than 7500 years.

The first real seawater Hf isotope data have only recently been published (Rickli et al., 2009; Zimmermann et al., 2009a;b; Rickli et al., 2010). In these studies it has been observed that the Hf concentration does not increase with the age of a water mass. In contrast to previous estimates, they concluded that the oceanic residence time for Hf is only in the order of a few hundred years and that Hf isotopes are only a useful tracer on a basin-wide scale. Furthermore, Rickli et al. (2009) suggested that the Southern Ocean is a potential Hf sink in that biogenic opal acts as an effective scavenger. Due to the very low number of seawater Hf concentrations and isotope analyses currently available, there are still a lot of open questions on the factors controlling the behavior and distribution of Hf in seawater.

The first investigations on the Nd isotope composition of seawater have been carried out in the early 1980s by Piepgras and Wasserburg (1980; 1982). From comparison of the Nd isotope composition of the Atlantic and the Pacific, they concluded that Nd is a valuable tracer for ocean circulation patterns. These authors also calculated the rate of exchange between the Pacific and the Atlantic from Nd isotope compositions and concentrations derived from one full depth profile in the Drake Passage. They suggested that the Nd budget of the Southern Ocean is to about 70 % governed by Atlantic contributions. This estimate, however, contrasted with the findings of Jeandel (1993), who proposed a higher Pacific contribution based on a more radiogenic (i.e., Pacific sourced) Nd isotope composition of AAIW in the Argentine Basin. The relative importance of the contribution of the respective ocean basins and therefore, of the cold and warm route in the ocean conveyor belt explained above is crucial to investigate past and present ocean circulation. In addition, potential contributions from the Antarctic continent to the Nd isotope composition of the Southern Ocean have until now not been considered.

1.6.2 Motivation and research questions

The subject of this study is a detailed investigation of the distribution of dissolved Hf and Nd isotopes in the Atlantic sector of the Southern Ocean. The combination of

Nd and Hf isotopes has been successfully applied for the characterization of continental weathering regimes, i.e., it has been suggested that coupled Nd-Hf isotope analyses of Hf and Nd allow to distinguish weathering regimes dominated by chemical weathering from those dominated by physical weathering (e.g. van de Flierdt et al., 2002). So far, no data from the modern Southern Ocean are available to confirm this hypothesis. The Antarctic continent is positioned in latitudes where chemical weathering is subordinate to physical weathering (e.g. Ehrmann et al., 1992), therefore the Hf-Nd isotope compositions of Southern Ocean seawater are expected to be affected by this weathering regime.

To better understand the processes governing the Hf and Nd budget in this key area of ocean circulation, a more detailed study is needed to allow a more reliable interpretation of paleo-oceanographic data. Given the numerous uncertainties, which still exist in Hf and Nd isotope geochemistry in the world ocean, this study is aimed at answering the following crucial research questions:

(1) Can the Hf isotope composition of seawater be used as a tracer for the global ocean circulation system, or is the applicability restricted to a basin-wide scale?

(2) What controls the Hf and Nd isotope composition of water masses in the Southern Ocean? Is it possible to distinguish Southern Ocean water masses by their Hf and Nd isotope compositions?

(3) Is the Hf and Nd isotope composition of seawater a promising tool to reconstruct past weathering regimes and ocean circulation patterns?

1.7 Outline of the thesis

The thesis is divided into five main sections. This introductory chapter (Chapter 1) gives a general overview of the global thermohaline circulation with focus on the Southern Ocean and Hf and Nd isotope systematics. Furthermore, the basic ideas of using these isotopes as (paleo)oceanographic tracers are introduced and the motivation of this study is presented.

The second chapter presents the applied methodology. It explains the chemical procedures and the analysis of the two isotope systems. This chapter is essentially a “cookbook” for the reliable extraction and measurement of Hf and Nd concentrations and isotope compositions from seawater samples. It also includes suggestions for

further improvements in the applied methodology.

Chapter 3 (Sources and input mechanisms of hafnium and neodymium in surface waters of the Atlantic sector of the Southern Ocean) examines the Hf and Nd isotope composition and concentration patterns in the surface waters of the Atlantic sector of the southern ocean. The results are discussed and compared to earlier studies on particulate signatures and are put into perspective with the geology on the surrounding landmasses. This chapter will be submitted as manuscript in an international scientific journal.

Chapter 4 (Hafnium and neodymium isotope composition of the Atlantic sector of the Southern Ocean) discusses the deep water Hf and Nd isotope composition and concentration and discusses the applicability of Hf and Nd as water mass tracers. This chapter has been submitted to Earth and Planetary Science Letters.

Finally, Chapter 5 comprises the general conclusions achieved in this study and an outlook for future research.

Chapter 2

Methodology

In this chapter a complete description of the applied analytical procedures for the extraction, purification and measurement of the seawater samples for Hf and Nd concentrations and isotope compositions is given.

The general methodology originates from the ones applied in previous studies (e.g. Rickli, 2008; Zimmermann et al., 2009a) and the protocols follow the ones approved by the GEOTRACES program for the measurement of radiogenic Nd and Hf isotopes. All samples were collected during the International Polar Year (IPY) cruise ANTXXIV/3 on the German R/V *Polarstern* from February to April 2008. The samples were collected in acid-cleaned 20 L LDPE-collapsible cubitainers. A complete flowchart of the sample treatment is illustrated in fig. 2.1 and the reagents used for the chemical processing are listed in tab. 2.1. The respective results are listed in tab. A1 to A3, in the Appendix.

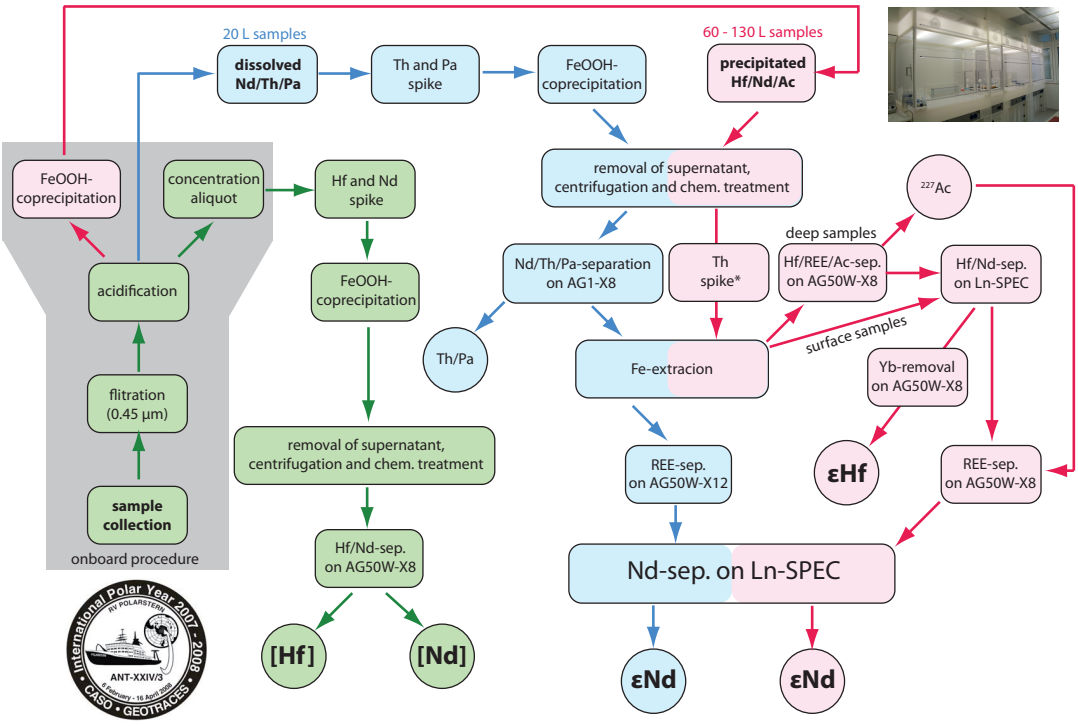

Figure 2.1: Schematic flowchart of the applied methodology. The gray shaded area represents the onboard procedures carried out on R/V *Polarstern*, whereas the remainder has been carried out in the home laboratory. The green boxes stand for "applied on all samples". The red boxes represent the large volume samples (≥ 60 L), which were primarily collected for the Hf isotope composition analysis. The blue boxes represent the smaller volume samples (20 L), which were collected for Nd, Th and Pa analyses.

Table 2.1: Reagents used for the chemical processing of the samples collected during ANTXXIV/3.
[a] double distilled for acidification on board

acid	product/grade	purification	usage
Milli-Q water	> 18 MΩ, Millipore	-	Chromatography
HCl	32 %, p.a.	Quartz distilled	Chromatography, sample dissolution
HNO3	65 %, p.a.	Quartz distilled[a]	Chromatography, sample dissolution
HF	40 %, Merck®, suprapure	-	Chromatography, sample dissolution
H_2O_2	30 %, Merck®, suprapure	-	Chromatography, sample dissolution
ammonia sol.	25 %, Merck®, suprapure	-	Iron co-precipitation
di-ethyl ether	> 99%, Roth®, p.a.	Back-extraction	Fe-extraction, cleaning of FeCl3
Ascorbic acid	solid	-	Reduce Fe(III) to Fe (II)
boric acid	solid	-	Dissolve fluorides
$FeCl_3$ x $6H_2O$	solid	Back-extraction	Co-precipitation
Citric acid	solid	-	Chromatography

2.1 Surface samples

2.1.1 Sample collection and onboard procedures for surface samples

Between 100 L and 130 L of seawater were taken for each sample mostly when the ship was underway. The collection was either carried out with a towed stainless steel fish, with the ship's own seawater intake system through polypropylene tubes, or with Niskin bottles on the CTD rosette from 25 m to 150 m water depth during station time. The samples were filtered (< 0.45 µm) within 12 hours after collection or directly during collection, if possible. Subsequent to filtration, the samples were acidified to pH ~2 with double distilled concentrated HNO_3 (see tab. 2.1 for the used reagents). From each sample an aliquot of 2 L was kept for concentration analysis. About 5 mg iron (Fe) per liter, in the form of previously cleaned dissolved Fe-chloride ($FeCl_3$, ~ 200 mg Fe per ml; see Appendix for the cleaning procedure) was added to the samples and equilibration was allowed for 24 hours. In a second step, ammonia solution (25%, suprapure) was added to bring the pH back to 8 in order to co-precipitate the dissolved trace metals with FeOOH (i.e. Hf and Nd). The supernatant was discarded and the residual FeOOH precipitate was transferred into 2 L wide mouth LDPE-bottles for transport to the home laboratory.

2.1.2 Home laboratory procedures of the surface samples

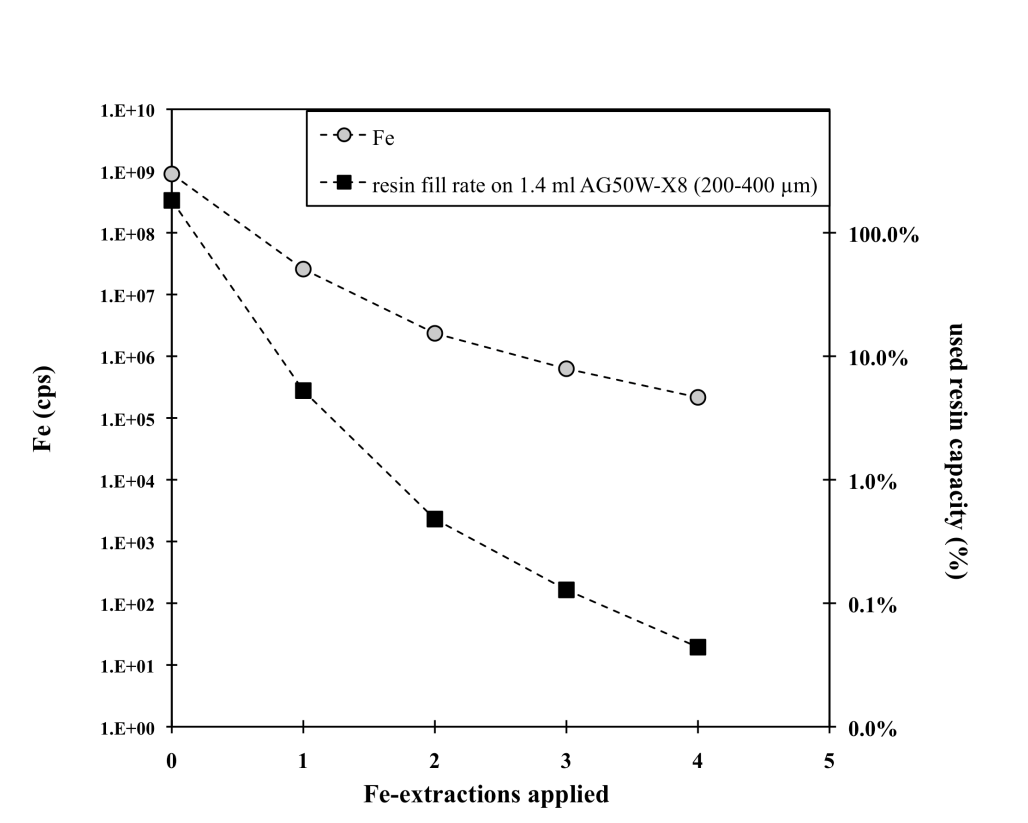

Figure 2.2: Efficiency of the applied Fe-extraction, tested on 0.5 ml $FeCl_3$ (corresponding to 100 mg Fe). The grey circles indicate the Fe content in the analyzed solution, where more than 90 % is already removed after one extraction. The black squares stand for the use of capacity of 1.4 ml AG50W-X8 (200-400 µm) resin.

The FeOOH precipitates were centrifuged for 10 minutes at 3500 rpm in the home laboratory at IFM-GEOMAR in Kiel (Germany). The precipitates were rinsed at least twice with de-ionized water (18.2 MΩ) followed by centrifugation to wash out major ions. The samples were removed from the centrifuge tubes with distilled 6M HCl into 60 ml Teflon vials and were evaporated to dryness on a hotplate over night. Subsequently 4 ml aqua regia was added and left for at least 24 hours at 110°C in the closed vials to destroy organic components. Thereafter the samples were evaporated to dryness again and transferred to Cl-form by adding 4 ml of 6M HCl followed by another evaporation step. Afterwards, 4 ml of 6M HCl was added to redissolve the samples. The previously added large amount of Fe was removed in order not to exceed resin capacity during the following ion chromatographic separation separation step. Iron was extracted by adding a suitable amount (in this case 4 ml, Tab. 2.2) of previously cleaned di-ethyl ether to the dissolved samples (see $FeCl_3$ cleaning procedure in the

Appendix chapter). The ether and the samples separate into two phases due to the density contrast and the iron was transferred into the ether phase by homogenization with a pipette tip, while the trace metals stayed in the acidic phase. The ether complex containing about 90 % of the iron (Fig. 2.2) was siphoned off with a pipette and discarded for each sample. This procedure, which is from hereon referred to as *Fe-extraction* was repeated twice or more until the sample solutions became pale yellow. Most of the samples formed a jelly-like precipitate, which scavenged about 90 % of the Hf from the sample. This precipitate was separated from the sample by centrifugation and dissolved by adding 2M HF. After evaporation, the remainder of the sample was added to this precipitate followed by another evaporation step.

Table 2.2: The amount of ether approximately needed to extract the Fe from the samples. The $FeCl_3$-solution contains ~ 200 mg/ml Fe.

	6M HCl (ml)	di-ethylether needed (ml)	Fe (g)
20 L sample: 0.5ml of Fe-sol	4	5	0.103
60 L sample: 3 x 0.5 ml	4	3 x 5 ml	0.310
120 L sample: 6 x 0.5 ml	4	6 x 5 ml	0.621

2.1.3 Chromatographic purification of Hf and Nd of the surface samples

Table 2.3: Applied chromatographic treatment of the samples. The shaded areas represent stages of sample loading or sample collection. The respective order of the columns for surface water and deepwater was: B, A, D (surface waters, Hf and Nd); A, B, A, D (deepwater, Hf, Ac/Nd) and C, D (Nd only). Recipe A has been slightly modified from Münker et al. (2001), whereas B is adapted from Pin and Zalduegui (1997).
(1) alternating HCl and HF
(2) 700 mg ascorbic acid is dissolved in 10 ml MQ on the same day of chromatography
(3) H_2O_2 is added to previously mixed 0.45M HNO_3 and 0.09M citric acid.

A: Hf/REE separation on 1.4ml AG50W-X8 (200-400µm)

volume	Acid	stage
8ml	6M HNO3 / 0.5M HF	pre-cleaning
2x1ml	MQ	change acid
0.5ml	1M HCl / 0.05M HF	pre-cleaning
1ml	1M HCl / 0.05M HF	pre-conditioning
0.5ml	**1M HCl / 0.05M HF**	**load and collect Hf**
2 ml	**1M HCl / 0.05M HF**	**collect Hf**
5ml	3M HCl	elute Fe
2x1ml	MQ	change acid
12ml	2M HNO3	elute Ba
6ml	**6M HNO3**	**collect Ac/REE**
6ml	6M HNO3 / 0.5M HF	clean
3x1ml	MQ	pass and store

B: Hf purification on 1ml Eichrom®LN-Spec (100-150µm)

volume	Acid	stage
2x15ml	6M HCl + 2M HF(1)	pre-cleaning
2ml	M.Q.	wash HF
2x3ml	3M HCl	pre-conditioning
4ml+08ml	**3M HCl + 0.4M ascorbic acid(2)**	**load**
8ml	**3M HCl**	**collect Nd**
50ml	6M HCl	elute matrix, REE
2x3ml	MQ	change acid
30ml	0.45M HNO3/0.09M Citric+1wt% H_2O_2(3)	elute Ti, W
2x3ml	MQ	change acid
5ml	2M HCl / 0.1M HF	elute Zr
6ml	**3M HCl / 0.2M HF**	**collect Hf**
2x25ml	6M HCl + 2M HF(1)	clean
2x3ml	1M HCl	pass and store

Tab. 2.3: continued.

C: REE separation on 0.8ml AG50W-X12 (200-400µm)

volume	acid	stage
8 ml	6M HCl	pre-cleaning
0.5 ml	1M HCl	pre-conditioning
1 ml	1M HCl	pre-conditioning
0.5 ml	**1M HCl**	**load sample**
3x0.6 ml	1M HCl	wash-in
5 ml	3M HCl	elute matrix
5 ml	**3M HCl**	**collect Sr**
2x1ml	MQ	change acid
8 ml	2.5M HNO_3	elute Ba
6 ml	**6M HNO_3**	**collect REE**
6 ml	6M HNO_3	clean
3x1ml	MQ	pass and store

D: Nd purification 2ml Eichrim®LN-Spec (50-100µm)

volume	acid	stage
8 ml	6M HCl	pre-clean
0.5 ml	0.1M HCl	pre-conditioning
1 ml	0.1M HCl	pre-conditioning
0.5 ml	**0.1M HCl**	**load sample**
0.5 ml	0.1M HCl	wash-in/elute Ba
7.5 ml	0.25M HCl	elute LREE
5 ml	**0.25M HCl**	**collect Nd**
8 ml	6M HCl	clean
1+1 ml	0.3M HCl	pass and store

The complete chromatographic schemes for all samples are listed in tab. 2.3. The samples were purified following the modified recipe of Münker et al. (2001), in which the samples are loaded in 4 ml 3M HCl + 0.8 ml 0.4M ascorbic acid to reduce remaining Fe in order not to exceed resin capacity (Tab. 2.3). The dissolved ascorbic acid solution was produced on the same day as the chromatographic procedures were carried out. About 700 mg of ascorbic acid (176.12 g/mol) was dissolved in 10 ml MQ, of which 0.8 ml was added to each sample dissolved in 4 ml 3M HCl. This recipe following Münker et al. (2001) was used as a matrix-independent purification of Hf, whereas remaining traces of ytterbium (Yb), which would have caused an isobaric interference on the mass spectrometer, were subsequently removed on an additional column with 1.4 ml of cation-exchange resin (BIORAD® AG50W-X8, 200-400 µm mesh-size) using 1M HCl / 0.05M HF (Fig. 2.1, Tab. 2.2). Furthermore, the purification

scheme of Münker et al. (2001) also separates rare earth elements (REE, including Nd) from the samples, which were washed and collected from the column immediately after loading the sample. The REE cuts from these columns were evaporated to dryness but still contained most of the previously added ascorbic acid. Adding 4 ml concentrated HNO_3 oxidized the ascorbic acid during carefully heating of the samples to ~ 90 °C in an open vial. The oxidizing HNO_3 mostly led to a vigorous reaction and when the reaction stopped the vial was closed and left on the hotplate over night at 90 °C to 100 °C. After subsequent evaporation the sample was further processed following Pin and Zalduegui (1997).

The respective Hf and Nd cuts were treated with 100 µl concentrated HNO_3 and 100 µl H_2O_2 (30 wt.%) for at least 2 hours and subsequently evaporated to dryness before measurement to avoid possible contamination by traces of resin in the sample and to reduce disturbing matrix effects. Finally, the samples were dissolved in 0.5M HNO_3 (Nd) and 0.5M HNO3 / 0.1M HF (Hf) for measurement on the MC-ICPMS.

2.2 Deepwater samples

2.2.1 Sample collection and onboard procedures of the deepwater samples

The sample volumes for the deep samples corresponded to 20 L for Nd and 60 L for Hf (Fig. 2.1). The onboard treatment of the large volume Hf samples followed the same procedure as of the surface samples described in section 2.1.1. The procedure for the 20 L Nd samples was reduced to only filtration (< 0.45 µm) and acidification to pH ~ 2. Further treatment of these samples was carried out in the home laboratory (see below).

2.2.2 Home laboratory procedures of the deepwater samples

The precipitates of the Hf samples were separated from the remaining supernatant by centrifugation and subsequently rinsed at least twice with MilliQ water to remove major ions. After the samples had been transferred into 60 ml teflon vials, they were treated with 4 ml of aqua regia for at least 24 hours at 110 °C to decompose organic components as described in section 2.1.2. Subsequently they were transferred into Cl-form by dissolution and evaporation in 4 ml of 6M HCl. Another 4 ml of 6M HCl were added to re-dissolve the samples. After complete dissolution, a previously weighed

^{228}Th-spike was added to each sample for determination of the ^{227}Ac (Actinium) activities, which will be discussed elsewhere. To separate the relatively large amount of Fe (300 mg) from the Hf, the Fe-extraction procedure described above was also applied for the 60 L samples (see section 2.1.2).

Similar to the surface samples, many deepwater samples formed jelly-like precipitates in 6M HCl, containing ~ 90 % of the Hf from the samples. These precipitates were removed in the same way as described in section 2.1.2. Due to remaining small amounts of calcium and magnesium in the samples, occasionally fluoride precipitates formed, which were re-dissolved in a mixture of 5 ml 6M HCl and 0.3M boric acid. This mixture was heated to up to ~ 100 °C in a closed Teflon vial. Within ~ 12 hours most of the fluoride precipitate was dissolved. After allowing the samples to cool down, they were transferred into suitable centrifuge vials. The samples were centrifuged for 10 minutes at 3500 rpm. The supernatant was taken out with a pipette and evaporated to dryness in Teflon vials. Subsequently the samples were dissolved in 1 ml 6M HCl and re-evaporated in order to transfer them into the Cl-form.

2.2.3 Chromatographic purification of Hf and Nd of the deepwater samples

In contrast to the surface samples, Hf was first separated from the main matrix including Nd and Ac through cation exchange chromatography (1.4 ml resin bed, Biorad® AG50W-X8, 200-400 µm mesh-size). The samples were loaded in 0.5 ml 1M HCl / 0.05M HF, and Hf was eluted by adding another 2 ml of the same reagent. Neodymium and Ac were collected in 6 ml 8M HNO3 after washing out the main part of the cation matrix and the remaining iron with 5 ml of 3M HCl (Tab. 2.3). The Ac/Nd cut was further processed at the Alfred-Wegener-Institute in Bremerhaven, Germany (AWI) following a modified procedure of Geibert and Vöge (2008). The Nd cuts were kept as a backup for the actual 20 L Nd isotope samples (see below). The Hf-cuts were further purified following the same modified separation scheme of Münker et al. (2001) as the surface samples (section 2.1.3). The total procedural blank was negligible at 15 pg to 20 pg compared to typical sample sizes of 4 ng to 5 ng.

The 20 L Nd aliquots were shared samples and were initially processed at Alfred-Wegener-Institut (AWI) in Bremerhaven (Germany) since thorium (Th) and protactinium (Pa) had to be separated first, because measurement of the ^{231}Pa concentration required addition of a short-lived ^{233}Pa spike (Venchiarutti et al., 2008).

The rare earth elements (REEs) including Nd were separated from Th and Pa using an anion exchange resin (Biorad® AG1-X8, 100-200 µm mesh-size) following the procedure described in Venchiarutti et al. (2008). Iron was subsequently separated from the REEs by solvent extraction at IFM-GEOMAR in Kiel, as outlined for Hf before. Further purification of the REEs was achieved through cation exchange chromatography (0.8 ml resin bed, Biorad® AG50-X12, 200-400 µm mesh-size), whereby major cations were removed first and the REEs were then eluted in 6M HNO_3. Neodymium was finally separated from Sm and the other REEs on columns filled with 2 ml LN-Spec resin (Eichrom®; Pin and Zalduegui (1997)). The Nd blanks were negligible at < 30 pg compared to more than 10 ng of Nd for each sample.

2.3 Hf and Nd isotope measurements

Table 2.4: Cup configuration on the *Nu plasma* MC-ICPMS for the Hf and Nd isotope composition measurements. Interfering masses are given in brackets.

Cup	H5	H4	H3	H2	H1	Ax	L1	L2	L3	L4
Mass (Hf)	^{182}W	^{180}Hf (^{180}W)	^{179}Hf	^{178}Hf	^{177}Hf	^{176}Hf (^{176}Yb)	175Lu	174Hf (^{174}Yb)	172Yb	-
Mass (Nd)	^{150}Nd (^{150}Sm)	^{148}Nd (^{148}Sm)	^{147}Sm	^{146}Nd	^{145}Nd	^{144}Nd (^{144}Sm)	143Nd	^{142}Nd (^{142}Ce)	140Ce	138Ba (^{138}Ce)

The Hf isotope compositions were measured on a *Nu plasma HR MC-ICPMS* at IFM-GEOMAR in manual time resolved mode due to the low Hf concentrations of the samples. The samples were dissolved in 250 µl to 500 µl 0.5M HNO_3 / 0.1M HF to obtain Hf concentrations of approximately 20 ppb corresponding and a total beam of at least 4 V. The measured Hf isotope compositions were corrected for instrumental mass bias to $^{179}Hf/^{177}Hf = 0.7325$ applying an exponential mass fractionation law. The JMC 475 standard was repeatedly measured during each run (n ≥ samples per run) and all $^{176}Hf/^{177}Hf$ ratios presented here were normalized to the accepted literature value of 0.28216 (Nowell et al., 1998). The external reproducibility ranged from ±0.5 ε_{Hf} to ±2.6 ε_{Hf} (2 S.D.) depending on sample size and was estimated by repeated measurements of both the JMC 475 standard and a certiPUR® ICPMS Hf-standard (with n ≥ number of samples per run).

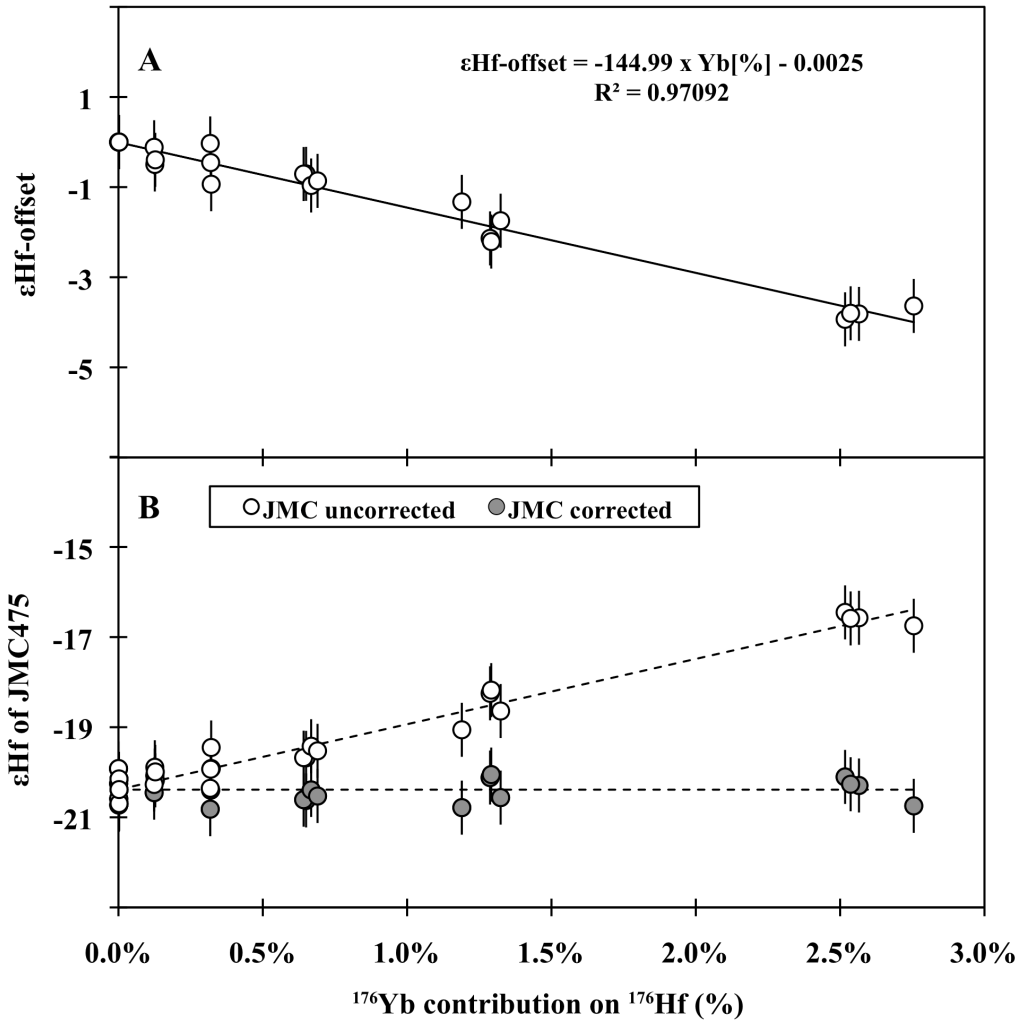

Figure 2.3: Graphs showing the change in Hf isotope composition when Yb is present during measurements. The change in Hf isotope composition correlates linearly with the amount of Yb (given in percent) on mass 176 (A). This resulted in a radiogenic offset in the isotope composition of an Yb doped JMC475 standard (B). The applied offset correction yields an average isotope composition of ε_{Hf} = -22.4 (±0.6 2 S.D.), identical to the initial value of the uncontaminated standard solution.

The samples were corrected for isobaric interferences of lutetium (Lu) and ytterbium (Yb) on mass 176 by monitoring ^{175}Lu and ^{172}Yb (see cup configuration in tab. 2.4). Most of the samples showed only little remaining Yb (< 0.3 % of the ^{176}Hf beam in the purified Hf) and corresponding interferences on ^{176}Hf were readily correctable following Chu et al. (2002). For some samples the Yb corrections were larger and corresponded to up to 2.2 % of the ^{176}Hf beam. Those data were corrected applying an offset correction obtained from a series Yb-doped JMC475 (Fig. 2.3) standards similar to Kemp et al. (2009). The systematic change in the Hf isotope composition of these standards depending on the amount of added Yb was linear

($R^2 = 0.971$, Fig. 2.3A) and the method is therefore considered reliable. The samples, which were corrected by this approach, are marked with a superscript "c" in tab. A3 (all results are listed in the Appendix).

The Nd isotope composition was either measured on a *Thermo Scientific TRITON 1 TIMS* or on the *Nu plasma* at IFM-GEOMAR. The measured isotope composition was corrected for instrumental mass bias after correcting for Sm contributions (see below) using $^{146}Nd/^{144}Nd = 0.7219$ applying an exponential mass fractionation law. The $^{143}Nd/^{144}Nd$ ratios were normalized to the accepted value for the JNdi-1 standard of 0.512115 (Tanaka et al., 2000). The external reproducibility on both instruments was between at ±0.3 and ±0.4 ε_{Nd} units (2 S.D.) estimated by repeatedly measuring JNdi-1 and an internal laboratory standard, with n = 4-6 on TIMS and n ≥ number of samples on the *Nu plasma MC-ICPMS*. Replicates measured on both mass spectrometers resulted in identical Nd isotope compositions within analytical error. On the *Nu plasma*, the larger samples containing 20 ppb to 50 ppb Nd were measured in 1 ml of solution in three blocks, each consisting of 15 cycles and an integration time of 10 second per cycle. The smaller samples containing less than 20 ng of Nd were measured manually in time resolved mode. These samples were dissolved in 250 µl to 500 µl to achieve a concentration of 20 ppb to 40 ppb. The uptake rate during one measurement was usually between 80 µl to 100 µl per minute, yielding a total integration time of 3 to 5 minutes per sample.

On the *TRITON TIMS* the samples were loaded on previously cleaned and de-gassed rhenium filaments in a 2 µl to 5 µl mixture of HCl and H_3PO_4. The samples were dried down directly on the filament. The samples were then mounted on a turret together with additional ionization filaments adjacent to the sample filaments. The fully loaded turret comprised up to 19 samples and two standards, which were measured repeatedly. The turret was then mounted in the ionization source, which was evacuated to $< 10^{-7}$ mbar. The samples were measured in nine blocks, each of them consisting of 10 to 15 cycles with an integration time of eight seconds per cycle. The number of measured cycles per block was dependent on signal strength, which was monitored on mass ^{144}Nd. A number of 10 cycles were measured during each block at 1 V on mass 144, whereas 15 cycles were used at 0.5 V. Isobaric interferences with Sm on mass 144 were monitored with ^{147}Sm on both instruments. The potential ^{144}Sm contribution on mass 144 was calculated by the natural abundances of Sm, assuming the same mass

fraction. The initial mass fractionation factor was calculated by the natural $^{146}Nd/^{145}Nd$ ratio of 2.0719 applying an exponential mass fractionation law and the resulting Sm contribution was subtracted from mass 144 prior to the final mass bias correction with the accepted $^{146}Nd/^{144}Nd$ ratio.

2.4 Hf and Nd concentration measurements by isotope dilution

2.4.1 Principles of isotope dilution and spike addition

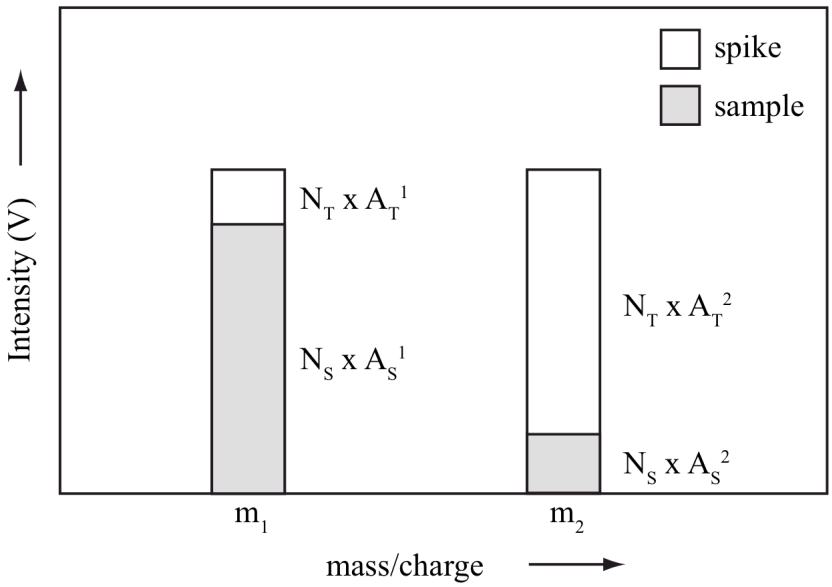

Figure 2.4: Principle of the isotope dilution (ID) technique in a schematic mass spectrum, modified after Heumann (1992). The naturally occurring isotopes (m_1 and m_2) of a given element have signal intensities, governed by the number of atoms (N_S) and their respective abundance (A_S). This is analog to the spike solution, indicated by a subscript "T". The resulting ratio of m_2/m_1 is a mixture of sample and spike is therefore dependent on (A) the amount of spike added and most importantly on (B), the amount of the element in the sample.

The isotope dilution (ID) technique has been proven to be a highly accurate method to determine the amounts or concentration of trace elements in a sample solution (see Heumann (1992) for a review). A schematic principle of the ID technique is illustrated in fig. 2.4. The ID method can be applied to any element, which has at least two stable or long-lived isotopes (m_1 and m_2). In this case, m_1 is more abundant in the sample (*S*) than m_2, usually identical to the natural isotope composition of the element. The spike (*T*), however, is enriched in isotope m_2. The amount of enrichment and spike addition to the sample must be exactly known to determine the amount of the analyzed element. From fig. 2.3 it is clear, that the measured mixed ratio (R_m) of m_2/m_1 is

produced by the amount of spike atoms added (N_T) and the amount of atoms of the same element in the sample (N_s). The largest uncertainty of ID technique is the amount of spike added, the isotope composition of the spike and the measurement of R_m. The isotope composition of a spike solution is in general well constrained and is crucial for the ID applicability. The measurement of R_m and its statistical error (σ) is of major importance for the uncertainty of an ID analysis and follows the law of error propagation (Riepe and Kaiser, 1966):

$$\sigma(\mathrm{N_s}) \approx \sqrt{\left[\sigma^2(\mathrm{N_T}) + f^2(R_\mathrm{m}) \times \sigma^2(R_\mathrm{m})\right]} \tag{2.1}$$

where (f) is the error multiplication factor of R, which is at minimum when the optimum R (R_{opt}) is reached:

$$\mathrm{R_{opt}} = \sqrt{\mathrm{R_T} \times \mathrm{R_s}} \tag{2.2}$$

The achievement of R_{opt} requires a circular argument, in that one has to estimate an expected amount or concentration of the analyzed element in the sample. The needed quality of estimation or the tolerance of R_{opt} is largely dependent on the enrichment of m_2 in the spike (Fig. 2.5). The employed Nd spike, for example, is enriched in ^{150}Nd by a factor of 846.5 compared to the natural abundance, whereas the Hf spike is enriched in ^{178}Hf only by a factor of 25.7 (see Appendix for spike composition). This means that the higher the enrichment factor of an isotope is, the broader is the range of R_m where the error propagation is at minimum (Fig. 2.5). All Hf samples reached ^{178}Hf/^{179}Hf ratios between 2.62 and 7.77 compared to the R_{opt} = 10.16. The ^{150}Nd/^{144}Nd ratios were between 2.5 and 10.3 compared to R_{opt} = 6.86.

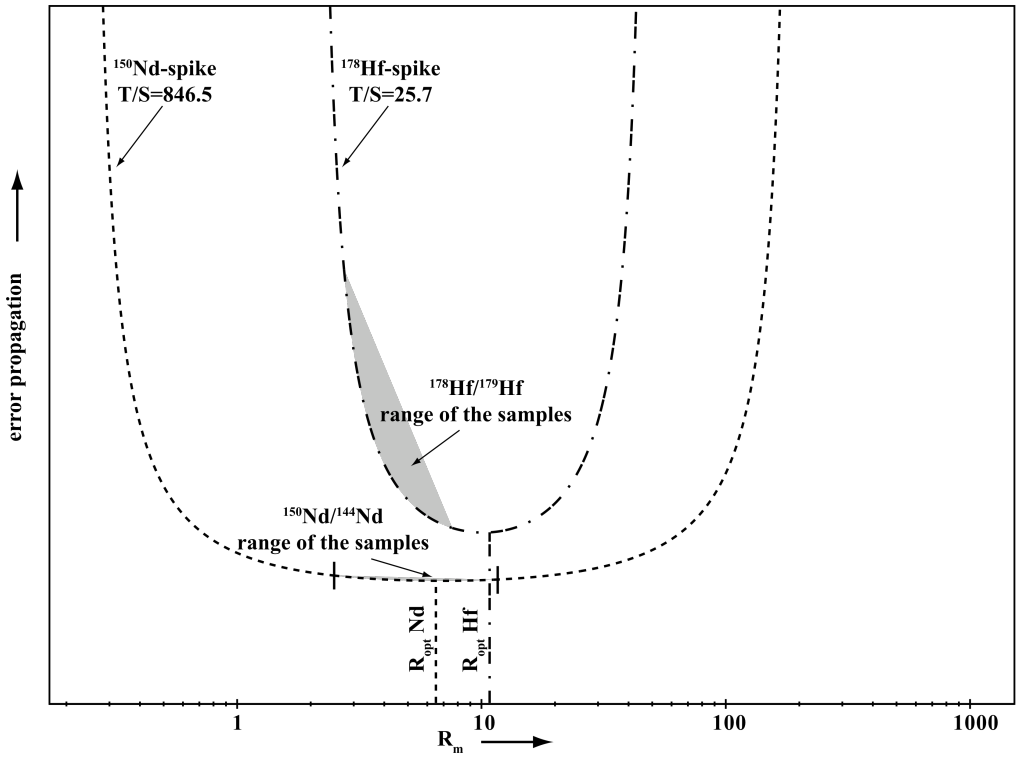

Figure 2.5: Dependency of error propagation on the mixed ratio (R_m). Indicated are the progressions of the Nd-spike (dashed line, with an enrichment factor of 846.5 on mass ^{150}Nd) and the Hf-spike (dashed-dotted line, with an enrichment factor of 25.7 on mass ^{178}Hf). The gray shaded area marks the mixed isotopic range of all samples achieved by the ID technique. For Nd this area is additionally marked by two strokes on the curve. The minima of the curves represent the respective optimum ratio (R_{opt}), being 10.16 for Hf and 6.86 for Nd.

2.4.2 Chemical treatment

The Hf and Nd elemental concentrations were obtained by application of the isotope dilution (ID) technique. The chemical procedure followed the one of Rickli et al. (2009). Previously weighed ^{178}Hf-single spike and ^{150}Nd/^{149}Sm double-spike solutions (see Appendix for the amounts of spike added) were added to an acidified 0.5 L aliquot of each sample, which was taken from the original 2 L aliquots, separately collected for concentration analysis (see sections 2.1.1 and 2.2.1). The samples were left for 4 to 5 days for complete isotopic equilibration, and 12 µl to 15 µl of $FeCl_3$ solution (~ 200 mg Fe per ml) were added to each sample. After 12 to 24 hours Fe was co-precipitated at pH 7 to 8 by adding 300 µl to 600 µl of ammonia solution (25 %, Merck® suprapure). The precipitates were centrifuged for 10 minutes at 3500 rpm and washed three times with Milli-Q water during subsequent centrifugation steps. The washed samples were transferred directly into Teflon vials and 300 µl of concentrated

HCl was added. After evaporation 0.5 ml of 1M HCl / 0.05M HF was added to redissolve the samples. The following purification of Hf and Nd was sufficient for subsequent mass spectrometric analysis using a single cation chromatographic separation step (1.4 ml resin bed, BIORAD® AG50W-X8, 200-400 µm mesh size). Hafnium was collected directly after loading onto the resin bed and washed down completely by adding another 2 ml of 1M HCl / 0.05M HF (Tab. 2.2). Neodymium was eluted after washing out the Fe with 5 ml of 3M HCl and the barium (Ba) with 12 ml 2M HNO_3. The respective Hf and Nd cuts were evaporated to dryness. Organic components were chemically removed prior to measurement on the MC-ICPMS by 0.5 ml 0.5M HNO_3 / 0.1 M HF + 100 µl H_2O_2 and 0.5M HNO_3 + 100 µl H_2O_2 for Hf and Nd, respectively.

2.4.3 Mass spectrometry

Table 2.5: Cup configuration on the *Nu plasma* MC-ICPMS for the Hf and Nd isotope dilution measurements. Interfering masses are given in brackets.

Cup	H6	H5	H4	H3	H2	H1	Ax	L1	L2	L5
Mass (Hf)	-	-	^{183}W	^{182}W	-	-	^{179}Hf	^{178}Hf	^{177}Hf	
Mass (Nd)	^{154}Sm	^{152}Sm	^{150}Nd (^{150}Sm)	^{149}Sm	^{148}Nd (^{148}Sm)	^{147}Sm	^{146}Nd	-	^{144}Nd (^{144}Sm)	^{138}Ba (^{138}Ce)

The concentration measurements were carried out on a *Nu plasma HR MC-ICPMS* (Tab. 2.5). The Nd samples were dissolved in 0.5 ml 0.5M HNO_3, whereas the Hf samples required the addition of traces of HF (0.1M) to redissolve. In order to guarantee complete dissolution, the samples were heated in a closed Teflon vial for ~ 1 hour. As long as the sample solution was still warm, the vial was tilted in a way to allow the solution to "touch" all droplets in the vial in order to catch the complete sample volume. The measurement for both elements was carried out in 30 cycles, each of them having eight seconds of integration time. Since Nd and Sm share common isotope masses (144, 148 and 150) and Sm was not separated from Nd by the applied chromatographic procedure (see section 2.3.1), an iterative interference correction was applied. Through this approach, not only the isobaric interferences, but also the instrumental mass bias were eliminated. The mass bias was corrected by assuming a fictional mass fractionation factor. This factor was used for the initial iteration. Every loop within the iteration optimized the fractionation factor. After five iterations no

significant changes were measurable and the obtained mass fractionation factor was applied for the mass bias correction. The amount of Nd was obtained by the mixed $^{150}Nd/^{144}Nd$ ratio of the spike and the natural ratio:

$$Nd[ng] = \left(\frac{\left((T \times C \times M_s)/M_T \right) \times A_T^{150} - {}^{150}Nd/_{144}Nd \times A_T^{144}}{\left({}^{150}Nd/_{144}Nd \times A_s^{144} - A_s^{150} \right)} \right) \times 1000 \qquad (2.3)$$

Where *T* is the amount of spike added in *g*, *C* is the concentration of the enriched isotope in the spike in *µg/g*, *M* is the atomic number in the spike (subscript *T*) and the natural element (subscript *s*) and *A* the abundance of the respective isotope in *percent*. The formula can be used for Hf as well, by substitution of the respective ratios, abundances and atomic numbers. For Hf the interference free $^{179}Hf/^{178}Hf$ ratio was measured to obtain the amount of Hf in the samples. The values were corrected for instrumental mass bias applying stable isotopes of tungsten (W), which has a mass similar to Hf and which was present in every sample. The mass fractionation factor was calculated by comparing the measured $^{182}W/^{183}W$ to the given $^{182}W/^{183}W = 1.850752$ (Taylor et al., 1994), using an exponential mass fractionation law.

Replicates for each element were processed and yielded an external reproducibility of better than 1% for Nd and between 3 and 10 % for Hf depending on the concentration. The procedural blanks were quantified by processing 0.5 liter of Milli-Q water in the same way as the samples and corresponded to less than 1 % in the case of Nd, for which no blank corrections were applied. The Hf content of the samples was closer to the blank level. The blank corresponded to 5 ±0.7 pg (n = 11), which was subtracted from all samples to achieve a correct seawater concentration (Tab. A4.2).

2.5 Recommendations on the methodology

The methodology applied in this study has been adopted and modified from previous studies (Rickli, 2009; Zimmermann et al., 2009a). For the first time, a liquid-liquid extraction method has been successfully employed for the seawater analysis of trace metals to remove the high amount of Fe induced by the FeOOH co-precipitation. This method has the advantage of reducing the chromatographic separation to a minimum of required ion exchange resin. After applying the Fe-extraction it was possible to purify the Hf of the surface samples of this study following the recipe of Münker et al. (2001). However, it has become apparent that using only one set of ion

exchange columns to purify the Hf is insufficient to quantitatively remove Yb and Lu, which have isobaric interferences with Hf on mass 176. These elements have been removed by loading the collected Hf cut on columns containing a 1.4 ml AG50W-X8 (200 µm to 400 µm) resin bed afterwards. Furthermore, applying the purification of Münker et al. (2001) the Nd yield was poor. The samples have been loaded onto the columns in a mixture of ascorbic acid and in the applied recipe the cuts containing the Nd were collected immediately after loading. In this way, the Nd cut contains a significant amount of ascorbic acid, which is very difficult to remove completely. The remaining ascorbic acid causes problems on the further purification of Nd because: (1) the sample does not completely dissolve and (2) the yield of the following cleaning steps is reduced by up to 80 %. A suggestion for future improvement could be that after the Fe-extraction, as soon as the amount of Fe is largely reduced, Hf and Nd should be separated first on 1.4 ml AG50W-X8 resin bed in order to: (1) separate Hf and Nd without any loss of the respective element and (2) remove the most of Yb and Lu before by applying the Hf purification after Münker et al. (2001). This method has been carried out in this order for the deep samples since it was not possible to separate Ac and Th from Hf after Münker et al. (2001). The high amounts of Yb occasionally remaining in these samples, did, however, mainly originate from a problem with column calibration.

Column calibrations were carried out by loading a standard solution on to the respective resin bed. A previously applied methodology involving doped standard solutions (e.g. Münker et al., 2001; Rickli, 2008) was used in order to estimate which element is washed out of the resin with defined amounts of specific acids. Sample matrices with high ion load, such as seawater, however, behave different from a pure standard solution during chromatographic separation. In this particular case, according to the column calibrations based on a standard solution, Yb and Lu are removed entirely already after washing with ~10 ml of 6M HCl, which is only a fifth of the actual volume finally used to remove these elements (Tab 2.3). The employment of the calibrations with the reduced amount of acid for seawater samples led to insufficient removal of Yb and Lu. These samples had to be corrected manually by an offset correction (see section 2.3). A further suggestion is therefore that calibration of chromatographic purification should be realized by either real or spiked real samples or a standard solution with an ion load similar to the analyzed sample.

A final remark is that due to the low amount of Hf in seawater, the volume of the aliquots for concentration measurements should be at least 1 L in order to reduce the blank/sample ratio. For a further improvement of the concentration measurements, a spike solution for Hf, where the enrichment factor of the spiked isotope is in the order of 500 to 1000 is recommended. This provides several advantages, such as: (1) the amount of spike can be reduced to a minimum to achieve the optimum ratio (R_{opt}, see section 2.4) and (2) the uncertainty is largely reduced, due to the expanded range, within which the error propagation is at minimum (see section 2.4).

Chapter 3

Sources and input mechanisms of hafnium and neodymium in surface waters of the Atlantic sector of the Southern Ocean*

* to be submitted as: Stichel T., Frank M., Rickli J., Hathorne E. C., Haley B. A., Jeandel C., Pradoux C., Sources and input mechanisms of hafnium and neodymium in surface waters of the Atlantic sector of the Southern Ocean.

Abstract

The first combined dissolved hafnium (Hf) and neodymium (Nd) isotope and concentration data from surface waters of the Atlantic sector of the Southern Ocean are presented here. The samples were collected along the Zero Meridian (ZM), in the Weddell Sea (WS) and in the Drake Passage (DP) during RV Polarstern expedition ANTXIV/3 in the frame of the International Polar Year (IPY) and the GEOTRACES program in 2008. The distribution of Hf and Nd concentrations is overall similar with essentially constant values (~0.3 pmol/kg and ~17 pmol/kg, respectively) between the area south of the Polar Front and the WS. Minima Hf and Nd concentrations were observed between the Subtropical Front (STF) and the Polar Front (PF). (~0.12 pmol/kg and ~8 pmol/kg, respectively). However, at the northernmost station located 200 km southwest of Cape Town a pronounced increase of the Nd concentration is observed, whereas the Hf concentration at the same time is at its minimum. This indicates a much lower amount of Hf than of Nd released by weathering of the Archean cratonic rocks of South Africa. From the southern part of the Subtropical Front (STF) to the Polar Front (PF) Hf and Nd show the lowest concentrations (less than 0.12 pmol/kg and 10 pmol/kg, respectively). This is most probably due to the limited terrigenous flux in this area, but may at least in parts also result from scavenging of Hf and Nd by biogenic opal.

In the vicinity of landmasses the Hf and Nd isotope composition is clearly marked by terrigenous inputs. In contrast, most of the Southern Ocean surface waters are characterized by the same isotope composition as the deep waters. It is only in the area of the Agulhas retroflection that Nd isotope values as low as $\varepsilon_{Nd} = -18.9$ are observed implying that unradiogenic inputs are supplied via the Agulhas Current (AC). The Nd isotope compositions become more radiogenic ($\varepsilon_{Nd} \sim -8$) towards the STF and within the Antarctic Circumpolar Current (ACC) and slightly decrease to $\varepsilon_{Nd} \sim -8.5$ in the Weddell Gyre (WG). Near the volcanic King George Island the isotopic data show significant increases to $\varepsilon_{Hf} = 6.1$ and $\varepsilon_{Nd} = -4.0$. The Hf concentration of these samples shows a maximum (0.38 pmol/kg), indicating an enhanced release of Hf from the mafic rocks of the Antarctic Peninsula. The Hf isotope composition in the studied area shows only a small range between $\varepsilon_{Hf} = 6.1$ at KGI and $\varepsilon_{Hf} = 2.8$ in the WG. Near the Antarctic continent the isotope composition drops from $\varepsilon_{Hf} \sim 5$ to $\varepsilon_{Hf} \sim 3$. This indicates a release

of unradiogenic Hf by glacial grinding and destruction of weathering resistant minerals such as zircon. The combined Hf and Nd isotope composition and concentration data from the studied area show that Hf is a sensitive tracer for prevailing physical weathering conditions, which is not the case for Nd. Neodymium isotopes show a factor of five larger range than Hf isotopes, which confirms Nd isotopes to be a highly sensitive tracer for the provenance of weathering inputs to surface waters of the ocean.

3.1 Introduction

3.1.1 Hafnium and neodymium isotopes as tracers in the sea

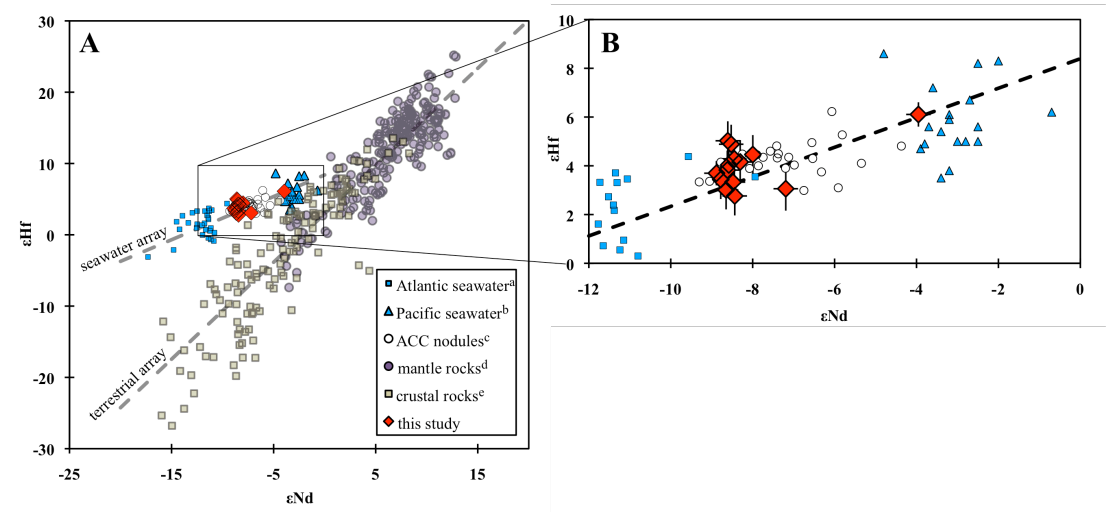

Figure 3.1: Hf and Nd isotope compositions of terrestrial rocks ("terrestrial array"), seawater and ferromanganese crusts ("seawater array"). The terrestrial array (Vervoort et al., 1999) is characterized by a larger ε_{Hf} variability than that of ε_{Nd} (A). The seawater array displays more radiogenic ε_{Hf} for a given Nd value (B). Atlantic Hf isotope compositions (Rickli et al., 2009) plot at the unradiogenic end of the array, whereas Pacific compositions (Zimmermann et al., 2009a) form the radiogenic part. The Hf and Nd isotope compositions of Southern Ocean seawater as well as of ferromanganese crusts and nodules (van de Flierdt et al., 2006) plot between Atlantic and Pacific compositions.

Dissolved radiogenic hafnium (Hf) and neodymium (Nd) isotope compositions (expressed as ε_{Hf} and ε_{Nd})[1] in seawater have been shown to provide insights into present and past ocean circulation and weathering conditions on land (e.g. Piotrowski et al., 2000; van de Flierdt et al., 2002; Frank et al., 2002). The global average residence time of Nd in the ocean is between 360 and 1500 years, which allows the use of Nd as a quasi-conservative tracer for advection of water masses over long distances (Jeandel et al., 1995; Tachikawa et al., 1999; Siddall et al., 2008; Arsouze et al., 2009). Hafnium, on the other hand, has an oceanic residence time, which is most likely on the order of

[1] $\varepsilon_{Hf} = \left(\frac{\left({}^{176}Hf / {}^{177}Hf \right)_{sample}}{\left({}^{143}Hf / {}^{144}Hf \right)_{CHUR}} - 1 \right) \times 10^4$ and $\varepsilon_{Nd} = \left(\frac{\left({}^{143}Nd / {}^{144}Nd \right)_{sample}}{\left({}^{143}Nd / {}^{144}Nd \right)_{CHUR}} - 1 \right) \times 10^4$

with CHUR = 0.282769 (Nowell et al., 1998) and 0.512638 (Jacobsen and Wasserburg, 1980) for Hf and Nd respectively.

only few hundred years (Rickli et al., 2009; Zimmermann et al., 2009b), implying that radiogenic Hf isotopes are useful tracers for water masses restricted to basin scales. However, there are also estimates of the residence time of Hf in seawater on the order of several thousand years (Godfrey et al., 2008; Godfrey et al., 2009). This discrepancy is mainly due to the lack of information available on the distribution of dissolved Hf in seawater. While the Nd input into the ocean is known to be governed by river and groundwater contributions, as well as exchange between sediments and seawater (Elderfield et al., 1990; Greaves et al., 1994; Jeandel et al., 1995; Haley et al., 2004; Lacan and Jeandel, 2005), the inputs contributing to the marine Hf budget are still debated. Hafnium in seawater is possibly delivered mainly by fluvial input (e.g. Bayon et al., 2006; Godfrey et al., 2008), but also hydrothermal inputs (Bau and Koschinsky, 2006) and exchange with marine sediments may play a role.

Comparison of the Hf and Nd isotope relationships in terrestrial rocks, referred to as the "terrestrial array" (Patchett et al., 1984; Vervoort et al., 1999), with available seawater data (Godfrey et al., 2009; Rickli et al., 2009a;b; Zimmermann et al., 2009a;b) reveals fundamental differences (Fig. 3.1A). The Hf and Nd isotope composition of terrestrial rocks is governed by the lutetium-hafnium (Lu/Hf) and samarium-neodymium (Sm/Nd) elemental fractionation during igneous processes. The radiogenic isotope systems of Hf and Nd are controlled by the decay of their respective parent isotopes ^{176}Lu and ^{147}Sm: Continental rocks are characterized by low Lu/Hf and low Sm/Nd leading to unradiogenic bulk Hf and Nd isotope compositions (low ε-values) over time. Mafic rocks (i.e. mantle-derived rocks) have higher Lu/Hf and Sm/Nd and are therefore more radiogenic (higher ε-value) in their bulk Hf and Nd isotope compositions. Compared to the terrestrial array, the available seawater Hf and Nd isotope compositions ("seawater array") are shifted to more radiogenic Hf isotope compositions for a given Nd isotope composition. The most plausible explanation is that during incongruent weathering of continental crust, unradiogenic Hf is retained in weathering resistant minerals, such as zircons, a process often referred to as the "zircon effect" (e.g. van de Flierdt et al., 2007). In addition, minerals with highly radiogenic Hf isotope composition have been shown to be more susceptible to weathering, thus causing preferential supply of radiogenic Hf to seawater (Bayon et al., 2006; van de Flierdt et al., 2007; Bayon et al., 2009). Rickli et al. (2010) suggested that areas with high atmospheric dust loads, such as the Sahara region, also contribute to the more

radiogenic Hf isotope composition. They showed that atmospheric sorting combined with a preferential release of Hf from traces of radiogenic apatite results in a surface water Hf isotope composition, which is ~10 ε_{Hf} units more radiogenic than the bulk dust composition. Therefore, both fluvial and atmospheric inputs are likely to contribute to a radiogenic Hf isotope composition in the ocean (Rickli et al., 2010). An alternative explanation, although so far not supported by direct data, is the input of radiogenic Hf through hydrothermal venting (White et al., 1986; Bau and Koschinsky, 2006). This source has been shown not to deliver any radiogenic Nd to deep waters (German et al., 1990; Halliday et al., 1992) and could also explain the observed decoupling of Hf and Nd isotopes and the offset to more radiogenic Hf isotope values in seawater.

Despite the fact that first analyses of the Hf and Nd isotope composition of different parts of the global ocean have already been published, the continental contributions and their supply pathways are still largely unconstrained, in particular in the Southern Ocean. Here we present the first combined surface water Hf and Nd isotope compositions and concentrations from the Atlantic sector of the Southern Ocean. With this new dataset we aim at a better understanding of the external inputs of Hf and Nd, as well as the mechanisms controlling their isotope composition.

3.1.2 Study area

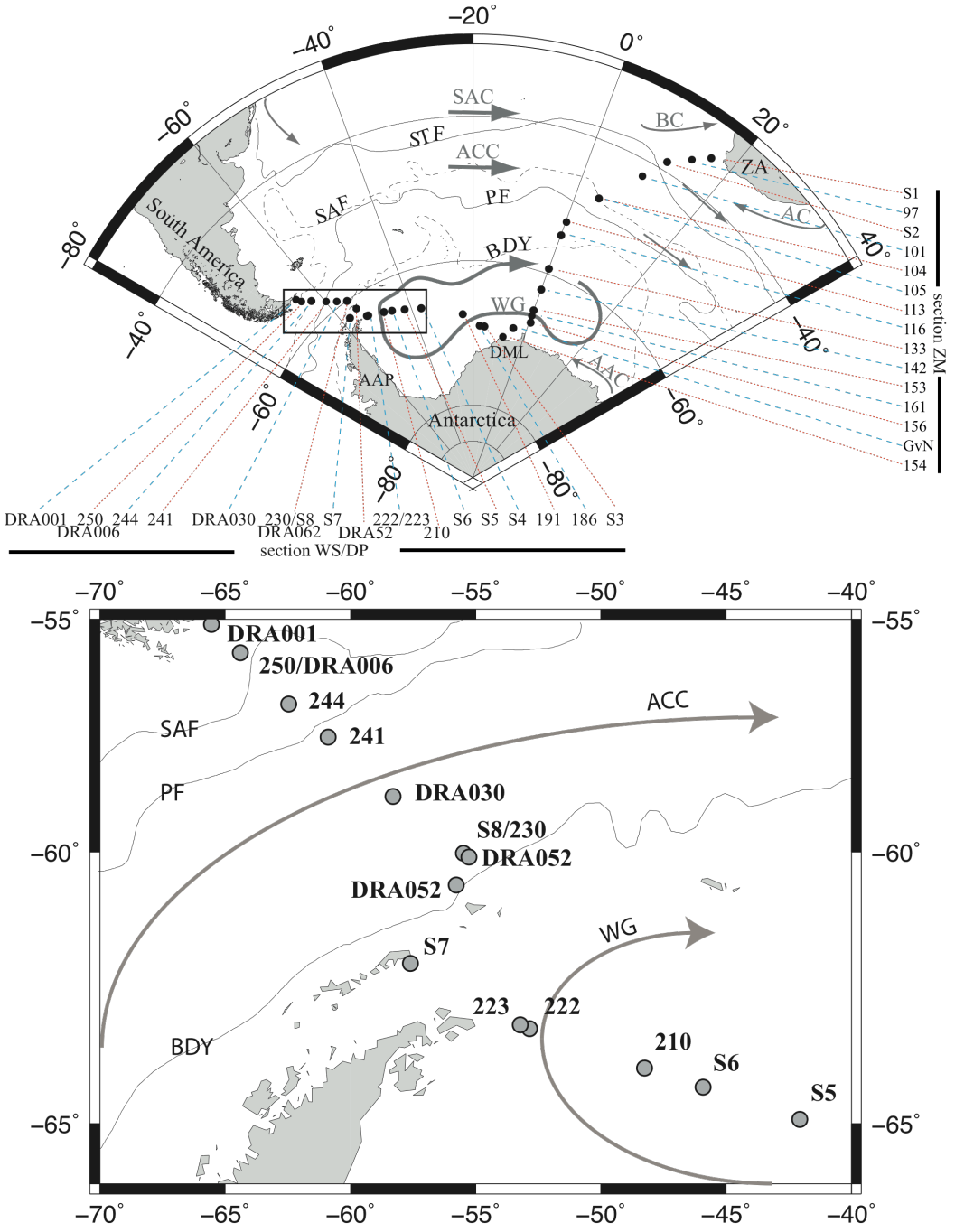

Figure 3.2: Overview of the study area (upper map) and detail of the area near the Antarctic Peninsula (lower map) with sample locations. The main hydrographic features are the Agulhas Current (AC), the Antarctic Circumpolar Current (ACC), the Benguela Current (BC), the South Atlantic Current (SAC) and the Weddell Gyre (WG). The dashed lines represent the approximate locations of the Southern Ocean frontal system from north to south, as described in Orsi et al. (1995): the Subtropical Front (STF) the Subantarctic Front (SAF), the Polar Front (PF) and the Southern ACC boundary (BDY).

The surface waters of the Southern Ocean (Fig. 3.2) are separated from those of the subtropical region further north by a pronounced meridional temperature and salinity gradient. This hydrographic boundary is referred to as the Subtropical Front (STF; Hofmann, 1985). The STF is the only front in the Southern Ocean that is not circumpolar, given that no subtropical waters are found in the Drake Passage between the Antarctic Peninsula and South America (Sievers and Emery, 1978; Sievers and Nowlin, 1984). The STF marks the transition between the relatively cold and fresh Subantarctic Surface Water (SASW) and the much warmer and saltier Subtropical Surface Water (STSW). This front develops in the western South Atlantic Ocean and is associated with an eastward transport of up to 37 Sv (1 Sv = 10^6 m^3s^{-1}). This flow decreases to less than 15 Sv towards South Africa, commonly called South Atlantic Current (SAC) where it turns north to feed the Benguela Current (Stramma and Peterson, 1990). South of the STF, a region of weak flow separates the SAC from the Antarctic Circumpolar Current (ACC), which dominates geostrophic eastward flow around the Antarctic continent. The ACC is bound to the south by cyclonically circulating gyres, such as the Weddell Gyre (Deacon, 1979; Klatt et al., 2005). Within the ACC, bands of horizontal density gradients, also associated with strong lateral currents, characterize the Subantarctic (SAF) and the Polar (PF) Fronts (Emery, 1977; Nowlin Jr. and Whitworth III, 1977; Whitworth III, 1980; Peterson and Stramma, 1991). From the PF to the Antarctic continent the relatively homogenous Antarctic Surface Water (AASW) is found, which forms the topmost layer above the warmer and saltier Upper (U) and Lower (L) Circumpolar Deep Water (CDW).

The Atlantic sector of the Southern Ocean is bounded by the landmasses of South Africa in the east, the Antarctic continent in the south and South America in the west (Fig. 3.2). The geology of South Africa mainly comprises the Archaean Kaapvaal Craton, which is surrounded by several orogenic belts of Proterozoic and Paleozoic ages. On top of this old basement the sedimentary Karoo Basin developed during the Paleozoic (Cole, 1992). The geological structure of the Antarctic continent can be roughly divided into the three tectonic domains comprising the East Antarctic Shield (EAS), the Transantarctic Mountains (TAM) and West Antarctica (WA). The EAS comprises a Precambrian to Ordovician igneous and sedimentary basement overlain by Devonian to Jurassic sediments. East Antarctica, in particular the Dronning Maud Land (DML), consists of tectonically approximately the same facies as South Africa

originating from the Pan-African orogeny during the collision of East and West Gondwana about 600 to 500 Ma ago (Thomas et al., 1993; Rogers et al., 1994). The TAM mark the boundary between East and West Antarctica. They represent sedimentary deposits from the Late Cambrian Ross orogeny, the Devonian to Permian Gondwana sediment cover and Jurassic tholeiites, which underwent uplift since the early Cretaceous (Dalziel, 1992; Fitzsimons, 2000). WA is a buildup of five crustal blocks, of which only three are of relevance for the studied area: the Haag Nunataks (HN), the Ellsworth Whitmore Mountains (EWM) and the Antarctic Peninsula (AAP). The HN represents a small crustal block between the AAP and the EWM consisting of Proterozoic amphibolites and orthogneisses (Millar and Pankhurst, 1987). The EWM form a 415 km long, NNE-SSW trending mountain chain being a terrane once situated at the margin of Gondwana prior to its break-up during the Jurassic (Dalziel, 1992; Storey, 2005). The sedimentary succession has similarities to the Gondwanian deposits from the TAM but additionally comprises mid-Cambrian volcanic rocks. Middle Jurassic granite intrusions related to the break-up of Gondwana are also found throughout the EWM. The AAP mainly consists of magmatic rocks of varying origin and is interpreted as a long-lived magmatic arc partly built on Cambrian continental crust (Millar et al., 2001). Most of the exposed rocks, however, are of Mesozoic and younger ages resulting from subduction on the western margin of the Peninsula, central arc magmatism (AAP Batholith), and back-arc sequences on the eastern side bounded by the Weddell Sea. In the Tertiary the batholitic intrusions were restricted to the western side of the AAP and ceased almost completely at ~50 Ma ago.

3.2 Methods

3.2.1 Sample collection and onboard procedures

Most samples were collected during the International Polar Year (IPY) cruise ANTXXIV/3 on the German research vessel *Polarstern* from February to April 2008. This cruise was also part of the international GEOTRACES program and all samples were collected and measured for their Nd and Hf concentrations and isotopic compositions according to the agreed GEOTRACES protocols. Between 100 L and 130 L of seawater were taken for each sample mostly when the ship was underway. The collection was either carried out by using a towed stainless steel fish with a teflon head, through which water was pumped directly into the ship's laboratory under trace metal

clean conditions, by polypropylene tubes using the ship's own seawater intake system, or by using Niskin bottles on the CTD rosette from 25 m to 150 m water depth during station time (Tab. A1). All samples were filtered (< 0.45 µm) within 12 hours after collection or directly during collection, when possible. The samples were then acidified to pH ~2 with double distilled, concentrated HNO_3. From each sample an aliquot of 2 L was kept for concentration analysis. About 500 to 600 mg iron (Fe), in the form of previously cleaned dissolved Fe-chloride, was added to the large volume samples and allowed equilbration for 24 hours. In a second step, ammonia solution (25%, suprapure) was added to bring the pH back to 8 in order to co-precipitate the dissolved trace metals with FeOOH (i.e. Hf and Nd). The supernatant was discarded and the residual FeOOH precipitate was transferred into 2 L wide mouth LDPE-bottles.

In addition five Nd samples collected in the Drake Passage during the expedition ANTXXIII/3 on *Polarstern* were included. For each sample 10 L of seawater was filtered and acidified as described above. The preconcentration was realized by co-precipitation with manganese hydroxide (MnOOH) after rising the pH to > 9. Similar to the sample described above, the supernatant was removed and the residual MnOOH was transferred to smaller bottles.

3.2.2 Further procedures in the home laboratory

The precipitate from the sample from ANTXXIV/3 was then centrifuged in the home laboratory of IFM-GEOMAR in Kiel (Germany) and was rinsed at least twice with de-ionized water (18.2 MΩ) to wash out major ions. The precipitate was removed from the centrifuge tubes with 6M HCl (sub boiled) into 60 ml Teflon vials and was evaporated to dryness on a hotplate over night. Then 4 ml aqua regia was added and left for at least 24 hours at 110°C in the closed vials to destroy organic components. Thereafter the samples were evaporated to dryness again and transferred to Cl-form by adding 4 ml of 6M HCl followed by another evaporation step. Afterwards, 4 ml 6M HCl was added to redissolve the samples. The previously added large amount of iron was removed in order not to exceed resin capacity during chromatographic separation. The iron was extracted by adding 4 ml of previously cleaned di-ethyl ether to the dissolved sample. The ether and the sample separated into two phases and the iron was transferred into the ether phase by homogenization, while the trace metals stayed in the acidic phase. The ethereal complex containing the iron was siphoned off

with a pipette and discarded. This iron extraction was repeated twice or more until the sample solution became pale yellow. The residual was then evaporated and re-dissolved in 4 ml 3M HCl.

Most of the samples formed a jelly-like precipitate, which scavenged about 90 % of the Hf from the sample. This precipitate was dissolved by adding 2M HF. Thereafter, the sample was purified following the modified recipe of Münker et al. (2001). This recipe was used as a matrix-independent purification for Hf, whereas remaining traces of ytterbium (Yb), which would have caused an isobaric interference on the mass spectrometer, were subsequently removed on an additional column with 1.4 ml of cation-exchange resin (BIORAD® AG50W-X8, 200-400 µm mesh-size) using 1M HCl and 0.05M HF. Furthermore, purification after Münker et al. (2001) also separated Rare Earth Elements (REE) from the sample, which were eluted from the column immediately after loading the sample. The REE cut was further processed following Pin and Zalduegui (1997). The respective Hf and Nd cuts were treated with 100 µl HNO_3 (concentrated, sub-boiled) and 100 µl H_2O_2 (30 wt.%, Merck-suprapur®) and subsequent evaporation to dryness before measurement to avoid possible contamination by traces of resin in the sample and to reduce potentially disturbing matrix effects. Finally the samples were dissolved in 0.5M HNO_3 (Nd) and 0.5M HNO3 + 0.1M HF (Hf) for measurement on the MC-ICPMS.

The additional samples from expedition ANTXXIII/3 were further treated at *LEGOS* in Toulouse (France) in that they followed a similar procedure as described in Lacan and Jeandel (2001).

3.2.3 Concentration measurements

Hafnium and Nd concentrations were obtained by isotope dilution (ID) similar to the method described by Rickli et al. (2009). Weighed ^{178}Hf-single spike and ^{150}Nd/^{149}Sm double-spike solutions were added to an acidified 0.5 L aliquot of each sample. The samples were left for 4 to 5 days for complete equilibration. Subsequently $FeCl_3$ solution was added to the samples and Hf and Nd were co-precipitated with FeOOH by adding ammonia to raise the pH to 8. For the mass spectrometric analysis, purification of Hf and Nd using a single cation chromatographic separation step (1.4 ml resin bed, Biorad® AG50W-X8, 200-400 µm mesh-size) was sufficient. The respective cuts containing Nd and Hf were evaporated to dryness and then oxidized by adding

200 µl of a 1:1 mixture of 0.5M HNO3 and H_2O_2 (30 wt.%) to reduce disturbing matrix effects during measurement on the MC-ICPMS. Replicates for each element were processed and yielded an external reproducibility of better than 1% for Nd and between 3 % and 10 % for Hf depending on concentration. Procedural blanks were quantified by processing 0.5 L of MQ-water in the same way as the samples and corresponded to less than 1% for Nd, where no blank corrections were applied. Due to their low concentrations, the Hf content of the samples was closer to the blank level. The blank amounted to 5 ±0.7 pg (n = 11, corresponding to 50 % of the smallest sample), which was subtracted from all samples to achieve a correct seawater concentration

In addition, rare earth element (REE) concentrations were determined using the *seaFAST* system (Elemental Scientific Inc.) connected to an *Agillent 7500 Series* quadrupole ICPMS. The seaFAST system performs preconcentration, matrix removal and online elution into the ICP-MS, enabling direct analysis of trace metals from undiluted seawater samples. For REE measurements 4 ml of acidified seawater was loaded onto the preconcentration column, the matrix washed away and the REE together with an Indium internal standard eluted directly into the PFA nebulizer. Calibration of the elution time each day using time resolved analysis reveals that the REEs are not fractionated on the seaFast column. The overall reproducibility of these analyses was better than 8 %, obtained by a repeatedly measured sample (n = 10), whereby it was independently shown that the REEs are not fractionated on the seaFast columns. The agreement with the isotope dilution measurements of the Nd concentrations was better than 10 % for most of the samples except for stations 116 and S7, which have 19 % and 12 % lower concentrations according to the *seaFAST* system, respectively. For this study only the lanthanum (La) – Yb ratios (La_N/Yb_N) are presented as markers of continental input at distinct sample sites, for which the uncertainty is estimated at ~ 2.5 %. All measured REEs were normalized to Post Achaean Average Shale (PAAS, Taylor and McLennan (1985)), which reflects the average composition of the upper continental crust.

3.2.4 Isotope measurements

The Hf isotopic composition was measured on a *Nu plasma HR MC-ICPMS* at IFM-GEOMAR applying manual time resolved data acquisition. The samples were dried down and re-dissolved in 250 to 500 µl 0.5M HNO_3 / 0.1M HF to obtain a Hf

concentration of ~20 ppb corresponding at total beam of at least 4 V. The measured Hf isotopic compositions were corrected for instrumental mass fraction bias to $^{179}Hf/^{177}Hf = 0.7325$ applying an exponential mass fractionation law. The $^{176}Hf/^{177}Hf$ ratios were normalized to the average of JMC 475 standards repeatedly measured during the same session with the accepted value of 0.28216 (Nowell et al., 1998). The external reproducibility for the set of samples in this study was ±0.8 ε_{Hf} (2 S.D.) and was estimated by repeated measurements of the JMC 475 Hf standard at the same concentration as the samples (with n ≥ number of samples per run). The Nd isotopic composition was either measured on the *Nu plasma* instrument as well, though in automatic mode, or on a Thermo Scientific Triton 1 TIMS. The measured isotopic composition was corrected for instrumental mass bias to $^{146}Nd/^{144}Nd = 0.7219$ applying an exponential mass fractionation law. The $^{143}Nd/^{144}Nd$ ratios were normalized to the average of the repeatedly measured JNdi-1 standard with the accepted ratio of 0.512115 (Tanaka et al., 2000). The external reproducibility was between ±0.3 ε_{Nd} and ±0.39 ε_{Nd} (2 S.D.) estimated by repeated measurements of the JNdi-1 standard, as well as of an internal laboratory standard. Duplicates measured on both instruments resulted in the same value within the error.

The additional samples from ANTXXIII/3 were measured on a MAT 261 TIMS, using the same method as above to correct for instrumental mass bias. The samples were corrected for machine bias by correcting a repeatedly measured La Jolla Nd standard with the accepted $^{143}Nd/^{144}Nd$ value of 0.511859, yielding an external reproducibility between ± 0.2 and 0.6 ε_{Nd} units.

3.3 Results

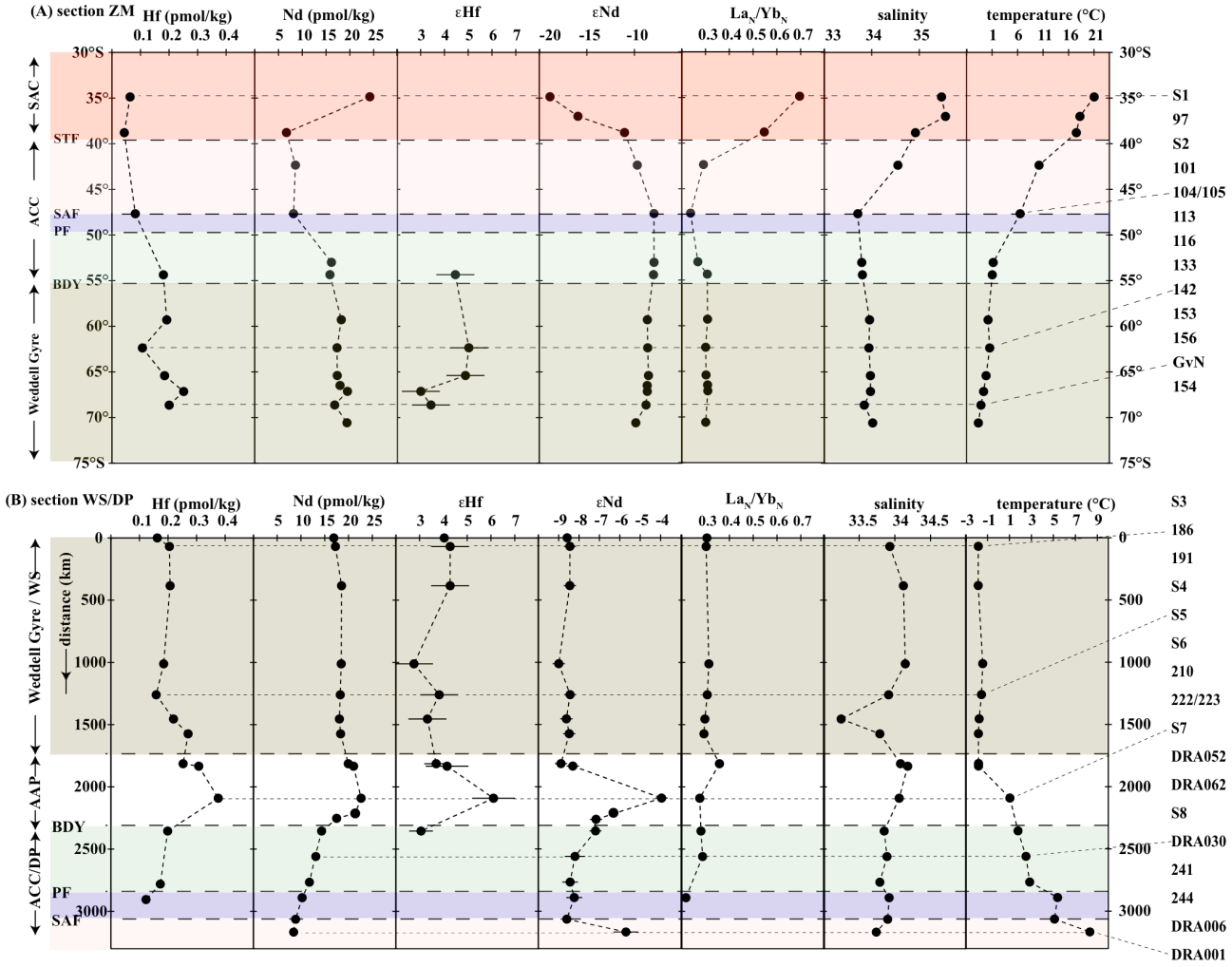

Figure 3.3: Composition of the surface samples along the Zero Meridian (A) and through the Weddell Sea and the Drake Passage (B). Note the different scales in ε_{Nd} and temperature between (A) and (B). Major hydrographic transitions are provided in the text. Hafnium and Nd concentrations largely follow a similar pattern in both sections with the exception that S1 in (A) shows a significantly elevated Nd concentration. The Hafnium and Nd isotope composition also follow similar trends where combined data are available. The only exceptions are stations 156 and GvN, where the ε_{Hf} drops to less radiogenic values, whereas ε_{Nd} does not. The La/Yb ratios are normalized to PAAS (Taylor and McLennan, 1985). Isosurface plots are shown in the Appendix (Fig. A1).

3.3.1 Hf and Nd concentrations

Both Hf and Nd concentrations show similar distribution patterns in the studied area with exceptions of stations S1 and 142 (Fig. 3.3A, see fig. A1 for isosurface plots), where Hf concentrations, in contrast to Nd, show local minima. The Hf concentration varies between 0.04 pmol/kg close to the STF (station S2) and 0.4 pmol/kg at station 161 near the Antarctic continent. This maximum concentration was found for a sample from 100 m water depth and represents the shallow part of LCDW, as indicated by the pronounced salinity anomaly. This sample is not included in fig. 3.3 and is not further discussed here, because it evidently does not reflect surface water properties. A second, broader maximum with a peak of 0.38 pmol/kg at station S7 was found near King George Island (KGI).

A local maximum at KGI, although not as pronounced as for the Hf, is also observed for Nd (reaching 22.6 pmol/kg). The highest Nd concentration of 24.2 pmol/kg was measured at station S1, about 200 km southwest of Cape Town, which contrasts with the second lowest concentration of Hf in this study at that location (0.06 pmol/kg). The Nd concentration then sharply decreases southward to a minimum value 6.7 pmol/kg at the STF (station S2). Towards the SAF, the concentrations for both elements remained on this low level. A pronounced southward increase in the concentrations of both elements is observed between the SAF (station 104/105) and the AAZ (station 113 and 116). From there on, the Hf and Nd concentrations stay relatively constant across the WG, although the Hf concentrations apparently show more scatter. This is, however, most likely caused by the low concentrations and the larger analytical uncertainties. Starting approximately at station S6 the Hf concentrations, and less pronouncedly also the Nd concentrations, rise continuously until station S7 north of the AAP (Fig. 3.3B). Further north in the DP Hf and Nd concentrations drop again to values similar to those found in the eastern Atlantic sector of the ACC.

3.3.2 Shale normalized La/Yb ratios

For this study we only use the ratio of light (LREEs) to heavy REE (HREEs), more specifically the PAAS-normalized La_N/Yb_N. The La_N/Yb_N data range from 0.69 to 0.20 (Fig. 3.3). The highest ratios were measured north of the STF, with a southward decrease from the maximum value of 0.69 at station S1 to 0.52 (station S2). Further south along the Zero Meridian the values drop from 0.29 at station 101 to 0.20 at the

SAF (station 105). South of the PF and in the WG the La_N/Yb_N is rather constant at values near 0.3. In the DP the values behave similarly with respect to the frontal positions in that the lowest ratios are found north of the PF (0.22, station 244) and there is no significant change of the La_N/Yb_N at those locations where elevated Hf and Nd concentrations are observed near the AAP.

3.3.3 Hf and Nd isotope composition

Overall, the Hf isotope composition of the surface waters does not show a large variability and ranges from $\varepsilon_{Hf} = 2.8$ to 5.0, whereby it is noted that for the stations north of 55° along the Zero Meridian and in the northern part of the Drake Passage the Hf concentrations in the samples were too low and therefore not measurable. A distinct deviation from the above range of Hf isotope data is station S7, where the most radiogenic value ($\varepsilon_{Hf} = 6.1$) is measured close to KGI (Fig. 3.2 and Fig. 3.3B). At the same station a similar excursion to more radiogenic values is also observed for Nd isotopes ($\varepsilon_{Nd} = -4.0$; Fig. 3.3B). At nearby station S8 north of KGI, the Nd isotope composition is still significantly higher than in the DP further north ($\varepsilon_{Nd} = -6.3$ to -7.2) whereas the Hf isotope composition is already back to low values ($\varepsilon_{Hf} = 3.1$). Another radiogenic Nd isotope excursion to $\varepsilon_{Nd} = -5.7$ is measured at station DRA001, close to the southern tip of Chile. However, within the ACC and the WG, the Nd isotope composition is rather uniform at ε_{Nd} values between -7.8 and -8.6 and only at station 154 a less radiogenic value was measured ($\varepsilon_{Nd} = -10.0$; Fig. 3.3A). Stations north of the STF have the least radiogenic Nd isotope compositions between $\varepsilon_{Nd} = -18.9$ and $\varepsilon_{Nd} = -11.0$ (Fig. 3.3A).

Combined Hf and Nd isotope compositions show that surface waters from the Southern Ocean are shifted towards more radiogenic Hf values for given Nd values when compared to the “terrestrial array” (Fig. 3.1B). Similar to previously published seawater data (Godfrey et al., 2009; Rickli et al., 2009, 2010; Zimmermann et al., 2009a,b), the surface waters in this study plot on the “seawater array”, as previously derived from analyses of ferromanganese crust and nodule surfaces (Albarède et al., 1998; David et al., 2001; van de Flierdt et al., 2006). All samples form an isotopically homogenous field, with the only exception of the samples collected in the vicinity of KGI, which plot on the more radiogenic part of the seawater array.

3.4 Discussion

3.4.1 Particles as potential sources for the dissolved Hf and Nd in the Southern Ocean?

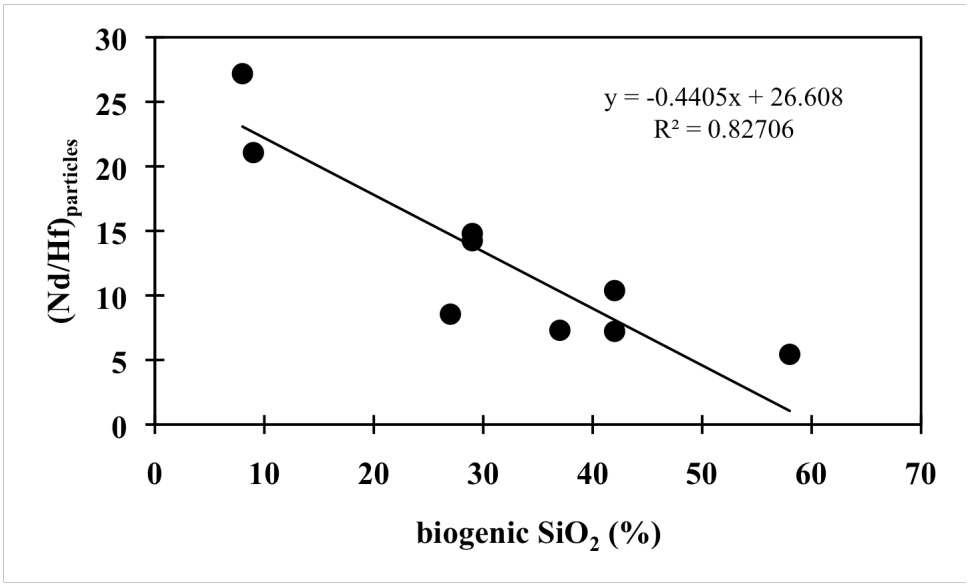

Figure 3.4: Nd/Hf ratio in particles plotted against their biogenic opal content (Hegner et al., 2007), indicating a preferential scavenging of Hf onto siliceous frustules.

Hf and Nd concentrations show remarkably similar distribution patterns, with a pronounced exception at station S1 southwest of Cape Town (Fig. 3.3A). There, the Hf concentration (0.08 pmol/kg) is one of the lowest of the entire sample set, whereas Nd is at its maximum (24.7 pmol/kg). It is unlikely that the low Hf concentration can be explained by strong particulate scavenging, because this would also have influenced the Nd concentration, as we will discuss below. One possible reason for the depletion of Hf in this region is a small amount of Hf supplied by weathering from South Africa. Further south, near the STF (station S2), the Hf concentration remains at the same low level, while the Nd concentration also drops to a minimum, suggesting either efficient removal or reduced input. Between the SAF and the ACC boundary (BDY), both elements show marked increases. A similar southward increase is also observed in the Drake Passage between stations 250 and S8. Hegner et al. (2007) showed that Nd concentrations adsorbed to particles are very low in the eastern Atlantic sector of the ACC and amount to less than ~1 pmol/L. This coincides with low aluminum (Al) and thorium (Th) concentrations, documenting very low terrigenous inputs. These authors proposed that scavenging of Nd from seawater on the order of only 5 % to 10 % of the available dissolved load would be sufficient to yield the observed Nd concentrations adsorbed to the particles. However, the slightly lower La_N/Yb_N ratios between 0.20 and

0.29 from the STF to the BDY compared to the WG (~ 0.3) suggest a removal at the surface, since LREE are preferentially scavenged to particles (e.g. Elderfield and Greaves, 1982). The low dissolved Nd concentrations in our surface water samples from the ACC can be explained by limited supply but additional scavenging cannot be excluded.

The dissolved Hf concentrations are also very low (less than 0.08 pmol/kg) in all three samples north of the PF. A comparison of our data with unpublished particulate Hf concentrations from the same study as the one by Hegner at al. (2007) shows that the Nd/Hf ratios of the particles reveal a strong coherence with biogenic opal (Fig. 3.4). This suggests that Hf is more efficiently scavenged from surface waters than Nd when siliceous frustules of diatoms are present. The implication is thus that biological activity, in particular diatom productivity, acts as a more effective sink for Hf than for Nd in the Southern Ocean. South of the ACC the dissolved concentrations for both elements are elevated and rather homogenous, with the exception of station 142, where the Hf concentration amounts to only 0.11 pmol/kg, i.e., only half of the average Hf concentration observed in other samples of this area. Hegner et al. (2007) also observed higher particulate Nd concentrations in the WG (more than 2 pmol/L) together with unradiogenic detrital Nd isotope compositions and high Al concentrations of up to 7.2 nmol/kg, supporting the idea of icebergs as potential vehicles of terrigenous material. However, the elevated concentrations of Nd (~ 18 pmol/kg) and Hf (~ 0.21 pmol/kg) observed in our study within the WG compared to north of the PF are most likely caused by accumulation of deep sourced Hf and Nd rather than derived from icebergs, as discussed below. The highest dissolved Hf and Nd concentrations south of the STF of 0.38 pmol/kg and 22.1 pmol/kg, respectively, were measured near the volcanic King George Island (KGI). This is in contrast to the low Hf concentration at S1, suggesting that volcanic rocks supply relatively more Hf into the ocean than continental deposits. The high dissolved concentrations of Hf and Nd match with the highest concentrations in their particulate fraction (2.88 pmol/L and 24.44 pmol/L, respectively) from unpublished data of Hegner et al. (2007), also implying a strong input from KGI.

3.4.2 Hf and Nd isotope signatures of the dissolved fraction

The Hf isotope composition of the surface waters is rather uniform (ε_{Hf} ranging between 2.8 and 5.0) with a radiogenic peak at KGI ($\varepsilon_{Hf} = 6.1$). However, there is a significant drop towards less radiogenic Hf values from station 153 ($\varepsilon_{Hf} = 4.9$) to the southernmost stations 156 and GvN ($\varepsilon_{Hf} = 3.0$ and $\varepsilon_{Hf} = 3.4$, respectively; Fig. 3.3A), which is, however, not accompanied by significant changes in Hf concentrations. The proximity of these stations to the Antarctic shelf suggests an unradiogenic Hf input from Dronning Maud Land (DML). In contrast, the Nd isotope data obtained from the same samples do not show such an excursion towards less radiogenic values, although the dissolved Nd isotope compositions are generally less radiogenic within the WG than within the ACC. This implies a more congruent release of Hf from weathering resistant accessory minerals, such as zircons due to glacial grinding of the exposed rocks on land. Evidence for such terrigenous inputs has previously been found in ferromanganese crusts, which recorded somewhat less radiogenic Hf isotope compositions than average data from the seawater array at regions where enhanced physical weathering prevails (Piotrowski et al., 2000; van de Flierdt et al., 2002; van de Flierdt et al., 2006). These authors concluded that for example the onset of Northern Hemisphere Glaciation was accompanied by enhanced physical weathering, leading to a more congruent release of Hf isotopes from the old continental crust in northern Canada and Greenland. Our data for the first time show that this is also reflected by modern seawater, supporting that Hf isotopes are a sensitive tracer for physical weathering inputs

However, there is also indication for an unradiogenic release of Nd from the shelf, as derived from the southernmost sample of the entire sample set closest to the Antarctic coast (station 154). This sample was taken close to the seafloor at ~ 135 m water depth and yielded an isotope composition of $\varepsilon_{Nd} = -9.9$, the least radiogenic value obtained south of the STF. The rather unradiogenic composition of the shelf sediments ($\varepsilon_{Nd} = -15$, van de Flierdt et al. (2007)) strongly support local boundary exchange at this station.

The most radiogenic values for both Hf ($\varepsilon_{Hf} = 6.1$) and Nd ($\varepsilon_{Nd} = -4.0$) are measured at KGI. This island is composed mainly of mafic volcanic rocks and can consequently supply highly radiogenic Hf and Nd isotope compositions to seawater. Previous studies on James Ross Island, which has the same geological origin as KGI (e.g. Machado et al., 2005) obtained highly radiogenic Hf and Nd compositions of the

rocks of ε_{Hf} ~7 (Sims et al., 2008) and ε_{Nd} ~5 (Hole et al., 1994; Kosler et al., 2009). In agreement with the high dissolved (this study) and particulate concentrations of Hf and Nd (Hegner et al., 2007), this most likely reflects modification of surface water by enhanced terrigenous supply. A similar excursion had been observed earlier near the volcanic Canary Island, where a surface water compositions of up to $\varepsilon_{Hf} = 10.2$ were measured (Rickli et al., 2010). Together with the observations from this study it supports that volcanic rocks readily release Hf and thus the radiogenic offset of Hf in the seawater array (Fig. 3.1) is most likely not only a result of incongruent weathering from continental deposits but also derived from a more congruent weathering input from radiogenic mafic rocks. The apparent terrigneous input from KGI contradicts the La_N/Yb_N data, which apparently do not indicate terrigenous imprint in that they are not elevated compared to the average WG value of ~ 0.3. Although there is a general enrichment of LREEs relative to HREEs, the REE composition of basalts from the South Shetland Island including KGI (Machado et al., 2005), the PAAS-normalized La/Yb from KGI generally only show values around 0.4. This is similar to the observed La_N/Yb_N in the surface waters and thus does not exclude terrigenous supply from KGI. The peak radiogenic Nd isotope signature of $\varepsilon_{Nd} = -4.0$ rapidly decreases to less radiogenic values of $\varepsilon_{Nd} = -6.3$ (DRA052) and $\varepsilon_{Nd} = -7.2$ (station S8 and DRA062) towards the DP, implying only limited spatial extension of the Nd supplied from the South Shetland Islands. This is also supported by the unradiogenic Hf isotope composition at station S8 ($\varepsilon_{Hf} = 3.1$), which does not indicate a radiogenic imprint of volcanic origin any more. A pronounced release of radiogenic Nd is again observed in the northern part of the DP (Fig. 3.3). At station DRA001 the Nd isotope composition of $\varepsilon_{Nd} = -5.7$ implies radiogenic input from the southern tip of South America, possibly derived from the Pali Aike Volcanic Field, which consist of lavas with $\varepsilon_{Nd} \sim 5$ (D'Orazio et al., 2000). In contrast to the near coast locations, the Nd isotope composition of the open DP is indistinguishable from the ACC signatures on the Zero Meridian at $\varepsilon_{Nd} \sim -8$.

Compared to the total range of ~ 15 ε_{Nd} units, a general homogeneity is observed for the Nd isotope distribution south of the STF, where the data only ranging from $\varepsilon_{Nd} = -6.4$ to -10.0, whereas a significant radiogenic peak occurs at KGI ($\varepsilon_{Nd} = -4.0$; Fig. 3.3B). However, within the Weddell Gyre (WG), the samples have ε_{Nd} values of -8.6 ± 0.2 (1 S.D.) and therefore tend to be less radiogenic than the average composition

of the ACC (ε_{Nd} = -7.8 ± 0.5,1 S.D.). This suggests that surface waters in the WG may be influenced by weathering contributions from the Proterozoic rocks of the Dronning Maud Land (DML) or the Ellsworth Whitmore Mountains (EWM), as also indicated by less radiogenic Hf values of ε_{Hf} = ~ 3 close to the Antarctic continent, as discussed above. This is further supported by the isotope composition of particles in the WG yielding values as low as ε_{Nd} < -15, suggesting an enhanced input of terrigenous material from East Antarctica by ice rafted debris (Hegner et al., 2007). Alternatively, the WG average Nd isotope composition is identical to the deepwater isotope composition of ε_{Nd} = -8.6 ± 0.1 (1 S.D.) in this area (see Chapter 4). This could imply that the Nd isotope compositions of surface waters are the result of vigorous mixing within the WG rather than the limited terrigenous input in this area. The accumulation of Nd is supported by relatively high surface water concentrations of ~18 pmol/kg in the WG and at the same time very low particle export, as indicated by scavenging experiments with Th and protactinium (Pa; Rutgers van der Loeff and Berger, 1993).

The highly unradiogenic Nd isotope compositions accompanied by high La_N/Yb_N of 0.52 to 0.69 of the samples in the SAC of $\varepsilon_{Nd} \leq$ -11.0 (Fig. 3.3A) most likely reflect inputs from old continental crust exposed in South Africa. These samples were taken close to the Agulhas retroflection, an area of enhanced admixture of waters from the Indian Ocean (Boebel et al., 2003; Richardson et al., 2003; You et al., 2003; E. Fahrbach, personal comm.). However, it is also possible, that the unradiogenic isotope composition is derived via a poleward directed undercurrent from the Angola Basin. Unradiogenic surface waters as low as ε_{Nd} = -16 were observed by Rickli et al. (2010) in the Angola Basin as far south as 17° S. However, these authors observed a trend towards more radiogenic values (ε_{Nd} = -14) further south, along with a freshening of surface waters, implying influences of Southern Ocean waters via the northward Benguela Current. The Nd values from our study, are as low as ε_{Nd} = -18.9 southwest of Cape Town (Station S1) and ε_{Nd} = -15.9 at Station 97 (Fig. 3.3A), and thus do not support a northern source. Supporting evidence is derived from surface sediments deposited around the South African coast, which were most likely transported via the Agulhas Current (AC). These sediments are on average less radiogenic (ε_{Nd} ~ -14) than those from the Cape Basin (ε_{Nd} ~ -12; Franzese et al., 2006). Hegner et al. (2007) also observed such unradiogenic ε_{Nd} values in suspended particles and showed that both the detrital fraction and the Fe-Mn-coatings of these particles most probably originated

from the Archean crust of South Africa. This supports an unradiogenic composition of waters transported via the AC. We therefore infer that the isotopic signal is derived from an East African origin advected by the AC rather than from the Cape Basin. The gradient towards the most radiogenic value of $\varepsilon_{Nd} = -11.0$ north of the STF indicates advection of subantarctic waters transported north via the Benguela Current.

3.5 Summary and conclusions

In this study the first combined surface water Hf and Nd isotope compositions and concentrations of surface waters from the Atlantic sector of the Southern Ocean are presented. The sample set comprises a wide range of Hf and Nd concentrations from low values in the South Atlantic Current (0.04 pmol/kg and 6.7 pmol/kg) to maximum values near King George Island (0.38 pmol/kg and 22.6 pmol/kg).

(1) The highest Nd concentrations were found in surface waters southwest of Cape Town. In the same sample, the low Hf concentration indicates restricted release of Hf during weathering of the South African continental crust. High La_N/Yb_Nbetween 0.5 and 0.7 reflect enhanced terrigenous input from South Africa. This is accompanied by the least radiogenic Nd isotope composition with values $\varepsilon_{Nd} \leq -11.0$ documenting inputs from weathering of Archean cratonic rocks exposed in South Africa, which were advected via the Agulhas Current.

(2) The low concentrations north of the Subantarctic Front most likely result from a combination of limited supply and biological productivity. A comparison of the particulate Nd/Hf ratio with biogenic SiO_2 reveals a preferential scavenging of Hf onto siliceous frustules. The lower Hf and Nd concentrations north of the PF increase southward to more constant values within the WG and indicate accumulation due to low biogenic particle fluxes and thus weak scavenging of trace metals.

(3) We observe indications of input from volcanic rocks by marked increases of Hf and Nd concentrations in the vicinity of King George Island. There, a pronounced radiogenic isotope excursion for both elements is observed ($\varepsilon_{Hf} = -6.1$; $\varepsilon_{Nd} = -4.0$) clearly reflecting terrigenous input from the volcanic South Shetland Islands. A similar influence from mantle-derived rocks on the Nd isotope composition is observed at the southern tip of Chile. This observation suggests that Hf is readily released from volcanic rocks.

(4) The Hf and Nd isotope compositions of the surface samples are shifted towards more radiogenic Hf values for given Nd values when compared to the "terrestrial array" and plot on the "seawater array". The least radiogenic Hf isotope compositions observed close to the Antarctic continent suggest a more congruent release due to enhanced physical weathering by glaciers because a similar shift towards less radiogenic Nd values is not observed for these samples. The combined Hf-Nd isotope composition of these surface waters is therefore apparently influenced by glacial weathering conditions on the Antarctic continent.

(5) The majority of the studied areas comprising the ACC and the Weddell Gyre shows essentially homogenous isotope compositions for Hf and Nd of $\varepsilon_{Hf} = \sim 4$ and $\varepsilon_{Nd} = \sim -8.5$, similar to previously studied deep water compositions and documents strong vertical mixing of Hf and Nd south of the Polar Front.

3. Sources and input mechanisms of hafnium and neodymium in surface waters of the Atlantic sector of the Southern Ocean.

Chapter 4

The hafnium and neodymium isotope composition of seawater in the Atlantic sector of the Southern Ocean*

* submitted to *Earth and Planetary Science Letters* as: Stichel T., Frank M., Rickli J., Haley B. A., The Hafnium and Neodymium Isotope Composition of Seawater in the Atlantic Sector of the Southern Ocean.

Abstract

We present the first combined dissolved hafnium (Hf) and neodymium (Nd) concentrations and isotope compositions of deepwater masses from the Atlantic sector of the Southern Ocean. Eight full depth profiles were analyzed for Hf and Nd and for four additional profiles only Nd was determined. Elemental concentration profiles show the typical behavior of particle reactive metals. In the upper few hundred meters Hf concentrations are depleted ranging between 0.2 pmol/kg and 0.4 pmol/kg in the upper few hundred meters and increasing to relatively constant values of around 0.6 pmol/kg in the deeper water column. North of the Polar Front (PF), the Nd concentrations generally increase linearly from about 10 pmol/kg at depths of ~ 200 m to up to 31 pmol/kg close to the bottom indicating uptake and release from biogenic opal. Within the Weddell Gyre (WG), however, Nd concentrations are essentially constant at 25 pmol/kg at depths greater than ~ 1000 m.

Hafnium essentially shows homogenous isotope compositions with values averaging at εHf = 4.6, whereas Nd isotopes mark distinct differences between water masses, such as modified North Atlantic Deep Water (NADW, ε_{Nd} = -11 to ε_{Nd} =-10) and Antarctic Bottom Water (AABW, ε_{Nd} = -8.6 to ε_{Nd} =-9.6), but also waters locally advected via the Agulhas Current can be identified by distinctly unradiogenic Nd isotope compositions. Mixing calculations suggest that a small fraction of Nd is removed by particle scavenging during mixing of water masses north of the PF. Nevertheless, the Nd isotope composition has apparently not been significantly affected by uptake and release of Nd from particles, as indicated by mixing calculations based on salinity and Nd isotope composition. Calculating the mixture of an approximated North Pacific and a North Atlantic end-member shows that Nd isotope and concentration patterns in the Lower Circumpolar Deep Water (LCDW) can be fully explained by ~ 30:70 contributions of these end-members.

4.1 Introduction

4.1.1 Radiogenic isotopes in seawater

Radiogenic isotopes have been widely used to investigate present and past ocean circulation patterns, hydrothermal inputs, or continental weathering regimes (e.g. Albarède and Goldstein, 1992; Albarède et al., 1997; Frank et al., 1999; Piotrowski et al., 2000; van de Flierdt et al., 2002; van de Flierdt et al., 2004). In particular, neodymium (Nd) and hafnium (Hf) have oceanic residence times comparable to the global ocean mixing time and can therefore be used as tracers for water masses and their mixing (Piepgras and Wasserburg, 1982; Lacan and Jeandel, 2005; Godfrey et al., 2008; Rickli et al., 2009; Zimmermann et al., 2009a). The global average residence time of Nd is relatively well constrained at 500 to 2000 years (Jeandel et al., 1995; Tachikawa et al., 1999; Tachikawa et al., 2003), although more recent estimates point to a somewhat lower number of < 500 years (Siddall et al., 2008; Arsouze et al., 2009). However, despite the fact there have been numerous studies on the Nd isotope distribution in seawater, large areas of the global ocean, including the Southern Ocean, still remain to a great part unconstrained, which results in persisting uncertainties concerning the residence time and the reflection of water mass distribution by Nd isotopes.

The global average residence time of Hf in seawater is much less certain with estimates ranging from 250 to 7500 years (Firdaus et al., 2008; Godfrey et al., 2008; Godfrey et al., 2009; Rickli et al., 2009; Zimmermann et al., 2009a). This uncertainty is mainly due to the lack of knowledge of the input sources and mechanisms of Hf in seawater, but also results from the sparse data available on dissolved Hf concentrations and isotope compositions of seawater. Nevertheless, a number of recent studies combining dissolved Hf and Nd isotope distributions from different areas of the global ocean have revealed similarities between the two radiogenic isotope systems with respect to distinct water mass signatures and their mixing (Zimmermann et al., 2009a,b; Rickli et al., 2009; Rickli et al., 2010). These studies suggest that the lower end of the above estimates of the seawater residence time of Hf is more plausible.

The Hf isotope budget of the global ocean has been indicated to be controlled by the intensity and prevailing regime of continental weathering (Piotrowski et al., 2000; van de Flierdt et al., 2002; van de Flierdt et al., 2007), which apparently results in a smaller Hf isotopic variability in seawater compared to that of Nd (Zimmermann et al.,

2009a,b; Rickli et al., 2009; Rickli et al., 2010). This is in contrast to crustal rocks, in which the range of Hf isotope variations is about a factor of 1.5 larger than for Nd isotopes (Patchett et al., 1984; Vervoort et al., 1999). The small variability of the Hf isotope composition in seawater could either indicate that weathering processes on land homogenized the Hf before entering seawater or that Hf has a significantly longer oceanic residence time than Nd. Alternatively, potential hydrothermal inputs of radiogenic Hf from mid-ocean ridges, which are Nd sinks (Halliday et al., 1992), may at least partly be responsible for the observed isotopic range of seawater Hf (Bau and Koschinsky, 2006). Whether such hydrothermal fluxes are significant for the oceanic Hf budget is not known, because there are currently no data on the Hf isotope composition or concentration of hydrothermal fluids. Additionally, it is not known to what extent such Hf influences ambient seawater. A prime factor for the observed small isotopic variability of Hf in seawater is most likely the isotopic fractionation of Hf during weathering processes. Whereas Nd isotopes are essentially released congruently (Andersson et al., 2001; Bayon et al., 2006), Hf isotopes are controlled by an incongruent release from Hf-bearing minerals during weathering (Patchett et al., 1984; Bayon et al., 2006). Zircons in particular have low Lu/Hf ratios, imparting highly unradiogenic Hf signatures (low ε_{Hf}) over time, which, however, are largely retained in these robust minerals during weathering (Patchett et al., 1984; Bayon et al., 2006; Bayon et al., 2009). In contrast, some easily weathered minerals with high Lu/Hf, such as sphene or apatite, release radiogenic Hf (high ε_{Hf}). A "zircon-free" crust is thus thought to be isotopically more uniform in Hf (van de Flierdt et al., 2007), which consequently leads to homogenized fluxes of Hf from the continents to the ocean and can explain the small Hf isotope variability in seawater (Rickli et al., 2010). The Nd and Hf isotope compositions are given in the ε - notation corresponding to the relative deviation of the $^{143}Nd/^{144}Nd$ and the $^{176}Hf/^{177}Hf$ of a sample from the CHondritic Uniform Reservoir (CHUR; $^{143}Nd/^{144}Nd = 0.512638$, Jacobsen and Wasserburg, 1980; $^{176}Hf/^{177}Hf = 0.282769$, Nowell et al., 1998) in parts per 10,000.

In this study we present full water depth for combined dissolved Hf and Nd isotopic compositions and concentrations in seawater samples from 14 sites in the Atlantic sector of the Southern Ocean. The main goal of this study is the first detailed investigation of the dissolved Nd and Hf isotope compositions of the water masses in this key area of the global thermohaline circulation. Furthermore we investigate whether

there are significant inputs of Hf and Nd from the Antarctic, as well as from the South American and African landmasses, which are characterized by a large range in types and ages of rocks and weathering regimes.

4.1.2 Hydrography

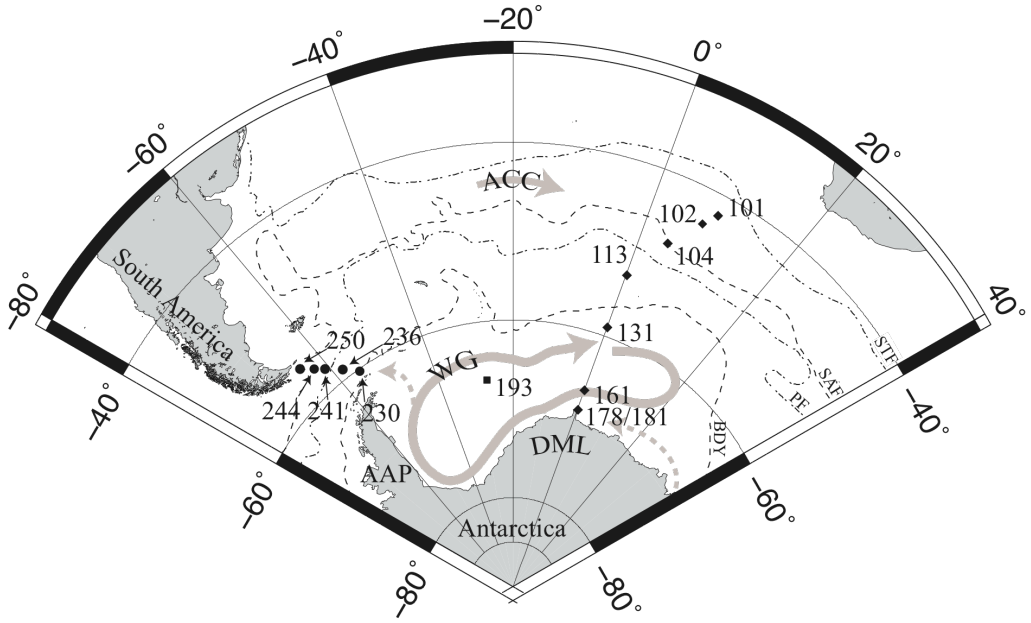

Figure 4.1: Sampling locations during expedition ANTXXIV/3 on the German research vessel *Polarstern*. The stations are grouped into three areas: the Zero Meridian comprising stations 101, 102, 104, 113, 131, 161, 178 and 181 (diamonds), the Weddell Sea (station 193, black square) and the Drake Passage (stations 230, 236, 241, 244 and 250, circles). Bold grey arrows indicate schematically the direction of the Antarctic Circumpolar Current (ACC) and the pathway of the Weddell Gyre (WG) and the pathway of AABW (grey dashed arrows). The black dashed lines represent the approximate positions of the Subtropical Front (STF), the Polar Front (PF) and the southern ACC boundary (BDY) as provided by Orsi et al. (1995). DML = Dronning Maud Land; AAP = Antarctic Peninsula.

The hydrography of the study area and its variability has been subject of many detailed studies (e.g Sievers and Nowlin, 1984; Orsi et al., 1995; Orsi et al., 1999; Stramma and England, 1999; Orsi et al., 2002). The circulation regime in the Atlantic sector of the Southern Ocean is dominated by the eastward flowing Antarctic Circumpolar Current (ACC), which is bounded to the north by the Subtropical Front (STF, Fig. 4.1). The major part of ACC itself essentially reaches from the surface to abyssal depths and is divided into Upper Circumpolar Deep Water (UCDW) and Lower Circumpolar Deep Water (LCDW) with neutral densities of $27.55\ kg/m^3 \leq \gamma^n \leq 28.27\ kg/m^3$ (Fig. 4.2). Another important current system in the

Atlantic sector of the Southern Ocean is the cyclonically circulating Weddell Gyre (WG), which is located between the southern ACC boundary (BDY) and the Antarctic continent in the Weddell Sea (WS; Fig. 4.1). The WG extends from the Antarctic Peninsula (AAP) to the Weddell-Enderby-Basin at about 20° E. The WG is fed by UCDW and LCDW from the ACC flowing in at intermediate depths, where it is then commonly called Warm Deep Water (WDW). Above WDW, Antarctic Surface Water (AASW) periodically gains density by brine injection during sea ice formation. Along the continental slopes of the WS these dense and cold surface waters sink down and mix with WDW. The part being dense enough to reach the bottom forms the Weddell Sea Bottom Water (WSBW), which is characterized by neutral densities of $\gamma^n \geq 28.40$ kg/m^3. These waters, however, are too dense to escape from the Weddell-Enderby Basin (Carmack and Foster, 1975). The less dense parts mix with WDW and feed into the Weddell Sea Deep Water (WSDW) directly, which is the densest water mass originating in the WS to permeate parts of the world ocean as AABW (28.40 kg/m^3 $\geq \gamma^n \geq$ 28.27 kg/m^3; e.g. Orsi et al., 1999; Heywood and King, 2002; Orsi et al., 2002; Klatt et al., 2005 and references therein). About 60% of the AABW in the Southern Ocean forms in the western WS, whereas the remainder is produced in the Amery Ice shelf region, at the Adélie Coast and in the Ross Sea (Gordon, 1971; Orsi et al., 1999; Stramma and England, 1999). Orsi et al. (1999) revisited the definition of AABW to point out that this water mass is not circumpolar due to its high density and is thus restricted to certain areas in the Atlantic sector, such as the Argentine Basin. The bottom water of Southern origin that covers the remainder of the Atlantic sector of the Southern Ocean is less dense than LCDW and is often termed ACC bottom water (Orsi et al., 1999).

Another important water mass originating in the Southern Ocean is northward flowing Antarctic Intermediate Water (AAIW), marked by relatively high dissolved oxygen and low salinities with a neutral density range of 27.13 kg/m^3 $\leq \gamma^n \leq$ 27.55 kg/m^3 (Whitworth III and Nowlin, 1987). AAIW originates from cooled surface waters of the ACC and is subducted northward at the Polar Front (Fig. 4.1). In the eastern Atlantic sector of the Southern Ocean AAIW is influenced by waters from the Indian Ocean, which are advected via the Agulhas Current (Wüst, 1935; Suga and Talley, 1995; Stramma and England, 1999; Roman and Lutjeharms, 2010).

Contributions from the north profoundly influence the water masses of the Southern Ocean. Southward flowing North Atlantic Deep Water (NADW) is separated into several branches at the northeastern tip of Brazil. A large fraction of NADW continues to flow eastward (Rhein et al., 1995), whereas the major part continues to flow southward into the southwestern Argentine Basin as part of the Deep Western Boundary Current. From here it is carried eastwards within the ACC (Stramma and England, 1999). Along its pathway NADW mixes with less dense waters originating from the southeast Pacific and the Indian Ocean, but is clearly identified by its characteristic deep salinity maximum within LCDW in the entire Atlantic sector of the Southern Ocean (Reid and Lynn, 1971).

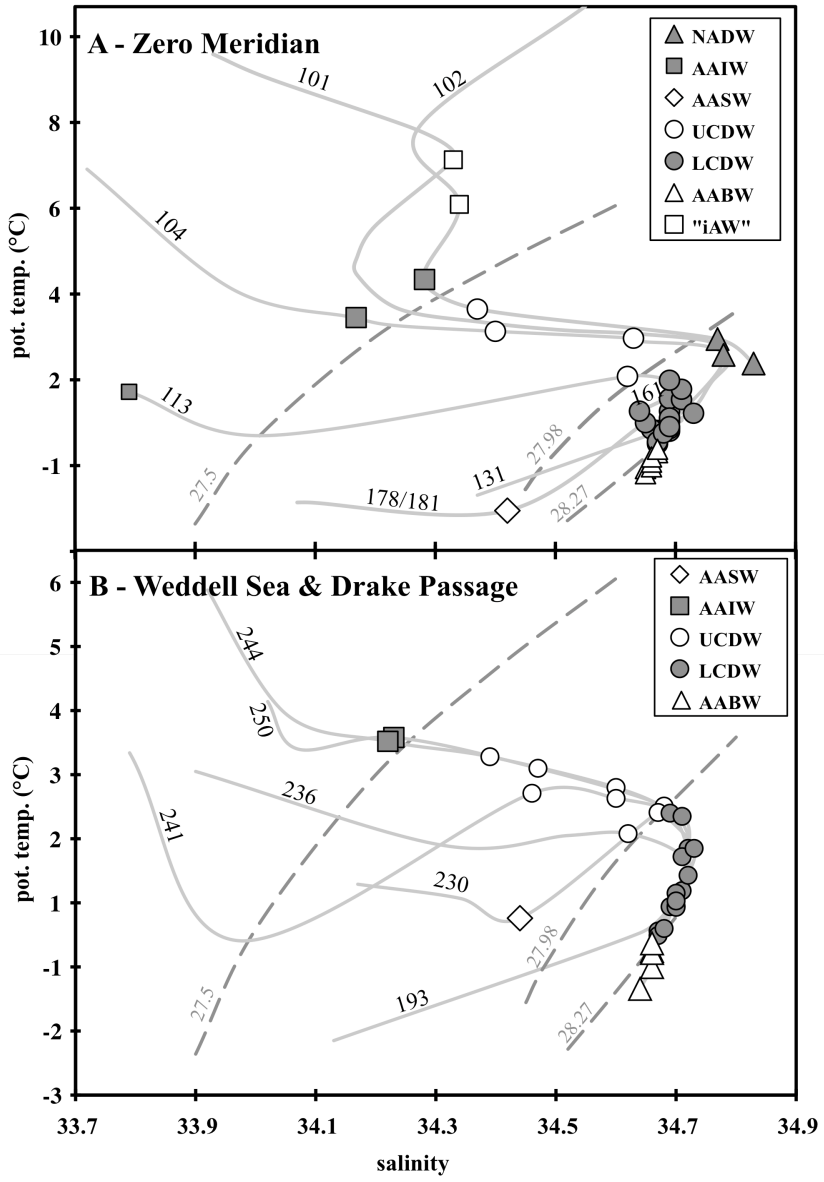

Figure 4.2: Measured potential temperature versus salinity at the sampling stations provided by Rohardt (2009); doi:10.1594/PANGAEA.727465. The symbols represent the sampled water masses: Antarctic Intermediate Water (AAIW, solid squares), "influenced by Agulhas Waters" ("iAW", open square), Upper Circumpolar Deep Water (UCDW, open circles) Lower CDW (LCDW, solid circles), Antarctic Bottom Water (AABW, open triangles) and North Atlantic Deep Water (NADW, solid triangle). The dashed lines indicate neutral densities (γ^n).

4.2 Methods

4.2.1 Sample collection and analytical procedures

Samples from 14 stations were taken from a depth range between 200 m and 4800 m with Niskin bottles mounted onto a CTD-rosette during the expedition ANTXXIV/3 from February to April 2008 onboard the German research vessel *FS*

Polarstern (Fig. 4.1). The expedition took place as part of the activities during the International Polar Year (IPY) 2008 and the chemical oceanographic investigations were part of the GEOTRACES program. The stations are geographically grouped as follows: *Zero Meridian* (stations 101, 102, 104, 113, 131, 161, 178 and 181), *Weddell Sea* (station 193) and *Drake Passage* (stations 230, 236, 241, 244 and 250).

The samples were collected in acid-cleaned 20 L LDPE-collapsible cubitainers and volumes corresponded to 20 L for Nd to 60 L for Hf. Each sample was filtered through a 0.45 µm Millipore® or Supor® filter within 12 hours after collection. The samples were then acidified to pH ~2 using double distilled concentrated nitric acid. For each sample a filtered aliquot of 2 L was separated for the measurement of Hf and Nd concentrations. The large volume (60 L) samples for Hf isotope analysis were further processed on board by adding 100 mg of iron (Fe) to each 20 L cubitainer in the form of previously purified dissolved Fe-chloride ($FeCl_3$, for purification method see below). After allowing 24 hours for equilibration, ammonia solution (25 %, Merck-suprapur®) was added to bring the pH up to 8 inducing the co-precipitation of the dissolved Hf and Nd with the iron hydroxides. After settling of the precipitate, most of the supernatant was discarded and the residue was transferred into 2 L PE-bottles for transport to the home laboratory.

The precipitates were then separated from the remaining supernatant by centrifugation and subsequently rinsed at least twice with MilliQ water to remove major ions. After the samples had been transferred into 60 ml teflon vials, they were treated with 4 ml of aqua regia for at least 24 hours at 110 °C to destroy organic components. Subsequently they were transferred into chloride by dissolution and evaporation in 4 ml of 6M HCl. Another 4 ml of 6M HCl were added to re-dissolve the samples. To separate the relatively large amount of Fe (300 mg) from the Hf a procedure similar to the one for cleaning the $FeCl_3$ solution was applied. This involves solvent extraction with 6M HCl and purified di-ethyl ether in equal amounts, whereby Fe forms an ethereal complex and trace metals stay in the acidic phase (Nachtrieb and Conway, 1948; Nachtrieb and Fryxell, 1948). The sample solutions were then stirred to dissolve the iron in the ether, which finally contained more than 90 % of the Fe and was removed by carefully siphoning the less dense Fe-ether complex from the acidic phase. This procedure was repeated to remove most of the residual Fe.

Many samples formed jelly-like precipitates in 6M HCl, containing ~ 90 % of the Hf from the samples. These precipitates were separated by centrifugation and subsequently dissolved in 2M HF. After evaporation the supernatant from the jelly precipitate was admixed again to each sample. Due to remaining small amounts of calcium and magnesium in the samples, occasionally fluoride precipitates formed, which were re-dissolved in a mixture of 6M HCl and 0.3M boric acid. Hafnium was then separated from the main matrix including Nd through cation exchange chromatography (1.4 ml resin bed, BIORAD® AG50W-X8, 200-400 µm mesh-size). The samples were loaded in 0.5 ml 1M HCl / 0.05M HF, and Hf was eluted adding another 2 ml of the same reagent. Neodymium was collected in 6 ml 8M HNO_3 after washing out the main part of the cation matrix and the remaining iron with 5 ml of 3M HCl. The Nd cuts were kept as a backup for the actual 20 L Nd isotope samples. The Hf-cuts were further purified following a slightly modified separation scheme of Münker et al. (2001). The total procedural blank for Hf was negligible at 15 pg to 20 pg compared to typical sample sizes of 4 ng to 5 ng.

The 20 liter Nd aliquots were shared samples and were initially processed at AWI since thorium (Th) and protactinium (Pa) had to be separated first, because measurement of the ^{231}Pa concentration required addition of a short-lived ^{233}Pa spike (Venchiarutti et al., 2008). The rare earth elements (REEs) including Nd were separated from Th and Pa using an anion exchange resin (BIORAD® AG1-X8, 100-200 µm mesh-size) following the procedure described in Venchiarutti et al. (2008). Iron was subsequently separated from the REEs by solvent extraction at IFM-GEOMAR in Kiel, as outlined for Hf above. Further purification of the REEs was achieved through cation exchange chromatography (0.8 ml resion bed, BIORAD® AG50-X12, 200-400 µm mesh-size), whereby major cations were removed first and the REEs were then eluted in 6M HNO_3. Neodymium was finally separated from Sm and the other REEs on 2 ml LN-Spec resin (EICHROM®; Pin and Zalduegui, 1997). The total procedure blank for Nd was lower than 30 pg, and thus negligible.

4.2.2 Hf and Nd concentration measurements

The Hf and Nd concentrations were obtained by isotope dilution (ID) following (Rickli et al., 2009). Previously weighed ^{178}Hf-single spike and ^{150}Nd/^{149}Sm double-spike solutions were added to an acidified 0.5 l aliquot of each sample. The samples

were left for 4 to 5 days for complete isotopic equilibration. $FeCl_3$ solution was added to the samples and Hf and Nd were co-precipitated with iron hydroxides by adding ammonia to raise the pH to 8. The purification of Hf and Nd was sufficient for subsequent mass spectrometric analysis using a single cation chromatographic separation step (1.4 ml resin bed, BIORAD® AG50W-X8, 200-400 µm mesh-size). The respective cuts containing Nd and Hf were evaporated to dryness and then oxidized by adding 200 µl of a 1:1 mixture of 0.5M HNO_3 and H_2O_2 (30 wt.%) to reduce disturbing matrix effects of organic components during measurement on the MC-ICPMS. Replicates for each element were processed and yielded an external reproducibility of better than 1% for Nd and between 3 and 10 % for Hf depending on concentration. The procedural blanks were quantified by processing 0.5 liter of MQ-water in the same way as the samples and corresponded to less than 1% in the case of Nd, for which no blank corrections were applied. The Hf content of the samples was closer to the blank level. The blank corresponded to 5 ±0.7 pg (n = 11), which was then subtracted from the samples to achieve a correct seawater concentration.

4.2.3 Hf and Nd isotope measurements

The Hf isotope compositions were measured on a *Nu plasma HR MC-ICPMS* at IFM-GEOMAR in manual time resolved mode due to the low Hf concentrations of the samples. The samples were dissolved in 250 to 500 µl 0.5M HNO_3 / 0.1M HF to obtain Hf concentrations of approximately 20 ppb corresponding at total beam of at least 4 V. The measured Hf isotope compositions were corrected for instrumental mass bias to $^{179}Hf/^{177}Hf = 0.7325$ applying an exponential mass fractionation law. The JMC 475 standard was repeatedly measured during each run (n ≥ samples per run) and all $^{176}Hf/^{177}Hf$ ratios presented here were normalized to the accepted literature value of 0.28216 (Nowell et al., 1998). The external reproducibility ranged from ±0.6 ε_{Hf} to ±2.6 ε_{Hf} (2 S.D.) depending on sample size and was estimated by repeated measurements of both the JMC 475 standard and a certiPUR® ICPMS Hf-standard (with n ≥ number of samples per run).

Most of the samples showed little remaining ytterbium (Yb; < 0.3 % of the ^{176}Hf beam in the purified Hf) and corresponding interferences on ^{176}Hf were readily correctable following Chu et al. (2002). For some samples the Yb corrections were larger and corresponded to up to 2.2 % of the ^{176}Hf beam. In order to avoid losing Hf

during repeated chromatographic separation, those data were corrected applying an offset correction obtained from a series Yb-doped JMC475 standards similar to Kemp et al. (2009). The systematic change in the Hf isotope composition of these standards depending on the amount of added Yb was linear ($R^2 = 0.971$) and the method was therefore considered reliable. The samples, which were corrected by this approach, are marked with a superscript "c" in Tab. 1.

The Nd isotope composition was either measured on a *Thermo Scientific TRITON 1 TIMS* or on the *nu plasma* at IFM-GEOMAR depending on the amount of Nd available for each sample. The smallest samples (< 20 ng) were measured in time-resolved mode on the *MC-ICPMS*. The measured isotopic composition was corrected for instrumental mass bias using $^{146}Nd/^{144}Nd = 0.7219$ applying an exponential mass fractionation law. The $^{143}Nd/^{144}Nd$ ratios were normalized to the accepted value for the JNdi-1 standard of 0.512115 (Tanaka et al., 2000). The external reproducibility on both instruments was between at ±0.3 and ±0.4 ε_{Nd} units (2 S.D.) estimated by repeatedly measuring JNdi-1 and an internal laboratory standard, with n = 4-6 on TIMS and n ≥ number of samples on the *nu plasma MC-ICPMS*. Replicates measured on both mass spectrometers resulted in identical Nd isotope compositions within analytical error.

4.3. Results

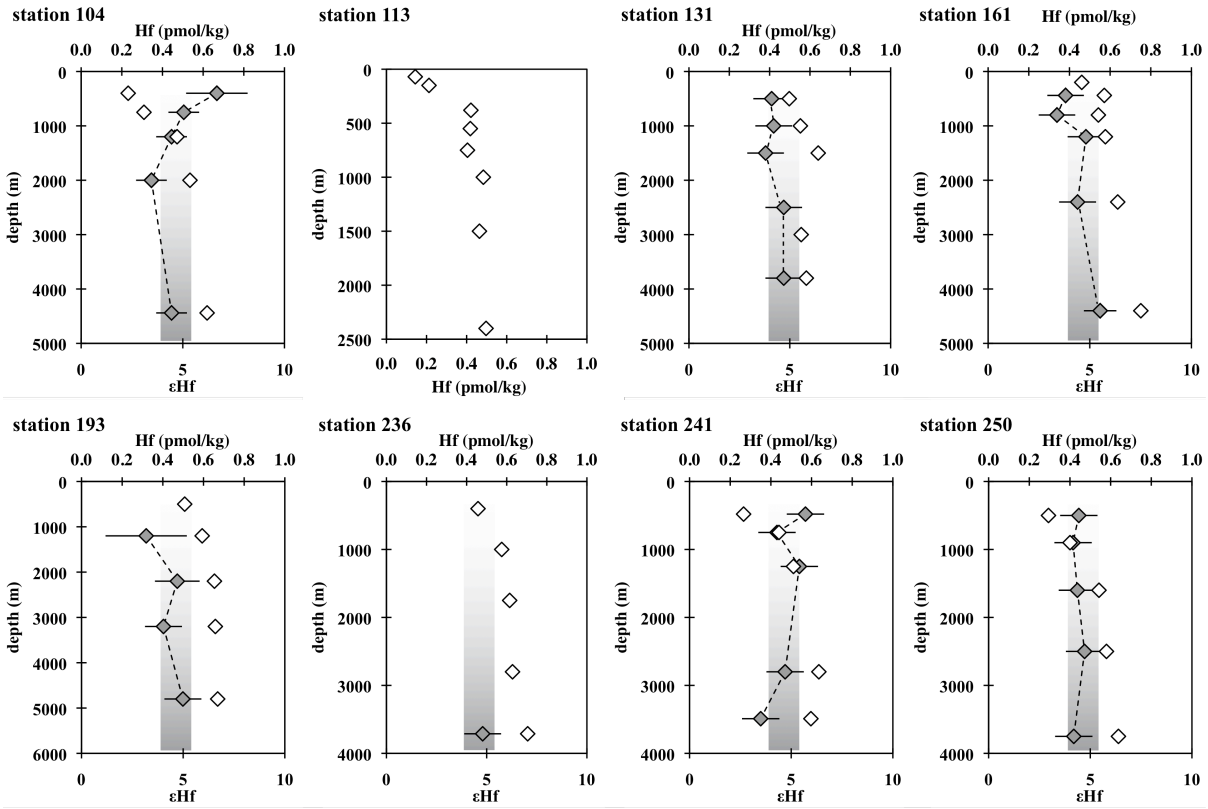

Figure 4.3: The Hf concentration (open diamonds) and isotopic composition (solid diamonds) as a function of depth at the sampled stations. Error bars for the isotopic composition represent 2 S.D. (external). Analytical errors for the concentrations are smaller than symbol size. Stations 101, 102 and 181 are omitted in this figure, because only one Hf isotope value of each station was obtained (see tab. 1). The grey bar marks the average Hf isotope composition of the entire sample set.

4.3.1 Hf and Nd concentration

Both elements show patterns typical for particle reactive metals in that lowest concentrations are observed in near surface waters (down to ~ 500 m depth, Figs. 4.3 and 4.4). The lowest concentrations in this shallow depth interval occur at stations near and north of the PF (stations 101, 104, 113, 241, 244 and 250) with 0.23 pmol/kg to 0.29 pmol/kg for Hf and 8.5 pmol/kg to 16.4 pmol/kg for Nd. These stations also exhibit the strongest increase in concentration with depth for both elements. However, the slope of the increase differs between Hf and Nd. The Hf concentrations only increase significantly within the upper 500 m to 1000 m to reach more or less constant values below. In contrast, Nd concentrations increase almost perfectly linearly with water depth ($R^2 > 0.93$). The stations in the WG (stations 131, 161, 178 and 193) show only minor increases with depth for both elements.

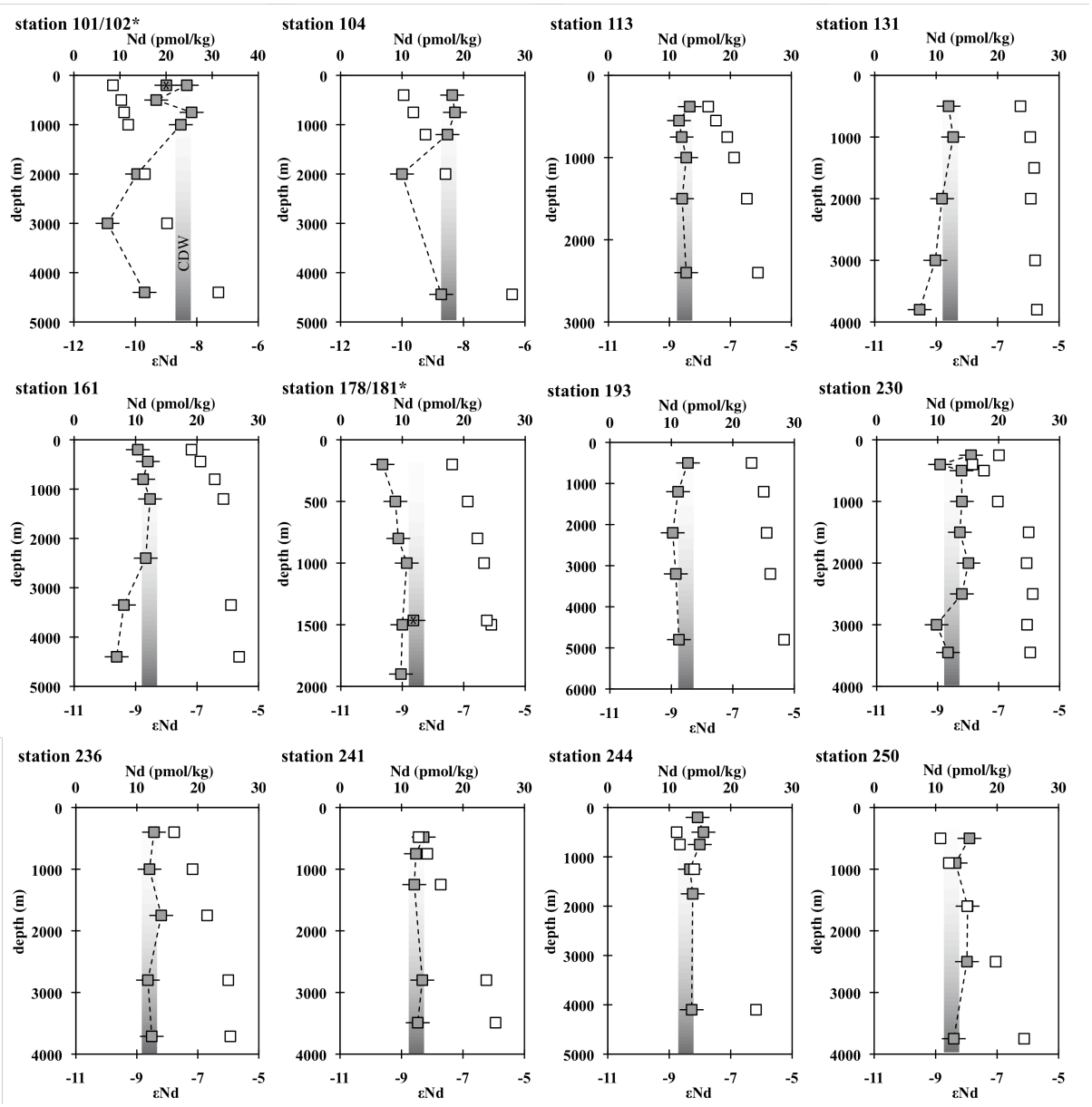

Figure 4.4: The Nd concentration (open squares) and isotope composition (solid squares) as a function of depth at the sampled stations. Error bars for the isotopic composition represent 2 S.D. (external). Analytical errors for the concentrations are smaller than symbol size. Single samples from stations 102 and 181 are combined at stations 101 and 178, respectively and are indicated as crosses. The gray bar marks the mean Nd isotope value of CDW for the entire samples set.

The highest concentrations are generally measured in deepest waters with Hf and Nd concentrations up to 0.75 pmol/kg (station 161) and 31.35 pmol/kg (station 104), respectively. The Hf concentration patterns for stations 131 and 241 are different, in that they show mid depth maxima at 1500 m (0.64 pmol/kg) and 2800 m (0.64 pmol/kg), respectively and slightly lower concentrations below (Fig. 4.3). The concentrations of both elements correlate well with dissolved silicon (Si) yielding an R^2 of 0.73 for Hf and 0.87 for Nd (Middag et al., 2010; Fig. 4.5). A potential increase in Hf

concentration at station 113, where hydrothermal activity left a strong imprint on the Fe and manganese (Mn) concentrations at depths between 1500 and 2000 m (Klunder et al., 2010; Middag, 2010; Middag et al., 2010), was not observed.

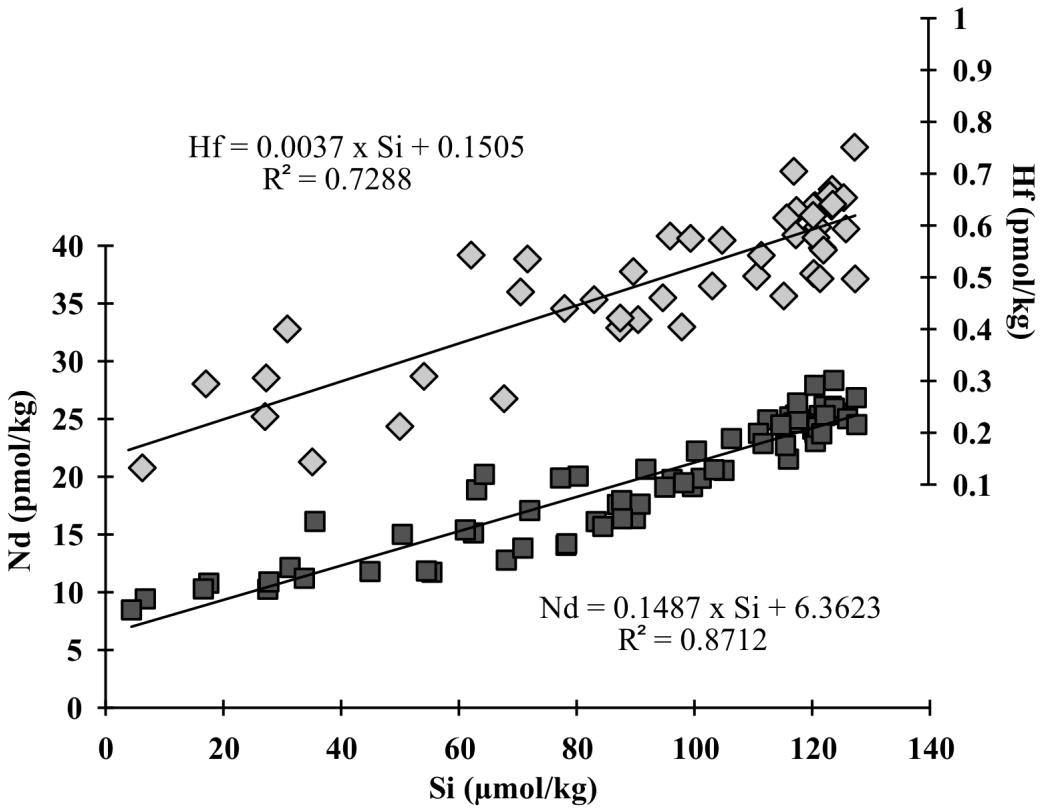

Figure 4.5: Concentrations of Hf (grey diamonds) and Nd (black squares) versus dissolved silica (Fahrbach and de Baar, 2010 and Middag et al. 2010). Neodymium yields a better correlation with dissolved Si than Hf, indicating a higher release from the frustules of diatoms in the Southern Ocean.

4.3.2 Hf isotope distribution

The Hf isotope compositions in the entire sample set show remarkably little deviation from an average $\varepsilon_{Hf} = 4.6$ (Fig. 4.3). The three most distinct samples yielded Hf isotope compositions of $\varepsilon_{Hf} = 3.2$, 6.7 and 7.0. These samples, however, have a poor external reproducibility of ±1.5 to ±2 ε_{Hf} (2 S.D.) due to very low amounts of available Hf. All other samples had much lower uncertainties (0.5 to 1 ε_{Hf} units) and did not reveal significant variations. In addition, the samples that needed larger Yb interference corrections (see section 2.3) are consistent with the rest of the dataset, indicating that these corrections are accurate.

4.3.3 Nd isotope distribution

The Nd isotope data in this study range from ε_{Nd} = -7.9 to ε_{Nd} = -10.9 (Fig. 4.4, Tab. A3). In the Drake Passage (DP) only show small variations between ε_{Nd} = -8.6 and -7.9 are observed. The only station in the Weddell Sea (WS, 193) yielded an average Nd isotope compositions of ε_{Nd} = -8.8 and no significant variations with depth. The eight stations from the Zero Meridian (ZM) and its vicinity show variations between ε_{Nd} = -10.9 and -8.4, whereby the least radiogenic values were measured at stations 101 (2000 m and 3000 m, ε_{Nd} = -9.9 and -10.9, respectively) and 104 (2000 m, ε_{Nd} = -10.0), which coincide with the salinity maximum of NADW (Fig. 4.2, Tab. A3). The Nd isotope composition of AABW averages at ε_{Nd} = -9.0 (±0.4, 1 S.D.), whereas the AABW values produced for the DP are slightly more radiogenic with ε_{Nd} = -8.5 to -9.0. In the WS and on the ZM, AABW ranges from ε_{Nd} = -8.7 to ε_{Nd} =-9.6, whereby the bottom samples of stations 131 and 161 (ε_{Nd} =-9.6 and ε_{Nd} = -9.5, respectively) are the least radiogenic ones. Samples from AAIW average at ε_{Nd} = -8.1 (±0.2). The values obtained at stations 101 (ε_{Nd} = -9.3) and 102 (ε_{Nd} = -9.0) were sampled within shallow local salinity maxima of the respective profiles, which suggests an influence from the Agulhas current, and is thus referred to here as "influenced by Agulhas Water" ("iAW"; Boebel et al., 2003; Roman and Lutjeharms, 2010; E. Fahrbach, pers. comm.). The two uppermost samples of stations 178 and 230 correspond to AASW, and yielded ε_{Nd} = -7.9 and -9.6, respectively. Most Upper and Lower CDW samples are isotopically indistinguishable from each other with average values of ε_{Nd} = -8.4 (±0.2) and ε_{Nd} = -8.6 (±0.2), respectively. An exception is observed at station 178 close to the Antarctic continent, where LCDW is on average less radiogenic (ε_{Nd} = -9.0 ±0.1) and at station 101 (4400 m, ε_{Nd} = -9.7).

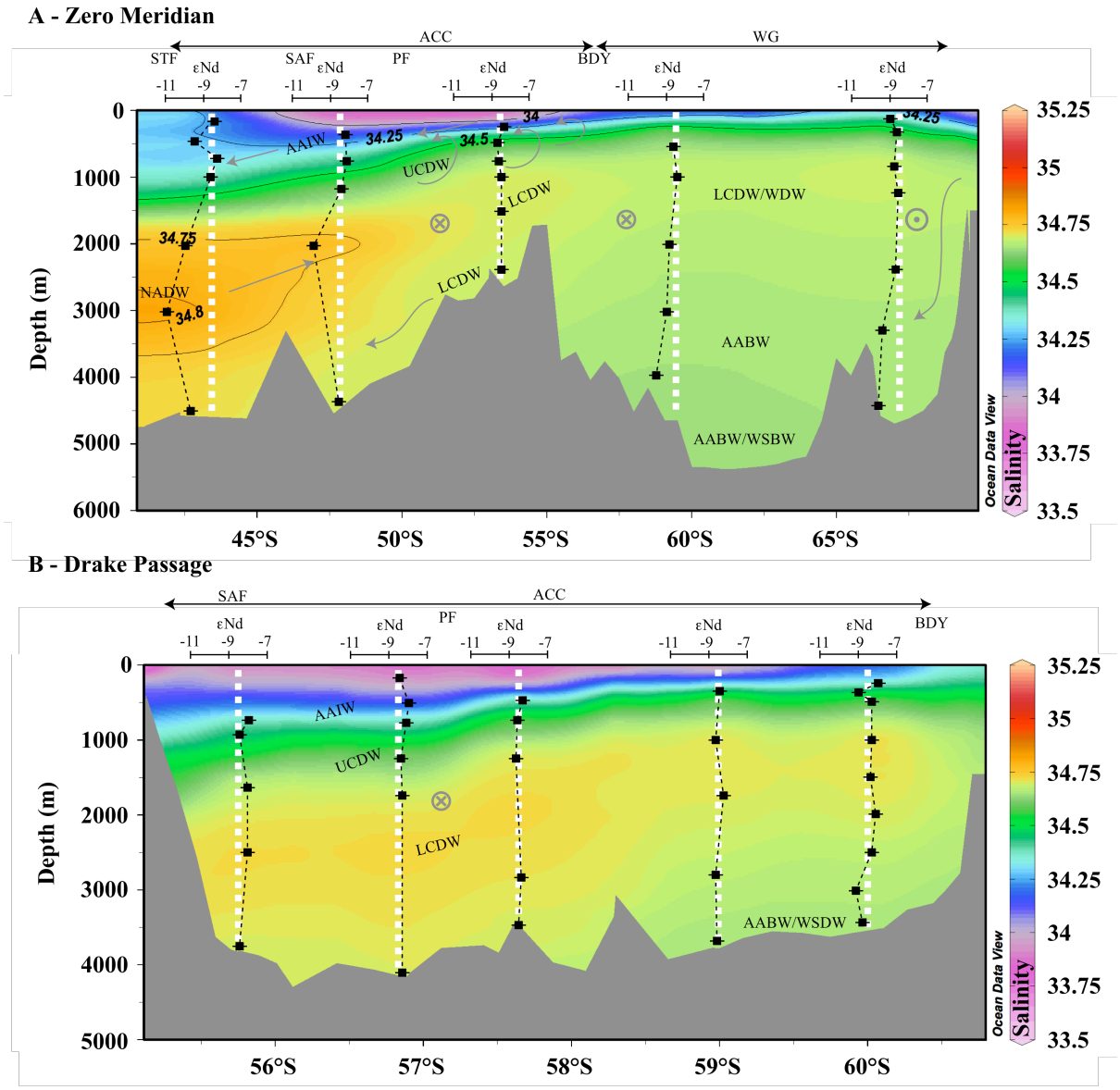

Figure 4.6: The Nd isotope distribution along the Zero Meridian (A) and across the Drake Passage (B). Crosses mark predominant eastward flow directions and the point symbol denotes westward flow. The color scales represent the salinity distribution of each section. Approximate positions of major water masses described in section 4.1.2 are indicated by their respective acronyms.

4.4 Discussion

4.4.1 Processes controlling Hf and Nd concentrations in the Southern Ocean

The distribution of the concentrations for both elements shows correlations with dissolved silicon (Si). In particular at the Polar Frontal Zone (between the PF and the SAF), where nutrients are upwelling and are consumed quickly, the subsurface concentrations of Hf and Nd are significantly lower than at all other stations. Dissolved Hf and Nd, similar to other trace metals, are most likely scavenged onto the relatively

large specific surface areas of diatoms, as already suggested by Rickli et al. (2009). The diatom frustules and the organic matter sinking down from the surface waters dissolve, which leads to a release of the previously scavenged trace metals. Modeling studies by Sarmiento et al. (2007) have shown that the Southern Ocean is the most important basin for opal dissolution. Thus, the close correlation of Hf and Nd concentrations with dissolved Si concentrations shown in fig. 4.5 likely reflects the release of Hf and Nd from remineralizing diatoms. The better correlation of Nd with dissolved Si ($R^2 = 0.87$) than that of Hf ($R^2 = 0.73$) suggests that Nd is removed more efficiently, but is also readily released again during diatom growth and dissolution. Samples taken near or at the PF (stations 104, 113, 241 and 250), where productivity and thus particle density is high (e.g. Rutgers van der Loeff and Berger, 1993), all show low Hf concentrations indicating efficient removal of Hf in the upper few hundred meters. The relatively high but constant values with greater depths however, imply a weaker remobilization of Hf from sinking particles and thus a more efficient removal from the water column. This contrasts with Nd, for which the increase in concentration is quasi linear. If diatom growth is a net sink for Hf, then the oceanic residence time of Hf should be shorter than for Nd, at least in areas where diatoms are the prevailing primary producers. A shorter oceanic residence time of Hf than of Nd has already been proposed by Rickli et al. (2009) and Zimmermann et al. (2009a). Based on Th and Pa distributions, Rutgers van der Loeff and Berger (1993) have shown that south of the ACC, i.e. in the WG, particle flux is largely reduced. This is in agreement with the findings in this study. All stations within the WG (131, 161, 178 and 193) but also in the southern DP (station 230) show rather constant and elevated concentrations for both elements between 0.4 pmol/kg to 0.75 pmol/kg for Hf and 19 pmol/kg to 28 pmol/kg for Nd. Significantly lower concentrations at these stations were only found in the upper 1000 m. This implies that remineralization for Nd and Hf is completed within the upper water column, in agreement with previous studies on remineralization in the Weddell Sea (Usbeck et al., 2002).

4.4.2 Hf isotope distribution in Southern Ocean water masses

The isotopic composition of Hf is relatively invariable throughout the entire sample set and most observed isotopic compositions are indistinguishable from the average value of $\varepsilon_{Hf} = 4.6$ (Tab. A3, Fig. 4.3). Distinction of water masses on the basis

of their Hf isotope compositions in the Southern Ocean is therefore not possible at the currently achievable external reproducibility of the data. Most likely, the vertical and lateral homogenization in the ACC removes all measureable isotopic differences in the water column. However, Hf isotope data obtained from ferromanganese crusts indicate that AABW incorporates isotopic fingerprints of Wilkes Land in East Antarctica (van de Flierdt et al., 2006), which implies an unradiogenic Hf input from the continent. In our study area, we do not observe such an imprint on Hf in AABW, and therefore conclude that AABW in the Atlantic sector does not receive significant Hf contributions from the Antarctic shelf. Either the Hf contributions from the Antarctic continent are too small to be distinguished in the water column or the Hf isotope compositions released from incongruent weathering are similar to the signatures of CDW. This question remains unresolved with the currently available data.

4.4.3 Nd isotope characteristics of Southern Ocean water masses

The overall Nd isotope composition of the water masses in the Atlantic sector of the Southern Ocean exhibits only small variations, probably due to the efficient horizontal and vertical homogenization within the ACC and the WG (Fig. 4.6). The average circulation time of a parcel of water in CDW around Antarctica is only about 50 to 70 years (Georgi, 1981), which is very short compared to the average oceanic residence time of Nd of at least several hundred years (Jeandel et al., 1995; Tachikawa et al., 1999; Tachikawa et al., 2003; Siddall et al., 2008; Arsouze et al., 2009). However, the Nd isotope distribution in the studied area allows distinguishing between northern (i.e. NADW) and southern (i.e. AABW) sourced water masses (Fig. 4.6A).

4.4.3.1 Nd isotope composition of intermediate waters

The AAIW (ε_{Nd} = -8.4 to ε_{Nd} =-7.9) has the most radiogenic Nd isotope composition found in the Atlantic sector of the Southern Ocean. More radiogenic values for AAIW of up to ε_{Nd} = -6.2 and ε_{Nd} = -6.8 (Jeandel, 1993), which may have indicated a higher Pacific contribution to AAIW through the DP, are not reproduced here. In the DP all five profiles from our study did not show any significant shifts towards such radiogenic values (Fig. 4.6B). This does not support Pacific waters being responsible for the highly radiogenic values of AAIW data observed by Jeandel (1993). However, the data for the deeper water masses presented here are in very good agreement with those of Jeandel (1993). This argues against analytical artifacts and leaves the reason for

the discrepancy in AAIW unexplained. The similarity of the Nd the composition of AAIW and CDW in our data set confirms strong vertical and horizontal homogenization in the Southern Ocean. Upwelling CDW comes close to the surface near the Antarctic continent and is then advected north where it eventually sinks at the PF to form AAIW. Along this pathway no significant change in the Nd isotope composition is observed in our data, arguing against any further addition of Nd with a different isotope composition to these waters before they are subducted as AAIW at the PF. At stations 101 (500 m) and 102 (200 m) slightly less radiogenic ε_{Nd} values of -9.3 and -9.0 were measured, which implies a contribution of waters other than the Southern Ocean in origin. These stations are located in an area where the Agulhas Current (AC) feeds South Atlantic waters (Boebel et al., 2003; Roman and Lutjeharms, 2010, E. Fahrbach pers. comm.), which is clearly documented by local salinity maxima at these depths. This suggests that a potential unradiogenic Nd isotope signature of the AC and can thus explain shifts to less radiogenic values in the area of the Agulhas retroflection. A rather unradiogenic composition of the AC is supported by surface sediments, being as low as $\varepsilon_{Nd} = -15.5$ to $\varepsilon_{Nd} = -11$ (Franzese et al., 2006) around the southeastern margin of South Africa.

4.4.3.2 Nd isotope composition of AABW

Despite the general isotopic homogeneity, the water column Nd isotope data clearly show that AABW from the WS and the ZM ($\varepsilon_{Nd} = -9.6$ to $\varepsilon_{Nd} = -8.7$) is systematically less radiogenic than CDW above ($\varepsilon_{Nd} = -8.3$ to $\varepsilon_{Nd} = -8.9$, Figs. 4.4 and 4.6). As mentioned in section 4.1.2, most of the AABW is formed in the western WS but is spatially restricted to the Weddell-Enderby Basin and the southern Drake Passage. AABW in the WS, including WSBW, shows ε_{Nd} values from -9.0 to -8.8. Similar values for AABW are found at stations 230 and 236 in the Drake Passage ($\varepsilon_{Nd} = -8.7$ to $\varepsilon_{Nd} = -9.0$), where AABW flows through a gap in the South Scotia Ridge and then continues westward into the Drake Passage (Wüst, 1935; Locarnini et al., 1993). The lower Nd isotopic values of AABW with neutral densities ($\gamma^n \sim 28.3$ kg/m^3) at stations 131 and 161 on the ZM ($\varepsilon_{Nd} = -9.5$ and $\varepsilon_{Nd} = -9.6$, respectively) most likely reflect inputs from unradiogenic continental sources in East Antarctica, as already proposed by van de Flierdt et al. (2006) on the basis of ferromanganese crust data. This is also supported by the pathway of dense waters that form through brine injection in the Amery Ice Shelf region and then flow westwards close to the Antarctic continent

before they mix with WSBW near the Zero Meridian in the Weddell-Enderby Basin to form AABW (Orsi et al., 1999; Heywood and King, 2002). Furthermore, at station 178, which was taken at the continental slope of Antarctica, the Nd isotope composition is relatively unradiogenic (ε_{Nd} = -9.6 to ε_{Nd} = -8.6, Tab. A3, Fig. 4.4). The least radiogenic value is obtained at 200 m depth, supporting an unradiogenic imprint on (sub)surface waters from Antarctica. Any direct mixing of AABW and NADW, which would also have a suitably low ε_{Nd} composition to cause the observed unradiogenic AABW signature, can be excluded due to the density contrast between NADW (γ^n = 27.7 kg/m^3 to γ^n = 28.27 kg/m^3) and locally formed AABW (γ^n > 28.3 kg/m^3). Given that the formation process of AABW involves admixture of saline shelf waters, a significant influence of Nd supplied from the Antarctic Continent is therefore consistent with the difference in the Nd isotope composition between AABW and CDW in the eastern Weddell Gyre. Apparently, release from suspended particles or a boundary exchange process (Lacan and Jeandel, 2005) provides a less radiogenic signature to seawater in this region. The Nd isotope composition of sedimentary deposits north of the Dronning Maud Land from the Zero Meridian to about 40° E ranges from ε_{Nd} = -10 to ε_{Nd} = -17 (van de Flierdt et al., 2007) and is thus the most likely source for an unradiogenic signature of AABW formed locally near East Antarctica. The slightly more radiogenic AABW values in the WS compared to the ZM signature indicate contributions from more radiogenic sources. Sediments from the western WS indeed show a more radiogenic ε_{Nd} signature of -9.6 (van de Flierdt et al., 2007) and can explain the observed small difference. The admixture of less radiogenic shelf waters rather than NADW can thus fully explain the range of Nd isotope signatures of AABW.

4.4.3.3 Modification of NADW in the ACC

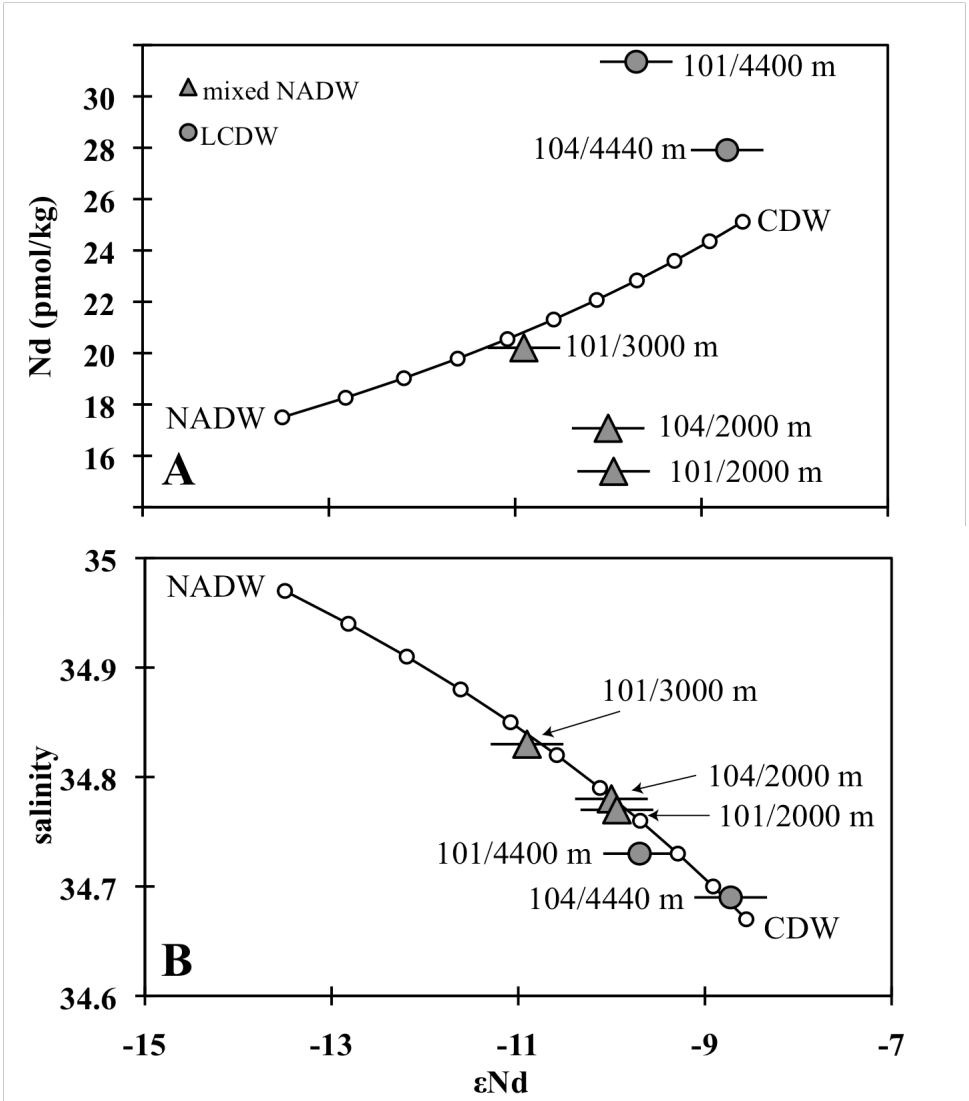

Figure 4.7: Two-component Nd isotope mixing between "conservative" CDW (this study, see text) and NADW (ε_{Nd} = -13.5±0.4; Nd = 17.5 pmol/kg; S = 34.97) from Piepgras and Wasserburg (1987) is shown on both plots. The mixing line is divided in 10 % fractions (open circles). Grey triangles and grey circles represent mixed NADW and LCDW from this study, respectively. The figure shows that mixed NADW from stations 101 (2000 m) and 104 (2000 m) is too low in Nd concentration to fit on the mixing line, whereas LCDW from stations 101 and 104 is too high (A). Conservative salinity (B), however, shows that mixed NADW from 2000 m is primarily a mixture of 60 % to 70 % CDW and 30 % to 40 % NADW.

As pointed out in section 4.4.3.2, NADW does not mix with AABW, but it does mix with CDW, given that NADW and CDW have a similar density by the time NADW arrives at 42°S (station 101). This is supported by a simple two component mixing calculation between undiluted NADW (ε_{Nd} = -13.5, 17.5 pmol/kg, Piepgras and

Wasserburg (1987)) and LCDW obtained in this study (ε_{Nd} = -8.6, 25.1 pmol/kg), which indicates that NADW (station 101, ε_{Nd} = -9.9 and station 104, ε_{Nd} = -10.0) is already highly diluted by Southern Ocean waters (Fig. 4.7A). However, the Nd concentrations of 15.4 pmol/kg (station 101) and 17.1 pmol/kg (station 104) found at 2000 m depth are too low to fit on the mixing line, from which a value of 19 pmol/kg to 20 pmol/kg would be expected for the corresponding isotope composition. This indicates that a fraction of the Nd is removed through scavenging during mixing with Southern Ocean waters. The NADW composition of station 101 at 3000 m depth on the other hand fits well on this mixing line, whereas the LCDW from 4400 m and from station 104 (4440 m) are too high in their concentrations. Apparently, the deep Nd concentrations do not behave conservatively and are influenced by biological uptake and remineralization, as already proposed by Rickli et al. (2009). We therefore applied a mixing calculation using ε_{Nd} and salinity, which is shown in fig. 4.6B. The chosen end-members for NADW are from Piepgras and Wasserburg (1987; salinity = 34.97) and for LCDW are from this study (salinity = 34.67). The resulting mixing array shows that both shallow (2000 m) NADW components from stations 101 and 104 are diluted by 60 % to 70 % with CDW. Both LCDW samples from stations 101 and 104 are even more CDW-dominated with amounts of 80 % and $\geq$ 90 %, respectively. Furthermore, the good match of NADW and LCDW from stations 101 and 104 with the mixing line implies that the resulting isotope compositions are primarily governed by mixing of water masses.

4.4.3.4 The Nd isotope composition of CDW only a result of mixing?

Piepgras and Wasserburg (1982) have shown that the overall Nd budget in average CDW is dominated by NADW and receives only smaller contributions from Pacific waters ($\varepsilon_{Nd} \approx$ -3.8, 52 pmol/kg; Piepgras and Jacobsen (1988)), which is general agreement in with the data from this study (Fig. 4.8). Our data suggest Atlantic contributions of 70 % to 75 % in the entire Atlantic sector of the Southern Ocean, whereas Piepgras and Wasserburg (1982) estimated a similar 50 % to 70 % contribution of Atlantic waters in the Drake Passage. As shown before, potential scavenging north of the PF removes Nd from the water column during mixing. As a consequence, the Nd concentrations in the Southern Ocean should be somewhat too low to represent

conservative mixing. This is indeed the case when the average composition of CDW is employed for the mixing calculation (Fig. 4.8, grey diamond).

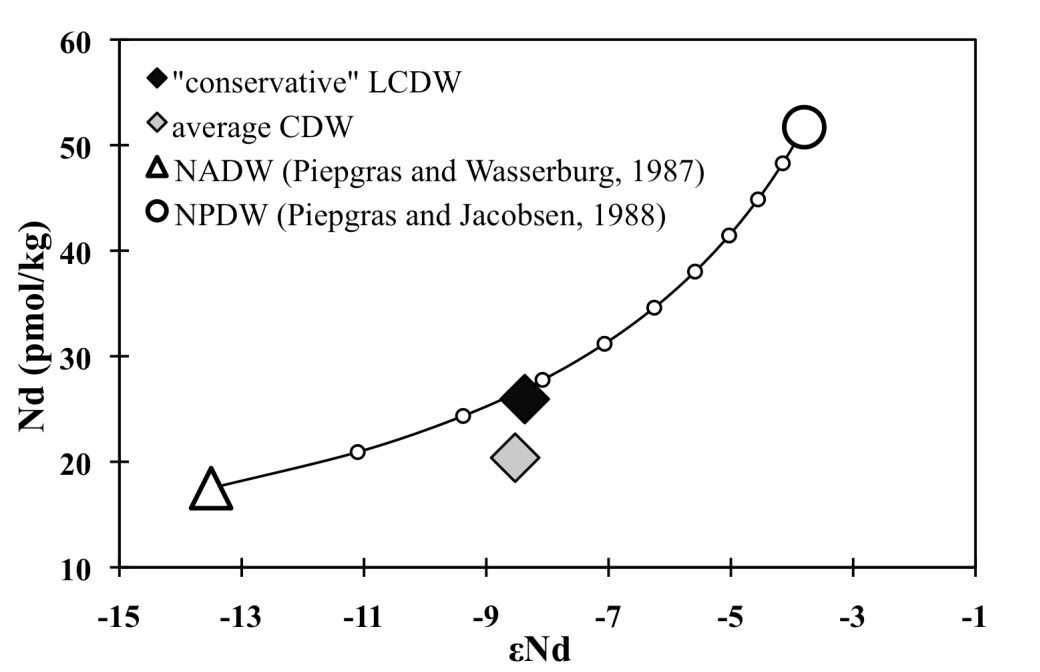

Figure 4.8: Two-component Nd isotope mixing between NPDW (ε_{Nd} = -3.8±0.3; 55.7 pmol/kg; open circle) and NADW (ε_{Nd} = -13.5±0.4; 17.5 pmol/kg; open triangle) from Piepgras and Jacobsen (1988) and Piepgras and Wasserburg (1987), respectively. The mixing line is divided into 10 % fractions (open circles). The "conservative" part of LCDW (black diamond) plots right on the mixing line, whereas mean CDW (grey diamond) plots somewhat below the mixing line.

North of the PF the Nd concentration of CDW is clearly influenced by particle uptake and release in the entire water column, as mentioned above. At the stations within the WG and in the southern DP, however, these vertical processes obviously cease at intermediate (~ 1000 m in the WG) or greater (~ 3000 m at station 236) depth, as indicated by largely constant Nd concentrations. This suggests that particle exchange processes do not alter these deep concentrations any more. The average Nd concentration of 25.1 (±1) pmol/kg at these stations is therefore used as the "conservative" Nd concentration of LCDW. Applying this value for the mixing calculations shows that Nd in LCDW can be explained by a mixing of Pacific and Atlantic waters without any significant contributions from the Antarctic continent (black diamond, Fig. 4.8). These considerations also show that Nd is not only transported in dissolved form but to some extent also adsorbed to particles as a result of scavenging as discussed above (see also Piepgras and Wasserburg, 1988). Obviously, the particulate load largely re-dissolves within LCDW south of the ACC, where it

generates the observed invariant concentrations and isotope compositions of the LCDW.

4.4.4 The Hf-Nd isotopes and the seawater array

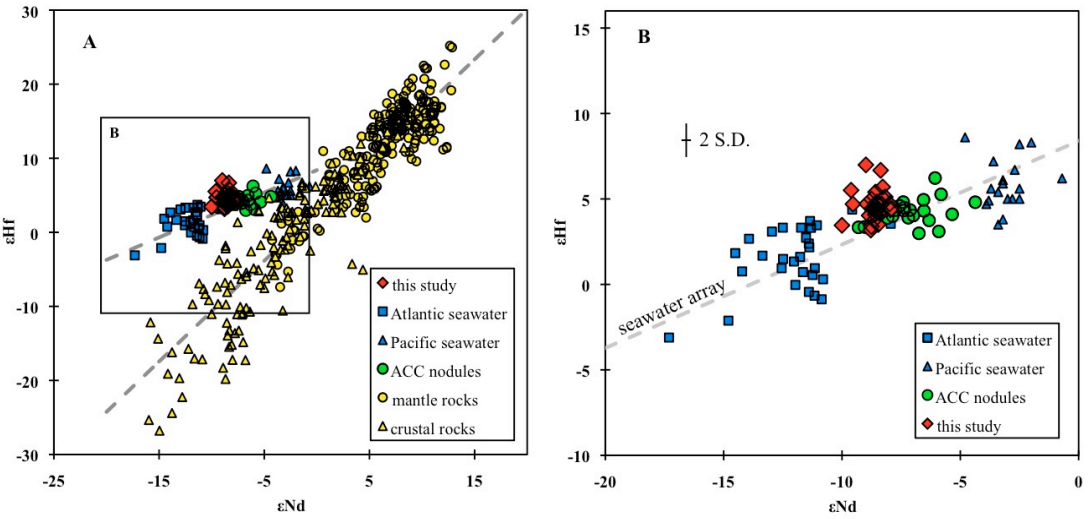

Figure 4.9: Hafnium and Nd isotope systematics of terrestrial rocks (Vervoort et al., 1999; van de Flierdt et al., 2007), ferromanganese nodules from the Southern Ocean (van de Flierdt et al., 2006) and seawater (Rickli et al., 2009; Zimmermann et al., 2009a, this study) (A). Blow up (B) shows that the data from this study (red diamonds) plot between Atlantic (blue squares, Rickli et al. (2009)) and Pacific compositions (blue triangles, Zimmermann et al. (2009a). The Hf isotope data agree well with the values obtained from ferromanganese nodules (green circles, van de Flierdt et al. (2006)). The Nd data show less radiogenic values than obtained from these nodules, indicating a stronger Pacific influence during the last Glacial period.

The combined Hf and Nd isotope composition show that the Southern Ocean waters are shifted towards more radiogenic Hf values compared to the "terrestrial array" (Figs. 4.9A and B). Similar to previous studies (Godfrey et al., 2009; Rickli et al., 2009; Rickli et al., 2010; Zimmermann et al., 2009a,b), our data plots on the "seawater array" derived from ferro-manganese crusts and nodules (e.g. Albarède et al., 1998; David et al., 2001; van de Flierdt et al., 2006). The samples form a narrow cluster located between Atlantic (Rickli et al., 2009) and Pacific seawater (Zimmermann et al., 2009a). The deepwater data obtained in this study agree very well with the distribution of the ferromanganese crust data from the same area (van de Flierdt et al., 2006) but are on average 1 ε-unit less radiogenic in the Nd isotope composition (Fig. 4.9B). The most likely explanation is that ferromanganese crusts integrate the overlying seawater composition over several tens of thousands of years, suggesting that the observed Nd isotope compositions are a mixture of at least the past glacial and the present

interglacial period. A more radiogenic signal of CDW and AABW would therefore imply a stronger input of Pacific sources or a weaker Atlantic input to the Southern Ocean during the last glacial period, which is consistent with high-resolution Nd isotope records from the Southern Ocean (e.g. Piotrowski et al., 2008). Such a difference is not observed for Hf isotopes, which supports a shorter seawater residence time and suggests that the glacial/interglacial variability of dissolved Hf isotopes in seawater of the Southern Ocean was small.

All recent studies on the dissolved Hf and Nd isotope distribution in seawater, including ours (Rickli et al., 2009; Rickli et al., 2010; Zimmermann et al., 2009a,b), indicated that Hf isotopes are of limited use as tracer for (past) water mass and ocean circulation. Besides the fact that it is more complicated to measure and that the continental range of Hf isotope variations is reduced through weathering processes prior to entering the ocean, the global residence time of Hf appears to be smaller than that of Nd, allowing a reflection of circulation and weathering inputs in the dissolved Hf isotope composition of seawater only on a basin scale.

Both elements exhibit only either small (in the case of Nd) or insignificant (in the case of Hf) variations in their isotope composition in the studied area. Continental inputs from Antarctica only significantly influence the Nd isotope composition of AABW, whereas this is not the case for Hf. This indicates that both isotope compositions are mainly governed by admixed contributions from the major ocean basins. For this reason, our results cannot contribute to the debate if the Hf budget in the world ocean is only governed by weathering inputs. The only supporting evidence comes from the lack of increased Hf concentrations at depths below 1500 m at station 113, where hydrothermal activity caused enhanced inputs of Mn and Fe (Klunder et al., 2010; Middag, 2010; Middag et al., 2010), arguing against significant hydrothermal contributions of Hf into the ocean.

4.5 Conclusions

Samples from 14 full water depth stations in the Atlantic sector of the Southern Ocean were analyzed for their Hf and Nd isotope composition and concentration. The concentration patterns for both elements are typical for particle reactive metals whereby the lowest values are observed in near surface waters with increasing values towards

greater depths. However, there are distinct differences between the distributions of the two elements with respect to the gradients of change:

(1) The concentration patterns for Hf show an increase in the upper water column and are nearly constant at greater depths. This suggests that scavenging of Hf onto particles and subsequent release are finalized at shallow depths.

(2) The Nd concentrations at stations north of the Polar Front increase linearly throughout the entire water column implying scavenging at the surface and continuous release with depth, which points to different affinities of Hf and Nd to particles.

(3) The concentration data suggest a shorter oceanic residence time of Hf than of Nd, which is in agreement with previous studies (Rickli et al., 2009; Zimmermann et al., 2009a) and also supports the Southern Ocean being a net sink for Hf.

The isotope compositions of both elements do not show large variations within most of the ACC and in the Weddell Gyre, but some distinct features are observed:

(4) The Hf isotope composition is remarkably constant and does not show any significant deviations from an average ε_{Hf} of 4.6. The data correspond well to previously measured ferromanganese crust data and The combined Hf and Nd isotope values plot in a narrow cluster on the "seawater array" and are in agreement with ferromanganese deposits from this area (van de Flierdt et al., 2006). The Nd data however are on average about 1 ε unit more radiogenic, implying a higher Pacific contribution in the last glacial period. The Hf data on the other hand does not experience such shift and suggests that the glacial/interglacial variability of dissolved Hf isotopes in seawater of the Southern Ocean was small.

(5) AABW is clearly less radiogenic in its Nd isotope composition than CDW above (ε_{Nd} = -8.4) along the Zero Meridian, documenting continental inputs from the Antarctic continent during formation of AABW. The inflow of NADW is clearly reflected by less radiogenic Nd isotope signatures north of 50°S. Admixture of waters from the Agulhas Current is reflected in unradiogenic ε_{Nd} values near the surface close to South Africa.

(6) Based on higher Nd concentrations than observed for modified NADW, a simple two component mixing model between NADW and LCDW suggests that opal scavenging influences the Nd budget of the Southern Ocean. This mixing model using

salinity clearly shows that the isotope composition of modified NADW is primarily controlled by water mass mixing.

(7) On a larger scale the Nd isotope composition of LCDW can be explained by a two component mixing of NPDW and NADW with a 70-75 % contribution of the Atlantic-sourced waters.

Acknowledgements

This study was funded by a grant of the Deutsche Forschungsgemeinschaft (DFG) to M.F. (project FR1198/2) within the priority program "*Antarctic Research" (SPP 1158)*. The authors would like to thank Jutta Heinze and Ana Kolevica for the priceless lab support and Folkmar Hauff and Anton Eisenhauer for providing assistance and machine time on the TIMS. Most importantly, we thank the chief scientists Eberhard Fahrbach and Hein de Baar, as well as Captain Stefan Schwarze and the crew of *Polarstern* for their contribution and braveness. Many thanks to Jan van Ooijen for the Si data and to Steven van Heuven to merge the ODV data. This paper is dedicated to those, who did not return from expedition ANT/XXIV-3.

Chapter 5

General conclusions and outlook

5.1 Summary and conclusions

The first systematic combined analyses of hafnium (Hf) and neodymium (Nd) isotope compositions and concentrations of seawater from the Atlantic sector of the Southern have been carried out in this study. The distribution patterns clearly reflect water mass mixing and show only limited influence of local weathering inputs.

The surface water data (Chapter 3) show that distribution of Hf and Nd concentrations closely follows the prevailing hydrography. In the Polar Frontal Zone (PFZ) and the Subantarctic Zone (SAZ) Hf and Nd concentrations are the lowest of the entire sample set (< 0.08 pmol/kg and < 9 pmol/kg, respectively). This documents that reduced terrigenous inputs together with particle scavenging. The high biological productivity and correlated particulate fluxes at the Polar Front (PF) and the Subantractic Front (SAF) enhance scavenging of Hf and Nd, mainly through the frustules of diatoms, and effectively remove both trace metals from the surface layer. This is corroborated by the surface data further south within the Weddell Gyre (WG), where particle flux is reduced and consequently the concentrations for both elements are generally higher. The highest concentrations for Hf are observed near King George Island (0.38 pmol/kg), which is obviously caused by weathering inputs from the dominantly volcanic rocks of this island, as confirmed by highly radiogenic Hf and Nd isotope compositions of these samples (ε_{Hf} = 6.1 and ε_{Nd} = -4.0).

This contrasts with the very low Hf concentration of 0.08 pmol/kg about 200 km southwest of Cape Town, where old continental rocks dominate the prevailing geology. In the same sample the Nd concentration is one of the highest of this data set (23 pmol/kg), thus excluding removal by particle scavenging as an explanation for the very low Hf concentration. The unradigenic Nd isotope composition of this surface water sample (ε_{Nd} = -18.9) together with elevated shale normalized La/Yb ratios suggests a predominant local input. Therefore, the most likely explanation is that only a small amount of the lithogenic Hf from this area is accessible to weathering and reaches the ocean.

A shift towards less radiogenic Hf isotope compositions close to Antarctica on the Zero Meridian is another example of continental inputs influencing the Hf budget in the Southern Ocean. This shift is interpreted as a signature originating from a more congruent release of Hf from the Archean rocks exposed nearby on the Antarctic

continent enabled by glacial grinding. From these regional findings it is concluded that the combination of Hf and Nd isotopes together with their concentration are promising proxies for changes in source provenance and weathering regime, which is in accordance with earlier findings obtained from ferromanganese deposits. Additionally, the new dataset of this study indicates that weathering of volcanic rocks is largely underestimated in the global Hf budget in seawater.

In Chapter 4 the combined Hf and Nd isotope composition of seawater deeper than 200 m are presented. The concentration patterns of both elements show a typical behavior of particle-reactive trace metals, where sub-surface waters are generally depleted and deeper waters are enriched. The gradient of enrichment of the two elements is, however, different in that Nd increases linearly at stations north of the PF, whereas the Hf concentration increases significantly only in the upper 1 to 2 km of the water column and essentially stays constant below. Both, Hf and Nd, correlate well with dissolved Si, whereas Nd shows a closer correspondence than Hf. It can be concluded that the vertical dynamics of both elemental concentrations are strongly influenced by uptake of and release from diatom frustules, as also indicated by the surface data. The different slopes of increase are most likely a function of a more efficient desorption of Nd from dissolving particles than of Hf. This strongly supports a shorter oceanic residence time of Hf than of Nd, at least in areas where diatoms are the prevailing primary producers.

In contrast to the surface waters, the Hf isotope compositions of the deeper Southern Ocean do not show significant deviations from the average value of $\varepsilon_{Hf} = 4.6$. Distinction of different water masses based on Hf isotopes, which is limited by the uncertainties of the measured values, is therefore not possible in the study area. The currently available seawater data for Hf isotopes show that the isotopic range in global seawater is only half of the Nd range. Comparison to the Nd isotope data confirms this low isotopic gradient for Southern Ocean water masses, which show a range from $\varepsilon_{Nd} = -8$ to $\varepsilon_{Nd} = -11$, which is even lower if only the waters south of the PF are considered, for which the total range is only about 1.5 ε units. Despite the relatively small isotopic range, some water masses, such as Antarctic Bottom Water (AABW; $\varepsilon_{Nd} \approx -9.5$), show significantly less radiogenic values than average Circumpolar Deep Water (CDW; $\varepsilon_{Nd} \approx -8.5$). This difference is only explainable by the admixture of less radiogenic Nd in near surface waters to CDW during the formation of AABW at distinct

areas around the Antarctic continent. A more significant modification of water masses is observed for North Atlantic Deep Water (NADW) north of the ACC. The Nd isotope composition of modified NADW (ε_{Nd} = -10 to ε_{Nd} =-11) can be explained by admixture of about 60 % to 70 % of southern sourced CDW, indicated by a simple two-component mixing calculation. The mixing calculation, however, reveals that the Nd concentration of modified NADW is 10 % to 20 % too low to fit on the mixing line. This additionally supports that Nd does not behave conservatively and a fraction of it is removed. The reason is particle scavenging at the Southern Ocean fronts, as also indicated by the Nd concentration data. On the other hand, using salinity instead of Nd concentration with the same isotope values shows that the observed isotope composition is entirely governed by water mass mixing. Therefore, it can be deduced that Nd isotopes behave as a quasi-conservative water mass tracer, despite the fact that the Nd concentration is clearly influenced by biological uptake and release. In the case of this study, this observation, which has been referred to as the Nd paradox, can be explained by the small isotopic differences between the water masses.

To summarize, the following conclusions of this study can be drawn in response to the scientific questions raised in the introduction of this thesis:

1. *Can the Hf isotope composition of seawater be used as a tracer for the global ocean circulation system or is the applicability only restricted to a basin-wide scale?*

   The findings of this study suggest that the Hf isotope composition of seawater has only a limited applicability to trace water masses and their mixing. The surface data have shown, however, that Hf isotopes are governed by changes in local weathering inputs. A more congruent release of Hf isotopes is observed when the catchment of the hinterland is of volcanic or mafic origin. Additionally, enhanced physical weathering of continental rocks, which are subjected to glacial grinding, apparently influences the local Hf isotope composition and shifts it towards less radiogenic values which is not the case for Nd. It can therefore be concluded that Hf isotopes largely reflect local signals, at best distributed on a basin scale, which is in agreement with the latest studies on Hf isotopes from other areas (e.g. Rickli et al., 2009, 2010).

2. *What controls the Hf and Nd isotope composition of water masses in the Southern Ocean? Is it possible to distinguish Southern Ocean water masses by their Hf and Nd isotope compositions?*

The answer to this question has partly been given already above. Weathering inputs largely control the Hf and Nd isotope composition in seawater. Although water mass distinction on the basis of Hf isotopes in the Southern Ocean is not possible based on these data, some conclusions on the input mechanisms of Hf into the ocean can be drawn. In the vicinity of landmasses, surface waters reflect the isotope composition of the prevailing geology of the hinterland. The hypothesis that weathering is the main contributor of Hf to the ocean is also supported by the lack of increased Hf concentrations where hydrothermal activity is present. Neodymium, on the other hand, is a very sensitive water mass tracer, even in areas where water mass mixing is vigorous, such as the Southern Ocean. For instance, the Nd isotope composition of AABW clearly reflects the admixture of Nd from former surface waters close to the shelf.

3. *Is the Hf and Nd isotope composition of seawater a promising tool to reconstruct past weathering regimes and ocean circulation patterns?*

Combined Hf and Nd isotopes can clearly contribute to the reconstruction of past weathering regimes. The main limitation, which arose in this study, is that surface water isotope compositions are obviously most affected by changes in the weathering regime. To reconstruct past weathering inputs on the basis of Hf isotopes, it is crucial to find suitable archives, in which Hf isotope signatures, preferably from surface waters, are preserved. Apparently, siliceous primary-producers (e.g. diatoms) readily scavenge both Hf and Nd from the surface layer. Neodymium isotopes have been shown to be suitable tracers to reconstruct past ocean circulation patterns. This study corroborates that it is possible to trace different water masses and to quantify their mixing relationships in the Southern Ocean. The clear distinction between AABW derived from East Antarctica and average CDW in the present day ocean is a key observation of this study. If the production or flow paths of AABW have changed in the past, it can be assumed that these changes have been recorded

by suitable archives, such as ferromanganese crusts, coatings of sedimentary particles, benthic foraminifera or fish teeth.

5.2 Outlook for future work

This work presents a detailed study of Hf and Nd isotope composition and concentration in the Atlantic sector of the Southern Ocean. To fully understand the processes, that govern the Hf and Nd isotope compositions of entire Southern Ocean, further investigations are required. The Indian and Pacific sectors of the Southern Ocean, for example, are completely unexplored in terms of Nd and Hf isotope compositions of modern seawater and a database needs to be produced. For the Atlantic sector of the Southern Ocean it has been shown in this study that AABW is distinct from CDW. The distinction is possible because AABW is formed near the Antarctic continent, and thus is influenced by the prevailing isotope composition of the local surface waters. Besides the Weddell Sea in the Atlantic sector, there are other areas, such as the Ross Sea in the Pacific sector or at the Amery Shelf in the Indian sector, where AABW is formed. In this study the Nd isotope composition of AABW on the Zero Meridian has its probable source area somewhere in East Antarctica, most likely in the vicinity of Amery Shelf. To corroborate this assumption, it further water column investigations are needed. To date, there are neither present day or paleo Hf and Nd data from the Enderby Basin, where AABW from the Amery shelf drains.

In this study no lateral differences in Hf and Nd isotope composition of CDW could be observed between the Drake Passage and the Zero Meridian. The reason for this is the effective mixing within the ACC. However, it would be of great advantage, if present day data of the South Pacific existed. The Hf and Nd isotope composition of this part of the Southern Ocean is to date only constrained by few analyses of ferromanganese deposits (Albarède et al., 1997; van de Flierdt et al., 2006).

Furthermore, this study shows that Nd is partly removed through particle scavenging when northern- and southern-sourced waters mix. The removal of Nd from the water column, therefore, influences to some extent the isotopic mass balance of Nd of the Southern Ocean. It has been shown that LCDW consists of a ~ 70 % Atlantic source. One of the questions, which arise from this finding, is whether the reason for this dominance of the Atlantic contribution is due to higher removal of Nd in the Pacific or whether it is related to a large difference in the geostrophic flow from the respective

ocean basins. This can only be answered by detailed studies in the Southeast Pacific sector.

References

Albarède, F., Goldstein, S.L., 1992. Geology World map of Nd isotopes in sea-floor ferromanganese deposits. Geology 20, 761-763.

Albarède, F., Goldstein, S.L., Dautel, D., 1997. The neodymium isotopic composition of manganese nodules from the Southern and Indian oceans, the global oceanic neodymium budget, and their bearing on deep ocean circulation. Geochimica et Cosmochimica Acta 61, 1277-1291.

Albarède, F., Simonetti, A., Vervoort, J.D., Blichert-Toft, J., Abouchami, W., 1998. A Hf-Nd isotopic correlation in ferromanganese nodules. Geophysical Research Letters 25, 3895-3898.

Andersson, P.S., Dahlqvist, R., Ingri, J., Gustafsson, Ö., 2001. The isotopic composition of Nd in a boreal river: a reflection of selective weathering and colloidal transport. Geochimica et Cosmochimica Acta 65, 521-527.

Arsouze, T., Dutay, J.-C., Lacan, F., Jeandel, C., 2009. Reconstructing the Nd oceanic cycle using a coupled dynamical – biogeochemical model. Biogeosciences 6, 2829-2846.

Bau, M., Koschinsky, A., 2006. Hafnium and neodymium isotopes in seawater and in ferromanganese crusts: The "element perspective". Earth and Planetary Science Letters 241, 952-961.

Bayon, G., Vigier, N., Burton, K.W., Jean Carignan, A.B., Etoubleau, J., Chu, N.-C., 2006. The control of weathering processes on riverine and seawater hafnium isotope ratios. Geology 34, 433.

Bayon, G., Burton, K.W., Soulet, G., Vigier, N., Dennielou, B., Etoubleau, J., Ponzevera, E., German, C.R., Nesbitt, R.W., 2009. Hf and Nd isotopes in marine sediments: Constraints on global silicate weathering. Earth and Planetary Science Letters 277, 318-326.

Bertram, C.J., Elderfield, H., 1993. The geochemical balance of the rare earth elements and neodymium isotopes in the oceans. Geochimica et Cosmochimica Acta 57, 1957-1986.

Boebel, O., Lutjeharms, J., Schmid, C., Zenk, W., Rossby, T., Barron, C., 2003. The Cape Cauldron: a regime of turbulent inter-ocean exchange. Deep Sea Research Part II: Topical Studies in Oceanography 50, 57-86.

Boyle, E.A., 1988. Cadmium: Chemical tracer of deepwater paleoceanography. Paleoceanography 3, 471-489.

Broecker, W.S., 1991. The great ocean conveyor belt. Oceanogrphy 4, 79-89.

Broecker, W.S., Peng, T.H., 1982. Tracers in the Sea. Eldigio Press, New York.

Carmack, E., Foster, T., 1975. On the flow of water out of the Weddell Sea. Deep Sea Research and Oceanographic Abstracts 22, 711-724.

Chu, N.-C., Taylor, R.N., Chavagnac, V., Nesbitt, R.W., Boella, R.M., Milton, J.A., German, C.R., Bayon, G., Burton, K., 2002. Hf isotope ratio analysis using multi-collector inductively coupled plasma mass spectrometry: an evaluation of isobaric interference corrections. Journal of Analytical Atomic Spectrometry 17, 1567-1574.

Cole, D.I., 1992. Evolution and development of the Karoo Basin, in: Wit, M.J. de, Ransome, I.G.D. (Eds.), Inversion Tectonics of the Cape Fold Belt, Karoo and Cretaceous Basins of Southern Africa. Balkema, Rotterdam, pp. 87-100.

Curry, W.B., Lohmann, G.P., 1983. Reduced advection into Atlantic Ocean deep eastern basins during last glaciation maximum. Nature 306, 577-588.

Dalziel, I.W.D., 1992. Antarctica - A Tale of 2 Supercontinents. Annual Review of Earth and Planetary Sciences 20, 501-526.

David, K., Frank, M., O'Nions, R.K., Belshaw, N.S., Arden, J.W., 2001. The Hf isotope composition of global seawater and the evolution of Hf isotopes in the deep Pacific Ocean from Fe-Mn crusts. Chemical Geology 178, 23-42.

Deacon, G.E.R., 1979. The Weddell gyre. Deep Sea Research Part A. Oceanographic Research Papers 26, 981-995.

D'Orazio, M., Agostini, S., Mazzarini, F., Innocenti, F., Manetti, P., Haller, M.J., Lahsen, A., 2000. The Pali Aike Volcanic Field, Patagonia: slab-window magmatism near the tip of South America. Tectonophysics 321, 407-427.

Ehrmann, W., Melles, M., Kuhn, G., Grobe, H., 1992. Significance of clay mineral assemblages in the Antarctic Ocean. Marine Geology 107, 249-273.

Elderfield, H., Greaves, M.J., 1982. The rare earth elements in seawater. Nature 296, 214-219.

Elderfield, H., Upstillgoddard, R., Sholkovitz, E., 1990. The rare earth elements in rivers, estuaries, and coastal seas and their significance to the composition of ocean waters. Geochimica et Cosmochimica Acta 54, 971-991.

Emery, W.J., 1977. Antarctic Polar Frontal Zone from Australia to the Drake Passage. Journal of Physical Oceanography 7, 811-822.

Fahrbach, E., de Baar, H.J.W. (Eds.), 2010. The expedition of the research vessel "Polarstern" to the Antarctic in 2008 (ANT-XXIV/3), in: Reports on Polar and Marine Research. Alfred-Wegener-Institute for Polar and Marine Research, p. 232. http://hdl.handle.net/10013/epic.34050

Firdaus, M.L., Norisuye, K., Nakagawa, Y., Nakatsuka, S., Sohrin, Y., 2008. Dissolved and labile particulate Zr, Hf, Nb, Ta, Mo and W in the western North Pacific Ocean. Journal of Oceanography 64, 247-257.

Fitzsimons, I., 2000. A review of tectonic events in the East Antarctic Shield and their implications for Gondwana and earlier supercontinents. Journal of African Earth Sciences 31, 3-23.

Frank, M., Reynolds, B.C., O'Nions, R.K., 1999. Nd and Pb isotopes in Atlantic and Pacific water masses before and after closure of the Panama gateway. Geology 27, 1147-1150.

Frank, M., 2002. Radiogenic isotopes: Tracers of past ocean circulation and erosional input. Reviews of Geophysics 109, 11.

Frank, M., Whiteley, N., Kasten, S., Hein, J.R., O'Nions, K., 2002. North Atlantic Deep Water export to the Southern Ocean over the past 14 Myr: Evidence from Nd and Pb isotopes in ferromanganese crusts. Paleoceanography 17.

Franzese, A.M., Hemming, S., Goldstein, S., Anderson, R., 2006. Reduced Agulhas Leakage during the Last Glacial Maximum inferred from an integrated provenance and flux study. Earth and Planetary Science Letters 250, 72-88.

Geibert, W., Vöge, I., 2008. Progress in the determination of 227Ac in sea water. Marine Chemistry 109, 238-249.

Georgi, D.T., 1981. On the Relationship Between the Large-Scale Property Variations and Fine Structure in the Circumpolar Deep Water. Journal of Geophysical Research 86, 6556-6566.

German, C.R., Klinkhammer, G.P., Edmond, J.M., Mitra, A., Elderfield, H., 1990. Hydrothermal scavenging of rare-earth elements in the ocean. Nature 345, 516-518.

Godfrey, L.V., Lee, D.C., Sangrey, W.F., Halliday, A.N., Salters, V.J.M., Hein, J.R., White, W.M., 1997. The Hf isotopic composition of ferromanganese nodules and

crusts and hydrothermal manganese deposits: Implications for seawater Hf. Earth and Planetary Science Letters 151, 91-105.

Godfrey, L.V., Field, M.P., Sherrell, R.M., 2008. The estuarine distributions of Zr, Hf and Ag in the Hudson River, and the implications for their continental and anthropogenic sources to seawater. Geochemistry, Geophysics, Geosystems 9.

Godfrey, L.V., Zimmermann, B., Lee, D.C., King, R.L., Vervoort, J.D., Sherrell, R.M., Halliday, A.N., 2009. Hafnium and neodymium isotope variations in NE Atlantic seawater. Geochemistry Geophysics Geosystems 10.

Goldstein, S.L., Onions, R.K., Hamilton, P.J., 1984. A Sm-Nd Isotopic Study of Atmospheric Dusts and Particulates from Major River Systems. Earth and Planetary Science Letters 70, 221-236.

Gordon, A.L., 1971. Oceanography of Antarctic waters, in: Reid, J.L. (Ed.), Antarctic Research Series. pp. 169-203.

Greaves, M., Statham, P., Elderfield, H., 1994. Rare earth element mobilization from marine atmospheric dust into seawater. Marine Chemistry 46, 255-260.

Haley, B. a, Klinkhammer, G.P., McManus, J., 2004. Rare earth elements in pore waters of marine sediments. Geochimica et Cosmochimica Acta 68, 1265-1279.

Halliday, N., Davidson, P., Owen, M., Olivarez, M., 1992. Metalliferous sediments and the scavenging residence time of nd near hydrothermal vents. Geophysical Research Letters 19, 761-764.

Hegner, E., Dauelsberg, H.J., Rutgers van der Loeff, M.M., Jeandel, C., Baar, H.J.W. de, 2007. Nd isotopic constraints on the origin of suspended particles in the Atlantic Sector of the Southern Ocean. Geochem. Geophys. Geosyst. 8.

Heumann, K.G., 1992. Isotope dilution mass spectrometry (IDMS) of the elements. Mass Spectrometry Reviews 11, 41-67.

Hoskin, P.W.O., Schaltegger, U., 2003. The Composition of Zircon and Igneous and Metamorphic Petrogenesis. Reviews in Mineralogy and Geochemistry 53, 27-62.

Hofmann, E.E., 1985. The Large-Scale Horizontal Structure of the Antarctic Circumpolar Current From FGGE Drifters. Journal of Geophysical Research 90, 7087-7097.

Hole, M.J., Saunders, A.D., Rogers, G., Sykes, M.A., 1994. The relationship between alkaline magmatism, lithospheric extension and slab window formation along continental destructive plate margins. spec. publ. geol. soc. london 81, 265-285.

Hoskin, P.W.O., Schaltegger, U., 2003. The Composition of Zircon and Igneous and Metamorphic Petrogenesis. Reviews in Mineralogy and Geochemistry 53, 27-62.

Heywood, K.J., King, B. a, 2002. Water masses and baroclinic transports in the South Atlantic and Southern oceans. Journal of Marine Research 60, 639-676.

Jacobsen, S.B., Wasserburg, G.J., 1980. Sm-Nd Isotopic Evolution of Chondrites. Earth and Planetary Science Letters 50, 139-155.

Jeandel, C., 1993. Concentration and isotopic composition of Nd in the South Atlantic Ocean. Earth and Planetary Science Letters 117, 581-591.

Jeandel, C., Bishop, J.K., Zindler, A., 1995. Exchange of neodymium and its isotopes between seawater and small and large particles in the Sargasso Sea. Geochimica et Cosmochimica Acta 59, 535-547.

Jeandel, C., Thouron, D., Fieux, M., 1998. Concentrations and isotopic compositions of neodymium in the eastern Indian Ocean and Indonesian straits. Geochimica et Cosmochimica Acta 62, 2597-2607.

Kemp, A.I.S., Foster, G.L., Scherstén, A., Whitehouse, M.J., Darling, J., Storey, C., 2009. Concurrent Pb–Hf isotope analysis of zircon by laser ablation multi-collector ICP-MS, with implications for the crustal evolution of Greenland and the Himalayas. Chemical Geology 261, 244-260.

Kinny, P.D., Maas, R., 2003. Lu – Hf and Sm – Nd isotope systems in zircon. Reviews in Mineralogy and Geochemistry 53, 327-341.

Klatt, O., Fahrbach, E., Hoppema, M., Rohardt, G., 2005. The transport of the Weddell Gyre across the Prime Meridian. Deep Sea Research Part II: Topical Studies in Oceanography 52, 513-528.

Klunder, M., Laan, P., Middag, R., De Baar, H.J.W., Ooijen, J.V., 2010. Dissolved Iron the Southern Ocean (Atlantic Sector). Deep Sea Research Part II: Topical Studies in Oceanography, in press, accepted manuscript.

Kosler, J., Magna, T., Mlcoch, B., Mixa, P., Nyvlt, D., Holub, F., 2009. Combined Sr, Nd, Pb and Li isotope geochemistry of alkaline lavas from northern James Ross Island (Antarctic Peninsula) and implications for back-arc magma formation. Chemical Geology 258, 207-218.

Lacan, F., Jeandel, C., 2001. Tracing Papua New Guinea imprint on the central Equatorial Pacific Ocean using neodymium isotopic compositions and Rare Earth Element patterns. Earth and Planetary Science Letters 186, 497-512.

Lacan, F., Jeandel, C., 2005. Acquisition of the neodymium isotopic composition of the North Atlantic Deep Water. Geochemistry Geophysics Geosystems 6.

Locarnini, R.A., Whitworth III, T., Nowlin Jr., W.D., 1993. The importance of the Scotia Sea on the outflow of Weddell Sea Deep Water. Journal of Marine Research 51, 135-153.

Lumpkin, R., Speer, K., 2007. Global Ocean Meridional Overturning. Journal of Physical Oceanography 37, 2550-2562.

Machado, a, Lima, E., Chemalejr, F., Morata, D., Oteiza, O., Almeida, D., Figueiredo, a, Alexandre, F., Urrutia, J., 2005. Geochemistry constraints of Mesozoic–Cenozoic calc-alkaline magmatism in the South Shetland arc, Antarctica. Journal of South American Earth Sciences 18, 407-425.

McCulloch, M.T., Wasserburg, G.J., 1978. Sm-Nd and Rb-Sr Chronology of Continental Crust Formation. Science (New York, N.Y.) 200, 1003-1011.

Middag, R., 2010. Dissolved Aluminium and Manganese in the Polar Oceans. Ph.D. thesis, University of Groningen, the Netherlands, 237 pp.

Middag, R., Baar, H.J.W. de, Laan, P., Cai, P.H., van Ooijen, J.C., 2010. Dissolved Manganese in the Atlantic Sector of the Southern Ocean. Deep Sea Research Part II, in press, accepted manuscript.

Millar, I.L., Willan, R.C.R., Wareham, C.D., Boyce, A.J., 2001. The role of crustal and mantle sources in the genesis of granitoids of the Antarctic Peninsula and adjacent crustal blocks. Journal of the Geological Society 158, 855-867.

Millar, I.L., Pankhurst, R.J., 1987. Rb–Sr geochronology of the region between the Antarctic Peninsula and the Transantarctic Mountains: Haag Nunataks and Mesozoic granitoids, in: McKenzie, G.D. (Ed.), Gondwana Six: Structure, Tectonics, and Geophys. Monogr. Ser. AGU, Washington, DC, p. 151–160.

Münker, C., Weyer, S., Scherer, E., Mezger, K., 2001. Separation of high field strength elements (Nb, Ta, Zr, Hf) and Lu from rock samples for MC-ICPMS measurements. Geochemistry, Geophysics, Geosystems 2.

Nachtrieb, N.H., Conway, J.G., 1948. The Extraction of Ferric Chloride by Isopropyl Ether. I. J. Am. Chem. Soc. 70, 3547-3552.

Nachtrieb, N.H., Fryxell, R.E., 1948. The Extraction of Ferric Chloride by Isopropyl Ether. II. J. Am. Chem. Soc. 70, 3552-3557.

Nowell, G.M., Kempton, P.D., Noble, S.R., Fitton, J.G., Saunders, A.D., Mahoney, J.J., Taylor, R.N., 1998. High precision Hf isotope measurements of MORB and OIB by thermal ionisation mass spectrometry: insights into the depleted mantle. Chemical Geology 149, 211-233.

Nowlin Jr., W.D., Whitworth III, T., 1977. Structure and Transport of the Antarctic Circumpolar Current at Drake Passage from Short-Term Measurements. Journal of Physical Oceanography 7, 788-802.

Orsi, A.H., Whitworth III, T., Nowlin, W.D., 1995. On the Meridional Extent and Fronts of the Antarctic Circumpolar Current. Deep-Sea Research Part I-Oceanographic Research Papers 42, 641-673.

Orsi, A.H., Johnson, G.C., Bullister, J.L., 1999. Circulation, mixing, and production of Antarctic Bottom Water. Progress In Oceanography 43, 55-109.

Orsi, A.H., Smethie Jr., W.M., Bullister, J.L., 2002. On the total input of Antarctic waters to the deep ocean: A preliminary estimate from chlorofluorocarbon measurements. Journal of Geophysical Research 107, 3122.

Patchett, P.J., White, W.M., Feldmann, H., Kielinczuk, S., Hofmann, A.W., 1984. Hafnium rare-earth element fractionation in the sedimentary system and crustal recycling into the earths mantle. Earth and Planetary Science Letters 69, 365-378.

Peterson, R., Stramma, L., 1991. Upper-level circulation in the South Atlantic Ocean. Progress In Oceanography 26, 1-73.

Piepgras, D.J., Wasserburg, G.J., 1980. Neodymium Isotopic Variations in Seawater. Earth and Planetary Science Letters 50, 128-138.

Piepgras, D.J., Wasserburg, G.J., 1982. Isotopic composition of neodymium in waters from the drake passage. Science 217, 207-214.

Piepgras, D.J., Wasserburg, G.J., 1987. Rare earth element transport in the western North Atlantic inferred from Nd isotopic observations. Deep Sea Research Part B. Oceanographic Literature Review 51, 1257-1271.

Piepgras, D.J., Jacobsen, S.B., 1988. The isotopic composition of neodymium in the North Pacific. Geochimica et Cosmocimica Acta 52, 1373-1381.

Pin, C., Zalduegui, J.F.S., 1997. Sequential separation of light rare-earth elements, thorium and uranium by miniaturized extraction chromatography: Application to isotopic analyses of silicate rocks. Analytica Chimica Acta 339, 79-89.

Piotrowski, A.M., Lee, D.-C., Christensen, J.N., Burton, K.W., Halliday, A.N., Hein, J.R., Gunther, D., 2000. Changes in erosion and ocean circulation recorded in the Hf isotopic compositions of North Atlantic and Indian Ocean ferromanganese crusts. Earth and Planetary Science Letters 181, 315-325.

Piotrowski, A., Goldstein, S., Hemming, S., Fairbanks, R., Zylberberg, D., 2008. Oscillating glacial northern and southern deep water formation from combined neodymium and carbon isotopes. Earth and Planetary Science Letters 272, 394-405.

Reid, J., Lynn, R., 1971. On the influence of the Norwegian-Greenland and Weddell seas upon the bottom waters of the Indian and Pacific oceans. Deep-Sea Research 18, 1063-1088.

Richardson, P., Lutjeharms, J., Boebel, O., 2003. Introduction to the "Inter-ocean exchange around southern Africa". Deep Sea Research Part II: Topical Studies in Oceanography 50, 1-12.

Rickli, J., 2008. The hafnium and neodymium isotopic composition of seawater and rivers. Ph.D. thesis, ETH-Zurich, Switzerland, 124 pp.

Rickli, J., Frank, M., Halliday, A.N., 2009. The hafnium–neodymium isotopic composition of Atlantic seawater. Earth and Planetary Science Letters 280, 118-127.

Rickli, J., Frank, M., Baker, A.R., Aciego, S., Souza, G. de, Georg, R.B., Halliday, A.N., 2010. Hafnium and neodymium isotopes in surface waters of the eastern Atlantic Ocean: Implications for sources and inputs of trace metals to the ocean. Geochimica et Cosmochimica Acta 74, 540-557.

Riepe, W., Kaiser, H., 1966. Massenspektrometrische Spurenanalyse von Calcium, Strontium und Barium in Natriumazid durch Isotopenverdünnungstechnik. Fresenius' Zeitschrift für Analytische Chemie 223, 321-335.

Rogers, J.J.W., Unrug, R., Sultan, M., 1994. Tectonic assembly of Gondwana. Journal of Geodynamics 19, 1-34.

Rohardt, G (2009): Continuous thermosalinograph oceanography along POLARSTERN cruise track ANT-XXIV/3, http://doi.pangaea.de/10.1594/PANGAEA.727465

Roman, R.E., Lutjeharms, J.R.E., 2010. Antarctic intermediate water at the Agulhas Current retroflection region. Journal of Marine Systems 81, 273-285.

Rutgers van der Loeff, M.M., Berger, G.W., 1993. Scavenging of ^{230}Th and ^{231}Pa near the Antarctic polar front in the South Atlantic. Deep-Sea Research 40, 339-357.

Sarmiento, J.L., Simeon, J., Gnanadesikan, a, Gruber, N., Key, R.M., Schlitzer, R., 2007. Deep ocean biogeochemistry of silicic acid and nitrate. Global Biogeochemical Cycles 21, 1-16.

Siddall, M., Khatiwala, S., Vandeflierdt, T., Jones, K., Goldstein, S., Hemming, S., Anderson, R., 2008. Towards explaining the Nd paradox using reversible scavenging in an ocean general circulation model. Earth and Planetary Science Letters 274, 448-461.

Sievers, A., Emery, J., 1978. Variability of the Antarctic Polar Frontal Zone in the Drake PassagesSummer 1976-1977. Journal of Geophysical Research 83, 3010-3022.

Sievers, H.A., Nowlin, W.D., 1984. The Stratification and water masses at Drake Passage. Journal of Geophysical Research-Oceans 89, 489-514.

Sims, K., Blichert-Toft, J., Kyle, P., Pichat, S., Gauthier, P., Blusztajn, J., Kelly, P., Ball, L., Layne, G., 2008. A Sr, Nd, Hf, and Pb isotope perspective on the genesis and long-term evolution of alkaline magmas from Erebus volcano, Antarctica. Journal of Volcanology and Geothermal Research 177, 606-618.

Stommel, H., 1958. The abyssal circulation. Race 5, 80-82.

Storey, B.C., 2005. ANTARCTIC, in: Selley, R.C., Cocks, L.R.M., Ian R Plimer (Eds.), Encyclopedia of Geology. Elsevier, Oxford, pp. 132-140.

Stramma, L., Peterson, R.G., 1990. The South Atlantic Current. Journal of Physical Oceanography 20, 846-859.

Stramma, L., England, M., 1999. On the water masses and mean circulation of the South Atlantic Ocean. Journal of Geophysical Research 104, 20863-20883.

Suga, T., Talley, D., 1995. Antarctic Intermediate Water circulation in the tropical and subtropical South Atlantic. Journal of Geophysical Reasearch 100, 13441-13453.

Tachikawa, K., Jeandel, C., Roy-Barman, M., 1999. A new approach to the Nd residence time in the ocean: the role of atmospheric inputs. Earth and Planetary Science Letters 170, 433-446.

Tachikawa, K., Athias, V., Jeandel, C., 2003. Neodymium budget in the modern ocean and paleo-oceanographic implications. Journal of Geophysical Research-Oceans 108, 3254.

Tanaka, T., Togashi, S., Kamioka, H., Amakawa, H., Kagami, H., Hamamoto, T., Yuhara, M., Orihashi, Y., Yoneda, S., Shimizu, H., Kunimaru, T., Takahashi, K., Yanagi, T., Nakano, T., Fujimaki, H., Shinjo, R., Asahara, Y., Tanimizu, M., Dragusanu, C., 2000. JNdi-1: a neodymium isotopic reference in consistency with LaJolla neodymium. Chemical Geology 168, 279-281.

Taylor, P.D.P., Valkiers, S., Vendelbo, D., De Bièvre, P., 1994. Determination of the isotopic composition and atomic weight of tungsten using gas source mass spectrometry: opening the route to the establishment of the traceability of tungsten amount measurements to the SI system. International Journal of Mass Spectrometry and Ion Processes 134, L7-L10.

Taylor, S.R., McLennan, S.M., 1985. The Continental Crust: Its Composition and Evolution. Blackwell Scientific, Boston, Mass.

Thomas, R.J., Veh, M.W. von, McCourt, S., 1993. The tectonic evolution of southern Africa: an overview. Journal of African Earth Sciences 16, 5-24.

Usbeck, R., Rutgers van der Loeff, M.M., Hoppema, M., Schlitzer, R., 2002. Shallow remineralization in the Weddell Gyre. Geochemistry Geophysics Geosystems 3, 1-18.

van de Flierdt, T., Frank, M., Lee, D.-C., Halliday, A.N., 2002. Glacial weathering and the hafnium isotope composition of seawater. Earth and Planetary Science Letters 201, 639-647.

van de Flierdt, T., Frank, M., Lee, D.-C., Halliday, A.N., Reynolds, B.C., Hein, J.R., 2004. New constraints on the sources and behavior of neodymium and hafnium in seawater from Pacific Ocean ferromanganese crusts. Geochimica et Cosmochimica Acta 68, 3827-3843.

van de Flierdt, T., Hemming, S.R., Goldstein, S.L., Abouchami, W., 2006. Radiogenic isotope fingerprint of Wilkes Land–Adélie Coast Bottom Water in the circum-Antarctic Ocean. Geophysical Research Letters 33, 1-5.

van de Flierdt, T., Goldstein, S., Hemming, S., Roy, M., Frank, M., Halliday, A., 2007. Global neodymium–hafnium isotope systematics — revisited. Earth and Planetary Science Letters 259, 432-441.

Venchiarutti, C., Jeandel, C., Roy-Barman, M., 2008. Particle dynamics study in the wake of Kerguelen Island using thorium isotopes. Deep-Sea Research Part I-Oceanographic Research Papers 55, 1343-1363.

Vervoort, J.D., Patchett, P.J., Blichert-Toft, J., Albarède, F., 1999. Relationships between Lu-Hf and Sm-Nd isotopic systems in the global sedimentary system. Earth and Planetary Science Letters 168, 79-99.

White, W., Patchett, J., BenOthman, D., 1986. Hf isotope ratios of marine sediments and Mn nodules: evidence for a mantle source of Hf in seawater. Earth and Planetary Science Letters 79, 46-54.

Whitworth III, T., 1980. Zonation and geostrophic flow of the Antarctic circumpolar current at Drake Passage. Deep Sea Research Part A. Oceanographic Research Papers 27, 497-507.

Whitworth III, T., Nowlin, W.D., 1987. Water Masses and Currents of the Southern Ocean at the Greenwich Meridian. Journal of Geophysical Research 92, 6462-6476.

Wüst, G., 1935. Schichtung und Zirkulation des Atlantischen Ozeans. Die Stratosphäre des Atlantischen Ozeans. Wissenschaftliche Ergebnisse der Deutschen Atlantischen Expedition auf dem Forschungs- und Vermessungsschiff "Meteor" 1925-1927 6, 109-288.

You, Y., Lutjeharms, J.R.E., Boebel, O., Ruijter, W.P.M. de, 2003. Quantification of the interocean exchange of intermediate water masses around southern Africa. Deep Sea Research Part II: Topical Studies in Oceanography 50, 197-228.

Zimmermann, B., Porcelli, D., Frank, M., Rickli, J., Lee, D., Halliday, A., 2009a. The hafnium isotope composition of Pacific Ocean water. Geochimica et Cosmochimica Acta 73, 91-101.

Zimmermann, B., Porcelli, D., Frank, M., Andersson, P.S., Baskaran, M., Lee, D.-C., Halliday, A.N., 2009b. Hafnium isotopes in Arctic Ocean water. Geochimica et Cosmochimica Acta 73, 3218-3233.

Appendix

Tab. A1: List of sampled stations for surface seawater composition analysis. The temperature and salinity is obtained from the ship's own PODAS system. The errors are given as external reproducibility. The results are discussed in Chapter 3.

station					device	depth (m)	T (°C)	salinity	εNd	error (2SD)	Nd (pMol)	εHf	error (2SD)	Hf (pMol)	La_N/Yb_N
S1	34° 53.15'	S	16° 40.7'	E	fish	5	21.03	35.47	-18.9	0.3	24.2			0.06	0.69
97	36° 59.60'	S	12° 45.40	E	CTD	100	18.23	35.55	-15.9	0.4					
S2	38° 48'	S	11° 35.8'	E	fish	5	17.53	34.92	-11.0	0.3	6.7			0.04	0.52
101	42° 20.60'	S	8° 59.20'	E	CTD	75	10.21	34.55	-9.7	0.4	8.6				0.29
104	47° 39.80'	S	4° 16.20'	E	CTD	75	6.41	33.72	-7.9	0.4	8.2				0.24
105	47° 39.00'	S	4° 16.60'	E	fish	5	6.50	33.71	-7.9	0.3	7.4			0.08	0.20
113	52° 59.80'	S	0° 02.00'	E	CTD	75	1.22	33.79	-7.9	0.4	16.1				0.27
113	52° 59.80'	S	0° 02.00'	E	CTD	150	0.20	34.02	-8.0	0.4	15.0				
116	54° 21.00'	S	0° 01.00'	E	fish	5	1.04	33.80	-8.0	0.3	15.8	4.5	0.8	0.18	0.29
133	59° 14.00'	S	0° 02.00'	E	fish	5	0.21	33.95	-8.6	0.3	18.2			0.19	0.31
142	62° 20.00'	S	0° 00.00'	E	fish	5	0.53	33.94	-8.6	0.3	17.3	5.0	0.8	0.11	0.30
153	65° 19'	S	0° 00.00'	E	fish	5	-0.18	33.97	-8.5	0.3	17.3	4.9	0.8	0.18	0.30
154	70° 34.50'	S	8° 07.38'	W	CTD	135	-1.69	34.02	-9.9	0.4	19.4			0.22	0.30
156	67° 08.00'	S	0° 24.00'	E	fish	5	-0.67	33.97	-8.6	0.3	19.5	3.0	0.8	0.25	0.31
161	66° 29.20'	S	0° 00.00'	E	CTD	100	0.77	34.64	-8.7	0.4	17.9			0.40	0.30
GvN	68° 31.8'	S	4° 39'	W	fish	5	-1.18	33.84	-8.8	0.3	16.8	3.4	0.8	0.20	
S3	69° 02'	S	15° 42'	W	snorkel	5	-	-	-8.6	0.3	16.9	4.0	0.8	0.16	0.30
186	69° 03'	S	17° 25'	W	CTD	25	-1.84	33.93	-8.4	0.3	17.2	4.3	0.8	0.20	0.30
191	67° 21.00'	S	23° 38.00'	W	CTD	25	-1.85	34.12	-8.5	0.3	18.5	4.3	0.8	0.21	
S4	65° 34'	S	36° 46'	W	snorkel	5	-1.44	34.15	-9.0	0.3	18.5			0.18	0.31
S5	64° 59'	S	42° 0'	W	snorkel	5	-1.55	33.91	-8.4	0.3	18.3	2.8	0.8	0.16	0.31
S6	64° 20'	S	46° 4.4'	W	snorkel	5	-1.76	33.25	-8.6	0.3	18.1	3.8	0.8	0.22	0.30
210	64° 2.8'	S	48° 15.4'	W	CTD	25	-1.83	33.79	-8.5	0.3	18.3	3.3	0.8	0.27	0.29
222	63° 21.00'	S	52° 51.00'	W	CTD	25	-1.82	34.08	-8.9	0.3	19.9	3.7	0.5	0.25	
222	63° 21.00'	S	52° 51.00'	W	CTD	50	-1.82	34.10	-8.9	0.4	21.2			0.29	0.36
222	63° 21.00'	S	52° 51.00'	W	CTD	100	-1.58	34.37	-8.9	0.4	19.9			0.30	
222	63° 21.00'	S	52° 51.00'	W	CTD	180	-1.22	34.49	-8.7	0.4	20.4			0.32	0.32

Tab. A1: continued.

station					device	depth (m)	T (°C)	salinity	εNd	error (2SD)	Nd (pMol)	εHf	error (2SD)	Hf (pMol)	La_N/Yb_N
222	63° 21.00'	S	52° 51.00'	W	CTD	280	-0.90	34.54	-8.7	0.4	21.3			0.35	0.33
222	63° 21.00'	S	52° 51.00'	W	CTD	400	-0.90	34.56	-9.1	0.3	22.5	3.9	0.8	0.34	0.31
223	63° 17.00'	S	53° 13.00'	W	CTD	25	-1.82	34.18	-8.3	0.3	21.1	4.2	0.9	0.31	
S7	62° 08.00'	S	57° 31'	W	snorkel	5	1.04	34.06	-4.0	0.3	22.6	6.1	0.5	0.38	0.28
S8	60° 03.00'	S	55° 24'	W	snorkel	5	1.78	33.85	-7.2	0.3	14.3	3.1	0.9	0.20	0.32
230	60° 06.00'	S	55° 16.40'	W	CTD	50	0.79	34.17	-6.9	0.4	18.9			0.31	0.29
230	60° 06.00'	S	55° 16.40'	W	CTD	150	0.57	34.34	-6.4	0.4	19.9			0.35	0.28
241	57° 37.20'	S	60° 53.80'	W	CTD	50	2.84	33.79	-8.4	0.4	11.8			0.17	0.27
244	56° 53.80'	S	62° 28.00'	W	CTD	25	5.38	33.92	-8.2	0.4	10.2			0.12	0.22
244	56° 53.80'	S	62° 28.00'	W	CTD	50	5.38	33.92	-8.2	0.4	9.6			0.09	0.22
250	55° 45.50'	S	64° 26.20'	W	CTD	150	3.64	34.02	-8.2	0.4	9.7				
DRA001[a]	55° 07.00'	S	65° 33.04'	W	CTD	50	8.32	33.74	-5.7	0.6	8.5				
DRA 006[a]	55° 45.00'	S	64° 30.00'	W	CTD	20	5.10	33.90	-8.6	0.3	8.9				
DRA030[a]	58° 52.00'	S	58° 18.00'	W	CTD	20	2.50	33.89	-8.2	0.5	14.7				
DRA052[a]	61° 50.00'	S	55° 26.00'	W	CTD	31	-	-	-6.3	0.3	21.4				
DRA062[a]	60° 39.00'	S	55° 47.00'	W	CTD	20	0.62	34.33	-7.2	0.4	17.7				

[a] samples from ANTXXIII/3

Table A2: Surface samples which have been analyzed for REEs on the *seaFAST* system. The results are discussed in Chapter 3.

station	depth (m)	La	Ce	Pr	Nd	Sm	Eu	Gd	Tb	Dy	Ho	Er	Tm	Yb	Lu
								(ppt)							
S1	5	4.19	5.37	0.90	3.84	0.74	0.18	0.90	0.12	0.85	0.19	0.62	0.08	0.45	0.07
S2	5	1.66	0.88	0.21	1.00	0.20	0.04	0.30	0.04	0.38	0.11	0.33	0.04	0.23	0.03
101	75	1.72	0.85	0.29	1.30	0.32	0.05	0.39	0.07	0.49	0.16	0.53	0.06	0.44	0.08
104	75	1.97	0.51	0.27	1.24	0.27	0.07	0.41	0.07	0.59	0.17	0.62	0.09	0.61	0.12
105	5	1.69	0.35	0.22	1.06	0.20	0.06	0.33	0.06	0.58	0.18	0.63	0.09	0.63	0.11
113	70	3.30	0.81	0.47	2.17	0.42	0.13	0.72	0.12	0.93	0.24	0.90	0.14	0.91	0.17
116	5	3.78	1.98	0.61	2.79	0.52	0.13	0.80	0.11	0.99	0.26	0.92	0.15	0.96	0.18
133	5	4.35	0.54	0.62	2.81	0.53	0.14	0.80	0.13	1.03	0.26	0.95	0.16	1.03	0.19
142	5	4.24	0.52	0.57	2.64	0.51	0.13	0.73	0.12	0.97	0.29	0.94	0.15	1.04	0.18
153	5	3.98	0.50	0.56	2.60	0.48	0.13	0.71	0.11	0.96	0.26	0.96	0.14	0.97	0.20
154	135	4.73	1.58	0.70	3.02	0.52	0.14	0.80	0.14	0.98	0.27	1.00	0.16	1.16	0.20
156	5	3.95	0.53	0.57	2.64	0.44	0.12	0.79	0.11	0.98	0.27	0.97	0.14	0.94	0.18
161	100	4.46	0.63	0.61	2.68	0.53	0.14	0.81	0.13	1.04	0.29	1.05	0.15	1.11	0.21
S3	5	4.16	0.57	0.58	2.72	0.46	0.13	0.76	0.12	1.03	0.27	0.97	0.15	1.03	0.18
186	25	4.15	0.57	0.58	2.74	0.46	0.13	0.80	0.11	0.88	0.27	1.01	0.14	1.01	0.17
S4	5	4.42	0.53	0.62	2.89	0.46	0.13	1.14	0.13	1.00	0.27	1.00	0.16	1.04	0.19
S5	5	4.31	0.47	0.63	2.91	0.56	0.15	0.89	0.12	1.06	0.31	1.02	0.14	1.04	0.18
S6	5	4.32	0.50	0.61	2.78	0.52	0.13	0.89	0.13	0.93	0.27	0.99	0.14	1.07	0.19
210	25	4.30	0.75	0.67	2.88	0.56	0.13	0.72	0.12	0.97	0.30	0.95	0.16	1.08	0.20
222	50	5.47	2.77	0.76	3.04	0.56	0.15	0.83	0.12	1.04	0.29	1.05	0.15	1.13	0.20
222	180	4.79	1.36	0.70	3.40	0.61	0.14	0.78	0.14	1.01	0.30	1.04	0.16	1.10	0.21
222	280	5.04	2.03	0.73	3.18	0.62	0.16	0.93	0.15	1.13	0.30	1.12	0.17	1.14	0.21
222	400	5.22	1.45	0.79	3.35	0.68	0.14	0.90	0.15	1.16	0.31	1.09	0.17	1.23	0.23
S7	5	4.66	2.24	0.82	3.69	0.75	0.18	1.02	0.15	1.18	0.33	1.10	0.18	1.25	0.23
S8	5	3.61	0.68	0.49	2.22	0.41	0.11	0.66	0.11	0.82	0.24	0.83	0.12	0.84	0.15
230	50	4.28	1.35	0.65	2.94	0.58	0.16	0.77	0.13	1.02	0.28	1.00	0.15	1.11	0.19
230	150	4.45	1.36	0.64	3.03	0.57	0.17	0.87	0.16	1.07	0.32	1.10	0.17	1.17	0.21

Table A2: continued.

station	depth (m)	La	Ce	Pr	Nd	Sm	Eu	Gd	Tb	Dy	Ho	Er	Tm	Yb	Lu
								(ppt)							
236	50	3.38	0.58	0.48	2.07	0.39	0.10	0.65	0.09	0.87	0.24	0.85	0.14	0.85	0.16
241	50	2.80	0.54	0.42	1.79	0.33	0.10	0.54	0.10	0.76	0.23	0.80	0.12	0.76	0.14
244	25	2.13	0.44	0.30	1.48	0.28	0.06	2.20	0.09	0.64	0.20	0.70	0.10	0.73	0.13
244	50	2.28	0.39	0.31	1.38	0.30	0.07	0.47	0.07	0.65	0.18	0.70	0.10	0.76	0.12
replicate															
131	2000	6.12	0.90	0.91	3.84	0.73	0.18	1.10	0.17	1.37	0.37	1.20	0.19	1.31	0.24
131	2000	5.84	0.90	0.85	3.91	0.70	0.19	1.17	0.16	1.19	0.34	1.16	0.18	1.34	0.25
131	2000	5.96	0.88	0.87	3.94	0.69	0.17	1.09	0.17	1.28	0.35	1.24	0.18	1.36	0.24
131	2000	5.85	0.88	0.87	3.69	0.75	0.17	1.11	0.17	1.28	0.33	1.14	0.16	1.28	0.22
131	2000	6.06	1.01	0.87	4.00	0.83	0.19	1.09	0.16	1.15	0.33	1.18	0.16	1.31	0.22
131	2000	6.12	0.90	0.91	3.84	0.73	0.18	1.10	0.17	1.37	0.37	1.20	0.19	1.31	0.24
131	2000	5.84	0.90	0.85	3.91	0.70	0.19	1.17	0.16	1.19	0.34	1.16	0.18	1.34	0.25
131	2000	5.96	0.88	0.87	3.94	0.69	0.17	1.09	0.17	1.28	0.35	1.24	0.18	1.36	0.24
131	2000	5.85	0.88	0.87	3.69	0.75	0.17	1.11	0.17	1.28	0.33	1.14	0.16	1.28	0.22
131	2000	6.06	1.01	0.87	4.00	0.83	0.19	1.09	0.16	1.15	0.33	1.18	0.16	1.31	0.22
average		5.97	0.91	0.87	3.87	0.74	0.18	1.11	0.17	1.25	0.34	1.18	0.18	1.32	0.23
RSD		1.95%	5.69%	2.48%	2.89%	7.20%	4.94%	2.78%	2.84%	6.48%	4.06%	3.34%	6.85%	2.35%	4.61%

Table A3: List of sampled stations for deep water composition analysis, presented in Chapter 4.

	depth (m)	pot. T[a] (°C)	salinity[a]	neutral density	ε_{Nd}	error (2SD)	Nd (pMol)	ε_{Hf}	error (2SD)	Hf (pMol)	Si[b] (µMol)	water mass (equivalent)
station 101 (depth: 4670 m)	200	7.33	34.27	26.902	-8.3	0.39	8.47				4.390	AAIW
42° 20.60'S / 8° 59.20'E	500	5.59	34.34	27.222	-9.3	0.39	10.3				16.60	"iAW"
	750	3.83	34.28	27.393	-8.2	0.39	10.9	5.1	0.8	0.31	27.73	AAIW
	1000	3.15	34.37	27.555	-8.5	0.39	11.8				44.91	UCDW
	2000	2.45	34.77	27.963	-9.9	0.39	15.4				61.10	NADW
	3000	1.88	34.83	28.091	-10.9	0.39	20.2				64.32	NADW
	4400	0.72	34.73	28.204	-9.7	0.39	31.4					
station 102 (depth: 4600m)	200	6.63	34.33	27.065	-9.0	0.39	9.42	7.0	1.5	0.13	6.740	"iAW"
44° 39.69'S / 7° 5.59'E												
station 104 (depth: 4550 m)	400	2.96	34.16	27.398	-8.4	0.39	10.3	6.7	1.5	0.23	27.54	AAIW
47° 39.80'S / 4° 16.20'E	750	2.63	34.40	27.644	-8.3	0.39	11.8	5.0	0.8	0.31	54.48	UCDW
	1200	2.47	34.63	27.847	-8.5	0.39	13.8	4.4	0.8	0.47	70.86	UCDW
	2000	2.08	34.78	28.027	-10.0	0.39	17.1	3.5	0.8	0.54	72.03	NADW
	4440	0.41	34.69	28.226	-8.7	0.39	27.9	4.4	0.8	0.62	120.5	LCDW
station 113 (depth: 2530 m)	70	1.22	33.79	27.222	-7.9	0.39	16.1			0.14	35.55	AAIW/AASW
52° 59.80'S / 0° 02.00'E	150	0.20	34.02	27.518	-8.0	0.39	15.0			0.21	50.39	AAIW
	380	1.58	34.62	27.943	-8.3	0.39	16.4			0.42	87.75	UCDW
	550	1.49	34.69	28.025	-8.7	0.39	17.6			0.42	90.78	LCDW
	750	1.28	34.71	28.077	-8.6	0.39	19.5			0.40	98.19	LCDW
	1000	1.04	34.71	28.117	-8.4	0.39	20.6			0.48	103.4	LCDW
	1500	0.61	34.69	28.183	-8.6	0.39	22.7			0.46	115.5	LCDW
	2400	0.26	34.68	28.236	-8.5	0.39	24.5			0.50	127.6	LCDW

Table A3: continued.

	depth (m)	pot. T[a] (°C)	salinity[a]	neutral density	ε_{Nd}	error (2σ)	Nd (pMol)	ε_{Hf}	error (2σ)	Hf (pMol)	Si[b] (µMol)	water mass (equivalent)
station 131 (depth: 4600 m)	500	0.36	34.69	28.217	-8.6	0.39	23.7	4.1[c]	0.9	0.50	121.6	LCDW (WDW)
59° 00.00'S / 0° 00.00'E	1000	0.06	34.67	28.260	-8.4	0.39	25.3	4.2[c]	0.9	0.55	122.2	LCDW (WDW)
	1500	-0.12	34.67	28.292			25.9	3.8[c]	0.9	0.64	123.8	AABW (WSDW)
	2000	-0.30	34.66	28.326	-8.8	0.39	25.4				123.8	AABW (WSDW)
	2500	-0.42	34.66	28.348				4.7[c]	0.9		122.0	AABW (WSDW)
	3000	-0.53	34.66	28.369	-9.0	0.39	26.1			0.56	122.0	AABW (WSDW)
	3800	-0.69	34.65	28.401	-9.5	0.39	26.4	4.7[c]	0.9	0.58	117.5	AABW (WSBW)
station 161 (depth: 4540 m)	200	1.06	34.69	28.088	-8.9	0.39	19.1			0.46	94.97	LCDW (WDW)
66° 29.20'S / 0° 00.00'E	440	0.77	34.69	28.146	-8.6	0.39	20.6	3.8	0.9	0.57	105.0	LCDW (WDW)
	800	0.52	34.69	28.196	-8.8	0.39	22.9	3.4	0.9	0.54	111.7	LCDW (WDW)
	1200	0.30	34.69	28.225	-8.5	0.39	24.3	4.8	0.9	0.58	120.9	LCDW (WDW)
	2400	-0.20	34.67	28.308	-8.7	0.39		4.4[c]	0.9	0.64	123.6	AABW (WSDW)
	3350	-0.42	34.66	28.348	-9.4	0.39	25.5				123.9	AABW (WSDW)
	4400	-0.57	34.65	28.378	-9.6	0.39	26.8	5.5	0.8	0.75	127.5	AABW (WSDW)
station 178 (depth: 2000m)	200	-1.55	34.42	27.981	-9.6	0.39	18.1				66.97	AASW
69° 23.00'S / 0° 00.00'E	500	0.50	34.65	28.105	-9.2	0.39	20.6				91.75	LCDW
	800	0.35	34.66	28.166	-9.1	0.39	22.2				100.3	LCDW
	1000	0.32	34.67	28.193	-8.9	0.39	23.3				106.3	LCDW
	1500	0.16	34.67	28.231	-9.0	0.39	24.5				114.7	LCDW
	1900	0.01	34.67	28.262	-9.0	0.39					118.3	LCDW
station 181 (depth 1500 m)	1465	0.28	34.67	28.204	-8.6	0.30	23.8	4.5	0.8	0.50	110.9	LCDW (WDW)
69° 36.00'S / 0° 00.00'E												
station 193 (depth: 4860 m)	500	0.44	34.69	28.197	-8.5	0.39	23.0			0.51	120.5	LCDW (WDW)
66° 36.20'S / 27° 14.60'W	1200	0.06	34.67	28.254	-8.8	0.39	25.0	3.2[c]	2.0	0.59	126.0	LCDW (WDW)

Table A3: continued.

	depth (m)	pot. T[a] (°C)	salinity[a]	neutral density	ε_{Nd}	error (2σ)	Nd (pMol)	ε_{Hf}	error (2σ)	Hf (pMol)	Si[b] (µMol)	water mass (equivalent)
station 193 (continued)	2200	-0.29	34.66	28.323	-9.0	0.39	25.5	4.7[c]	1.1	0.65	125.6	AABW (WSDW)
	3200	-0.50	34.66	28.366	-8.9	0.39	26.1	4.0[c]	0.9	0.66	123.3	AABW (WSDW)
	4800	-0.84	34.64	28.429	-8.8	0.39	28.3	5.0[c]	0.9	0.67	123.7	AABW (WSBW)
station 230 (depth: 3500 m)	250	0.26	34.44	27.894	-7.9	0.39	20.1				80.25	AASW
60° 06.00'S / 55° 16.40'W	400	1.91	34.67	27.956	-8.9	0.39	15.7				84.44	UCDW
	500	1.79	34.69	27.990	-8.2	0.39	17.6				86.93	LCDW
	1000	1.35	34.73	28.095	-8.2	0.39	19.9				101.2	LCDW
	1500	0.93	34.72	28.156	-8.3	0.39	24.9				112.5	LCDW
	2000	0.53	34.70	28.205	-8.0	0.39	24.6				121.6	LCDW
	2500	0.10	34.68	28.254	-8.2	0.39	25.6					LCDW
	3000	-0.13	34.66	28.286	-9.0	0.39	24.7				116.9	AABW (WSDW)
	3450	-0.28	34.66	28.312	-8.7	0.39	25.2				116.2	AABW (WSDW)
station 236 (depth: 3770 m)	400	1.58	34.62	27.939	-8.4	0.39	16.1			0.46	83.32	UCDW
58° 59.60'S / 58° 08.60'W	1000	1.22	34.71	28.088	-8.6	0.39	19.1			0.58	99.67	LCDW
	1750	0.65	34.70	28.182	-8.2	0.39	21.5			0.61	116.0	LCDW
	2800	-0.01	34.67	28.267	-8.6	0.39	25.0			0.63	117.6	LCDW
	3712	-0.25	34.66	28.306	-8.5	0.39	25.3	4.8	0.9	0.70	117.2	AABW (WSDW)
station 241 (depth: 3460 m)	480	2.21	34.46	27.752	-8.3	0.39	12.8	5.7	0.9	0.27	68.06	UCDW
57° 37.20'S / 60° 53.80'W	750	2.13	34.60	27.865	-8.5	0.39	14.2	4.3	0.9	0.44	78.31	UCDW
	1250	1.85	34.71	27.996	-8.6	0.39	16.4	5.4	0.9	0.51	89.97	LCDW
	2800	0.69	34.71	28.186	-8.3	0.39	23.8	4.7	0.9	0.64	120.5	LCDW
	3490	0.43	34.70	28.217	-8.5	0.39	25.3	3.5	0.9	0.60	121.2	LCDW
station 244 (depth: 4170 m)	200	3.45	34.05	27.249	-8.1	0.39					13.66	AAIW
56° 53.80'S / 56° 55.14'W	500	3.02	34.22	27.453	-7.9	0.39	11.2				33.75	AAIW/UCDW
	750	2.78	34.39	27.617	-8.0	0.39	11.7				55.41	UCDW

Table A3: continued.

	depth (m)	pot. T[a] (°C)	salinity[a]	neutral density	ε_{Nd}	error (2σ)	Nd (pMol)	ε_{Hf}	error (2σ)	Hf (pMol)	Si[b] (µMol)	water mass (equivalent)
station 244 (continued)	1250	2.30	34.60	27.846	-8.3	0.39	14.1				78.19	UCDW
	1750	1.90	34.69	27.968	-8.2	0.39					84.53	LCDW
	4100	0.45	34.70	28.215	-8.3	0.39	24.1				120.1	LCDW
station 250 (depth: 3800 m)	500	3.08	34.23	27.458	-7.9	0.39	10.8	4.4	0.7	0.29		AAIW
55° 45.40'S / 64° 26.00'W	900	2.60	34.47	27.708	-8.4	0.39	12.1	4.2	0.6	0.40		UCDW
	1600	2.01	34.68	27.941	-8.0	0.39	15.1	4.4	0.6	0.54		UCDW
	2500	1.35	34.72	28.085	-8.0	0.39	19.8	4.7	0.6	0.58		LCDW
	3750	0.44	34.70	28.217	-8.4	0.39	24.4	4.2	0.6	0.64		LCDW

[a] from the onboard scientific crew of the Alfred Wegener Institut (AWI), Bremerhaven, Germany; doi:10.1594/PANGAEA.727465.

[b] from Fahrbach and de Baar (2010) and Middag et al. (2010)

[c] values with higher ^{176}Yb contribution on ^{176}Hf than 0.3 % and a manual correction was applied.

Errors are given as external errors.

Tab. A4.1: Hf spikes added to the samples and the corrected $^{179}Hf/^{178}Hf$ and reciprocal ratios.

ID-series	LabID	Station	Depth (m)	Hf-spike (g)	Sample (kg)	$\frac{^{179}Hf}{^{178}Hf}$	$\frac{^{178}Hf}{^{179}Hf}$	Hf (pg)	Hf (pMol)	Dupl. (1SD)	Hf-blank (pg)
1	TS080ID	250	500	0.15345	0.4963	0.321	3.117	28.97	0.37		
1	TS081ID	250	900	0.22914	0.5072	0.304	3.284	37.48	0.47		
1	TS082ID	250	1600	0.29322	0.5103	0.305	3.276	48.28	0.61		
1	TS083ID	250	2500	0.38385	0.5273	0.278	3.599	50.08	0.65		
1	TS084ID	250	3800	0.45763	0.5008	0.270	3.709	55.72	0.71		
1	TS102ID	241	480	0.19580	0.5060	0.299	3.339	30.66	0.34		
1	TS103ID	241	750	0.24932	0.4876	0.304	3.293	40.49	0.51		
1	TS104ID	241	1250	0.29380	0.5028	0.299	3.342	45.92	0.58		
1	TS105ID	241	2800	0.37714	0.4829	0.294	3.405	56.20	0.71		
1	TS106ID	241	3490	0.45602	0.4870	0.270	3.699	55.85	0.67		
1	TS149ID	236	500	0.14984	0.4930	0.366	2.736	43.34	0.53		
1	TS150ID	236	1000	0.22385	0.4965	0.341	2.931	50.92	0.65		
1	TS151ID	236	1500	0.30245	0.4940	0.318	3.142	55.82	0.69		
1	TS152ID	236	2500	0.37497	0.4854	0.294	3.405	55.91	0.70		
1	TS153ID	236	3700	0.45415	0.4978	0.281	3.561	60.74	0.78		
1	TS154ID	193	500	0.14911	0.4938	0.374	2.676	46.99	0.58		
1	TS155ID	193	1200	0.22788	0.4943	0.344	2.910	53.07	0.67		
1	TS156ID	193	2200	0.29711	0.4882	0.326	3.064	58.96	0.73		
1	TS157ID	193	3200	0.37700	0.4959	0.299	3.344	58.81	0.73		
1	TS158ID	193	4800	0.45734	0.4927	0.280	3.575	60.59	0.74		
1	TS184ID	161	1200	0.29658	0.4873	0.313	3.194	52.29	0.65		
1	TS185ID	161	800	0.22706	0.4945	0.339	2.949	50.62	0.61		
1	TS186ID	161	440	0.14898	0.4916	0.382	2.616	51.62	0.64		
1	TS187ID	161	4400	0.45541	0.5233	0.290	3.445	65.97	0.82		
1	duplicate	250	500	0.14923		0.323	3.092	28.83	0.35	2.62%	
1	duplicate	241	2800	0.37805	0.4443	0.288	3.474	53.63	0.66	4.79%	
1	duplicate	193	4800	0.45883		0.272	3.682	56.80	0.69	4.92%	
1	blank1	blank		0.14945	0.4683	0.159	6.299	6.83	0.08		6.83
1	blank2	blank		0.15004	0.4685	0.132	7.592	5.12	0.06		5.12
2	TS216ID	105	0	0.29615	0.4948	0.159	6.274	13.63	0.15		
2	TS217ID	S 1	0	0.29750	0.4962	0.147	6.805	12.03	0.14		
2	TS218ID	S 2	0	0.29720	0.4742	0.129	7.774	9.79	0.12		
2	TS220ID	GVN-fish	0	0.29856	0.4285	0.204	4.891	20.94	0.27		
2	TS222ID	S 3	0	0.29875	0.4822	0.201	4.984	20.26	0.24		
2	TS223ID	191	0	0.29762	0.4780	0.220	4.540	23.94	0.28		
2	TS224ID	186	0	0.29919	0.4558	0.213	4.693	22.63	0.28		
2	TS225ID	222	25	0.29786	0.4892	0.241	4.154	28.50	0.33		
2	TS226ID	116	0	0.29906	0.4892	0.211	4.750	22.12	0.25		
2	TS228ID	142	0	0.29829	0.4663	0.168	5.956	14.94	0.18		
2	TS229ID	S 4	0	0.29881	0.4810	0.211	4.745	22.14	0.26		

Tab. A4.1: continued.

ID-series	LabID	Station	Depth (m)	Hf-spike (g)	Sample (kg)	$\frac{^{179}Hf}{^{178}Hf}$	$\frac{^{178}Hf}{^{179}Hf}$	Hf (pg)	Hf (pMol)	Dupl. (1SD)	Hf-blank (pg)
2	TS230ID	S 5	0	0.29841	0.4880	0.200	4.994	20.17	0.23		
2	TS231ID	210	0	0.29873	0.4641	0.240	4.160	28.49	0.34		
2	TS232ID	133	0	0.29789	0.4744	0.213	4.701	22.45	0.27		
2	TS233ID	223	0	0.29794	0.4942	0.261	3.837	33.66	0.38		
2	Fe-blank	blank	Fe only	0.50001		0.036	28.034	1.96			1.96
2	duplicate	105	0	0.29695	0.4918	0.171	5.849	15.32	0.17	8.67%	
2	duplicate	S 1	0	0.29737	0.5017	0.149	6.703	12.32	0.14	0.86%	
2	duplicate	S 2	0	0.29742	0.49760	0.1368	7.31	10.76	0.12	3.29%	
3	TS177ID	131	3000	0.37891	0.5075	0.295	3.387	57.26	0.63		
3	TS178ID	131	1500	0.29932	0.4957	0.334	2.998	63.43	0.72		
3	TS179ID	131	900	0.23058	0.5033	0.349	2.867	56.41	0.63		
3	TS180ID	131	400	0.14967	0.5019	0.381	2.623	51.29	0.57		
3	TS181ID	131	b-100	0.49784	0.5053	0.267	3.745	59.31	0.66		
3	TS182ID	156	0	0.34905	0.5124	0.227	4.408	29.70	0.32		
3	TS208ID	104	400	0.14982	0.4875	0.314	3.189	26.52	0.30		
3	TS209ID	104	750	0.22901	0.5278	0.300	3.332	36.07	0.38		
3	TS210ID	104	1200	0.29668	0.4917	0.303	3.298	47.98	0.55		
3	TS211ID	104	2000	0.37806	0.4870	0.287	3.489	53.08	0.61		
3	TS212ID	104	b-100	0.49871	0.5020	0.273	3.667	62.30	0.70		
3	TS213ID	101	750	0.22964	0.5025	0.293	3.412	34.06	0.38		
3	TS214ID	102	200	0.22863	0.4974	0.219	4.563	18.22	0.21		
3	blank4	blank		0.49670	0.4808	0.074	13.485	7.15	0.08		7.15
4	TS215ID	154	135	0.19891	0.5032	0.281	3.563	26.57	0.30		
4	TS221ID	151/153	0	0.20016	0.4968	0.262	3.819	22.84	0.26		
4	TS234ID	113	70	0.19990	0.4914	0.240	4.167	19.00	0.22		
4	TS235ID	113	150	0.20049	0.5069	0.276	3.617	25.85	0.29		
4	TS236ID	113	380	0.30060	0.4887	0.290	3.454	43.27	0.50		
4	TS237ID	113	500	0.29866	0.4976	0.292	3.428	43.79	0.49		
4	TS238ID	113	750	0.39945	0.4956	0.253	3.952	42.35	0.48		
4	TS239ID	113	1000	0.49796	0.5017	0.247	4.056	50.00	0.56		
4	TS240ID	113	1500	0.59815	0.5072	0.222	4.507	48.79	0.54		
4	TS241ID	113	2400	0.79777	0.5105	0.196	5.090	52.12	0.57		
4	duplicate	113	2400	0.79852	0.5203	0.197	5.068	52.57	0.57	0.75%	
4	TS243ID	S 8	0	0.20116	0.5200	0.248	4.039	20.37	0.22		
4	blank5	blank		0.79541	0.4965	0.047	21.111	5.50	0.06		5.50
5	TS244ID	S 7	0	0.29825	0.5126	0.270	3.705	36.39	0.40		
5	TS245ID	222	50	0.29827	0.5093	0.240	4.172	28.28	0.31		
5	TS246ID	S 6	0	0.29901	0.5170	0.210	4.762	22.02	0.24		
5	TS219ID	181	1435	0.79706	0.5111	0.187	5.343	47.87	0.52		
5	blank6	blank		0.4953	0.4924	0.032	30.933	1.53	0.02		1.53
5	blank7	blank		0.49665	0.4948	0.038	26.223	2.25	0.03		2.25

Tab. A4.1: continued.

ID-series	LabID	Station	Depth (m)	Hf-spike (g)	Sample (kg)	$\frac{^{179}Hf}{^{178}Hf}$	$\frac{^{178}Hf}{^{179}Hf}$	Hf (pg)	Hf (pMol)	Dupl. (1SD)	Hf-blank (pg)
5	blank8	blank		0.49606	0.4959	0.034	29.005	1.80	0.02		1.80
5	blank9	blank		0.49845	0.4846	0.039	25.538	2.39	0.03		2.39
5	duplicate	S 7	0	0.29791	0.5063	0.268	3.732	35.77	0.40	0.34%	
5	duplicate	222	50	0.29875	0.5182	0.243	4.107	29.24	0.32	1.15%	
6.1	TS039ID	236	50	0.19872	0.5138	0.243	4.116	19.37	0.21		
6.1	TS048ID	241	50	0.20012	0.5089	0.200	4.997	13.51	0.15		
6.1	duplicate	241	50	0.19956	0.5132	0.232	4.310	17.74	0.19	18.58%	
6.1	TS056ID	244	25	0.20089	0.5077	0.195	5.123	12.97	0.14		
6.1	TS057ID	244	50	0.20032	0.5201	0.173	5.790	10.51	0.11		
6.1	TS058ID	244	200	0.19967	0.5141	0.223	4.489	16.41	0.18		
6.1	TS060ID	244	500	0.19987	0.523	0.267	3.739	23.89	0.26		
6.1	TS091ID	230	50	0.19984	0.52	0.298	3.359	30.82	0.33		
6.1	TS092ID	230	150	0.19998	0.509	0.309	3.233	34.09	0.38		
6.1	TS093ID	230	250	0.19982	0.5254	0.318	3.144	36.79	0.39		
6.1	TS094ID	230	400	0.20001	0.5213	0.324	3.086	38.87	0.42		
6.1	duplicate	230	400	0.20000	0.5137	0.322	3.106	38.10	0.42	0.38%	
6.1	TS095ID	230	500	0.19984	0.5094	0.330	3.028	41.09	0.45		
6.2	TS108ID	193	200	0.19987	0.5089	0.322	3.107	38.06	0.42		
6.2	TS172ID	222	100	0.2002	0.5189	0.292	3.424	29.44	0.32		
6.2	TS173ID	222	180	0.20038	0.5049	0.299	3.350	31.13	0.35		
6.2	TS174ID	222	280	0.19935	0.5092	0.308	3.245	33.66	0.37		
6.2	TS175ID	222	bottom	0.19923	0.511	0.307	3.252	33.44	0.37		
6.2	TS127ID	161	100	0.19838	0.5045	0.323	3.095	38.23	0.42		
6.2	duplicate	161	100	0.19945	0.5132	0.320	3.126	37.33	0.41	2.90%	
6.2	TS128ID	161	200	0.2	0.5108	0.338	2.961	44.03	0.48		
6.2	duplicate	161	200	0.20041	0.5144	0.334	2.995	42.60	0.46	2.83%	
6.2	blank10	blank		0.20011	0.4907	0.053	19.009	1.66	0.02		1.66
6.2	blank11	blank		0.20011	0.4858	0.052	19.173	1.64	0.02		1.64
6.2	blank12	blank		0.19956	0.4873	0.035	28.949	0.73	0.01		0.73

Tab. A4.2: Nd spikes added to the samples and the corrected $^{150}Nd/^{144}Nd$ ratio.

ID-series	LabID	Station	Depth (m)	Nd-spike (g)	Sample (kg)	$\frac{^{150}Nd}{^{144}Nd}$	Nd (ng)	Nd (pMol)	Dupl. (1SD)	Nd-blank (pg)
1	TS080ID	250	500	0.05041	0.4963	5.170	0.77	10.79		
1	TS081ID	250	900	0.06974	0.5072	6.140	0.89	12.14		
1	TS082ID	250	1600	0.08960	0.5103	6.280	1.11	15.14		
1	TS083ID	250	2500	0.15097	0.5273	7.728	1.50	19.76		
1	TS084ID	250	3800	0.15153	0.5008	6.684	1.76	24.40		
1	TS102ID	241	480	0.05023	0.5060	4.324	0.93	12.78		
1	TS103ID	241	750	0.07035	0.4876	5.551	1.00	14.20		
1	TS104ID	241	1250	0.07042	0.5028	4.727	1.19	16.38		
1	TS105ID	241	2800	0.09057	0.4829	4.381	1.66	23.81		
1	TS106ID	241	3490	0.15108	0.4870	6.613	1.78	25.30		
1	TS149ID	236	500	0.05016	0.4930	3.571	1.15	16.12		
1	TS150ID	236	1000	0.06985	0.4965	4.108	1.37	19.14		
1	TS151ID	236	1500	0.08931	0.4940	4.649	1.53	21.52		
1	TS152ID	236	2500	0.15017	0.4854	6.672	1.75	25.00		
1	TS153ID	236	3700	0.15034	0.4978	6.441	1.82	25.34		
1	TS154ID	193	500	0.04885	0.4938	2.516	1.64	23.05		
1	TS155ID	193	1200	0.06939	0.4943	3.205	1.78	25.03		
1	TS156ID	193	2200	0.08947	0.4882	4.024	1.80	25.50		
1	TS157ID	193	3200	0.15042	0.4959	6.290	1.87	26.10		
1	TS158ID	193	4800	0.15093	0.4927	5.881	2.01	28.33		
1	TS184ID	161	1200	0.06963	0.4873	3.348	1.71	24.29		
1	TS185ID	161	800	0.04927	0.4945	2.549	1.63	22.87		
1	TS186ID	161	440	0.04929	0.4916	2.823	1.46	20.55		
1	TS187ID	161	4400	0.15031	0.5233	5.824	2.03	26.84		
1	duplicate	250	500							
1	duplicate	241	2800	0.09000	0.4443	4.755	1.51	23.54	0.80%	
1	duplicate	193	4800							
1	blank1	blank			0.4683					
1	blank2	blank			0.4685					
2	TS216ID	105	0	0.08395	0.4948	9.083	0.53	7.38		
2	TS217ID	S 1	0	0.08352	0.4962	2.997	1.73	24.19		
2	TS218ID	S 2	0	0.08358	0.4742	10.32	0.46	6.68		
2	TS220ID	GVN	0	0.08335	0.4285	4.786	1.04	16.81		
2	TS222ID	S 3	0	0.08353	0.4822	4.277	1.18	16.90		
2	TS223ID	191	0	0.08419	0.4780	3.989	1.28	18.53		
2	TS224ID	186	0	0.08225	0.4558	4.360	1.13	17.24		
2	TS225ID	222	25	0.08352	0.4892	3.622	1.41	19.94		
2	TS226ID	116	0	0.08348	0.4892	4.486	1.12	15.81		

Tab. A4.2: continued.

ID-series	LabID	Station	Depth (m)	Nd-spike (g)	Sample (kg)	$\frac{^{150}Nd}{^{144}Nd}$	Nd (ng)	Nd (pMol)	Dupl. (1SD)	Nd-blank (pg)
2	TS228ID	142	0	0.08365	0.4663	4.323	1.16	17.30		
2	TS229ID	S 4	0	0.08272	0.4810	3.915	1.28	18.46		
2	TS230ID	S 5	0	0.08301	0.4880	3.915	1.29	18.26		
2	TS231ID	210	0	0.08274	0.4641	4.074	1.23	18.33		
2	TS232ID	133	0	0.08302	0.4744	4.032	1.25	18.20		
2	TS233ID	223	0	0.08321	0.4942	3.402	1.50	21.06		
2	Fe-blank	blank	Fe onl.	0.20190		192.2	0.00			2.28
2	duplicate	105	0	0.08277	0.4918	9.280	0.51	7.15	2.20%	
2	duplicate	S 1	0	0.08266	0.5017	2.917	1.77	24.40	0.61%	
2	duplicate	S 2	0	0.08228	0.4976	10.03	0.46	6.46	2.32%	
3	TS177ID	131	3000	0.15119	0.5075	6.188	1.91	26.09		
3	TS178ID	131	1500	0.08040	0.4957	3.540	1.86	25.94		
3	TS179ID	131	900	0.06056	0.5033	2.758	1.84	25.30		
3	TS180ID	131	400	0.05067	0.5019	2.497	1.72	23.71		
3	TS181ID	131	b-100	0.15216	0.5053	6.220	1.91	26.23		
3	TS182ID	156	0	0.05059	0.5124	2.921	1.44	19.49		
3	TS208ID	104	400	0.05076	0.4875	5.542	0.72	10.26		
3	TS209ID	104	750	0.06119	0.5278	5.362	0.90	11.84		
3	TS210ID	104	1200	0.08108	0.4917	6.447	0.98	13.82		
3	TS211ID	104	2000	0.13218	0.4870	8.427	1.20	17.07		
3	TS212ID	104	b-100	0.15241	0.5020	5.914	2.02	27.91		
3	TS213ID	101	750	0.06117	0.5025	6.064	0.79	10.89		
3	TS214ID	102	200	0.05064	0.4974	5.877	0.68	9.42		
3	blank4	blank		0.20272	0.4808	203.6	0.00	-0.02		-1.54
4	TS215ID	154	135	0.05044	0.5032	2.975	1.41	19.39		
4	TS221ID	151/153	0	0.05042	0.4968	3.331	1.24	17.35		
4	TS234ID	113	70	0.05670	0.4914	4.007	1.14	16.13		
4	TS235ID	113	150	0.05092	0.5069	3.768	1.10	15.01		
4	TS236ID	113	380	0.05073	0.4887	3.587	1.15	16.37		
4	TS237ID	113	500	0.07067	0.4976	4.472	1.27	17.63		
4	TS238ID	113	750	0.07092	0.4956	4.106	1.39	19.48		
4	TS239ID	113	1000	0.10110	0.5017	5.356	1.49	20.60		
4	TS240ID	113	1500	0.10129	0.5072	4.853	1.66	22.70		
4	TS241ID	113	2400	0.15137	0.5105	6.530	1.81	24.51		
4	duplicate	113	2400	0.15175	0.5203	6.460	1.83	24.39	0.35%	
4	TS243ID	S 8	0	0.05039	0.5200	3.802	1.08	14.34		
4	blank5	blank		0.20240	0.4965	143.3	0.03	0.43		30.97
5	TS244ID	S 7	0	0.08099	0.5126	3.917	1.67	22.64		

Tab. A4.2: continued.

ID-series	LabID	Station	Depth (m)	Nd-spike (g)	Sample (kg)	$\frac{^{150}Nd}{^{144}Nd}$	Nd (ng)	Nd (pMol)	Dupl. (1SD)	Nd-blank (pg)
5	TS245ID	222	50	0.08508	0.5093	4.377	1.56	21.23		
5	TS246ID	S 6	0	0.08070	0.5170	4.770	1.35	18.08		
5	TS219ID	181	1435	0.08086	0.5111	3.751	1.75	23.76		
5	TS188ID	101	75	0.08052	0.5085	9.705	0.63	8.56		
5	TS189ID	101	200	0.08064	0.5096	9.791	0.62	8.47		
5	TS190ID	101	500	0.06054	0.512	6.226	0.76	10.29		
5	TS192ID	101	1000	0.06090	0.5182	5.451	0.88	11.79		
5	TS193ID	101	2000	0.08103	0.5224	5.506	1.16	15.40		
5	TS194ID	101	3000	0.08088	0.5153	4.324	1.50	20.21		
5	TS195ID	101		0.12110	0.5147	4.189	2.33	31.35		
5	blank6	blank		0.20236	0.4924	192.136	0.003	0.04		3.08
5	blank7	blank		0.20179	0.4948	189.036	0.004	0.06		4.40
5	blank8	blank		0.20237	0.4959	204.633	neg.	neg.		neg.
5	blank9	blank		0.20265	0.4846	205.123	neg.	neg.		neg.
5	TS199ID	104	75	0.08089	0.5172	10.033	0.61	8.16		
5	TS200ID	104	200	0.08063	0.508	8.764	0.70	9.57		
5	duplicate	S 7	0	0.07573	0.5063	3.722	1.65	22.65	0.04%	
5	duplicate	222	50	0.08075	0.5182	4.111	1.58	21.19	0.13%	
5	TS139ID	178	200	0.08065	0.5152	4.773	1.35	18.11		
5	TS140ID	178	500	0.08090	0.503	4.335	1.50	20.65		
5	TS142ID	178	800	0.08080	0.5142	3.964	1.65	22.22		
5	TS143ID	178	1000	0.08120	0.5147	3.808	1.73	23.30		
5	TS145ID	178	1500	0.07717	0.5143	3.475	1.82	24.49		
6.1	TS039ID	236	50	0.06014	0.5138	4.610	1.04	14.06		
6.1	TS048ID	241	50	0.06052	0.5089	5.518	0.86	11.78		
6.1	duplicate	241	50	0.06085	0.5132	5.354	0.90	12.13	2.08%	
6.1	TS056ID	244	25	0.06089	0.5077	6.332	0.75	10.25		
6.1	TS057ID	244	50	0.06114	0.5201	6.624	0.72	9.57		
6.1	TS058ID	244	200	0.09203	0.5141	7.281	0.98	13.17		
6.1	TS060ID	244	500	0.09136	0.523	8.272	0.85	11.21		
6.1	TS061ID	244	750	0.09137	0.5246	7.906	0.89	11.73		
6.1	TS062ID	244	1250	0.10204	0.5144	7.539	1.04	14.06		
6.1	TS067ID	244	bottom	0.12207	0.5096	5.434	1.77	24.12		
6.1	TS068ID	250	150	0.06107	0.5149	6.592	0.72	9.71		
6.1	TS069ID	250	300	0.09139	0.52	8.312	0.84	11.22		
6.1	TS091ID	230	50	0.06091	0.52	3.517	1.42	18.87		
6.1	TS092ID	230	150	0.06109	0.509	3.426	1.46	19.89		
6.1	TS093ID	230	250	0.06100	0.5254	3.299	1.52	20.05		

Tab. A4.2: continued.

ID-series	LabID	Station	Depth (m)	Nd-spike (g)	Sample (kg)	$\frac{^{150}Nd}{^{144}Nd}$	Nd (ng)	Nd (pMol)	Dupl. (1SD)	Nd-blank (pg)
6.1	TS094ID	230	400	0.09163	0.5213	6.076	1.18	15.70		
6.1	duplicate	230	400	0.09128	0.5137	6.098	1.17	15.81	0.50%	
6.1	TS095ID	230	500	0.09131	0.5094	5.564	1.29	17.59		
6.1	TS096ID	230	1000	0.09149	0.5156	4.922	1.48	19.87		
6.1	TS097ID	230	1500	0.10176	0.5128	4.424	1.84	24.92		
6.1	TS098ID	230	2000	0.10180	0.5119	4.489	1.82	24.59		
6.1	TS099ID	230	2500	0.12141	0.5337	4.901	1.97	25.59		
6.1	TS100ID	230	3000	0.12189	0.5068	5.342	1.80	24.66		
6.2	TS101ID	230	bottom	0.12129	0.5093	5.191	1.85	25.18		
6.2	TS108ID	193	200	0.06076	0.5089	3.221	1.55	21.17		
6.2	TS133ID	161	3350	0.12155	0.5184	5.054	1.91	25.52		
6.2	TS165ID	131	2000	0.11947	0.5235	4.951	1.92	25.39		
6.2	TS167ID	131	3800	0.12100	0.5161	4.899	1.96	26.38		
6.2	TS172ID	222	100	0.06064	0.5189	3.346	1.49	19.87		
6.2	TS173ID	222	180	0.06065	0.5049	3.345	1.49	20.44		
6.2	TS174ID	222	280	0.06080	0.5092	3.200	1.57	21.32		
6.2	TS175ID	222	bottom	0.09123	0.511	4.415	1.66	22.47		
6.2	TS127ID	161	100	0.06041	0.5045	3.760	1.31	17.93		
6.2	duplicate	161	100	0.06053	0.5132	3.689	1.34	18.03	0.39%	
6.2	TS128ID	161	200	0.06037	0.5108	3.507	1.41	19.10		
6.2	duplicate	161	200	0.06085	0.5144	3.532	1.41	18.97	0.48%	
6.2	blank10	blank		0.20292	0.4907	187.901	0.00	0.07		4.93
6.2	blank11	blank		0.20299	0.4858	209.673	neg.	neg.		neg.
6.2	blank12	blank		0.20348	0.4873	208.673	neg.	neg.		neg.

Table A5: Composition of the Sm/Nd double spike.

mass	conc (µmol/g)	error	conc (µg/g)	abun. spike	abun. nat
141.90773	0.0000533		0.0075590	0.41%	27.16%
142.90982	0.0000317		0.0045267	0.24%	12.18%
143.91010	0.0000644		0.0092617	0.49%	23.86%
144.91258	0.0000282		0.0040797	0.21%	8.30%
145.91313	0.0000573		0.0083622	0.44%	17.17%
147.91690	0.0000486		0.0071952	0.37%	5.74%
149.92090	0.0128481	±0.0000283	1.9261987	97.84%	5.62%
146.91489	0.0000153		0.0022522	0.38%	14.99%
148.91718	0.0039945	±0.0002668	0.5948497	99.23%	13.82%
151.91973	0.0000158		0.0023946	0.39%	26.75%
Nd	**ratio spike**	**ratio nat**			
146/144	0.8905	0.7205204		$146/145_{spike}$	2.03567
143/144	0.4922	0.5111204		$146/145_{nat}$	2.06867
150/144	199.6356	0.2358372		$150/145_{spike}$	456.3744
145/144	0.4374	0.3483005			
142/144	0.8277	1.1397398			
148/144	0.7558	0.2408728			
Sm				enr. of ^{150}Nd	846.50
149/152	253.423	0.5167470			
147/152	0.97257	0.5606665			
Atomic num. spike					
149.806					
Atomic num. nat.			R_{opt}	$1/R_{opt}$	
144.24			6.861595801	0.145738692	

Table A6: Composition of the Hf spike.

mass	conc (pmol/g)	error	conc (pg/g)	abun. spike	abun. nat
173.94007				0.00%	0.16%
175.94142				0.00%	5.26%
176.94323				1.54%	18.60%
177.94371	0.18		32.0298678	94.90%	27.28%
178.94583				1.84%	13.62%
179.94656				1.69%	35.08%
	ratio spike	**ratio nat**			
180/178		1.2858792			
179/178	0.0194	0.4992871			
177/178		0.6816184			
176/178		0.1928221			
174/178		0.0059382		enr. of ^{178}Hf	25.74
Atomic num. spike					
177.95					
Atomic num. nat.			R_{opt}	$1/R_{opt}$	
178.49			0.098418336	10.16070829	

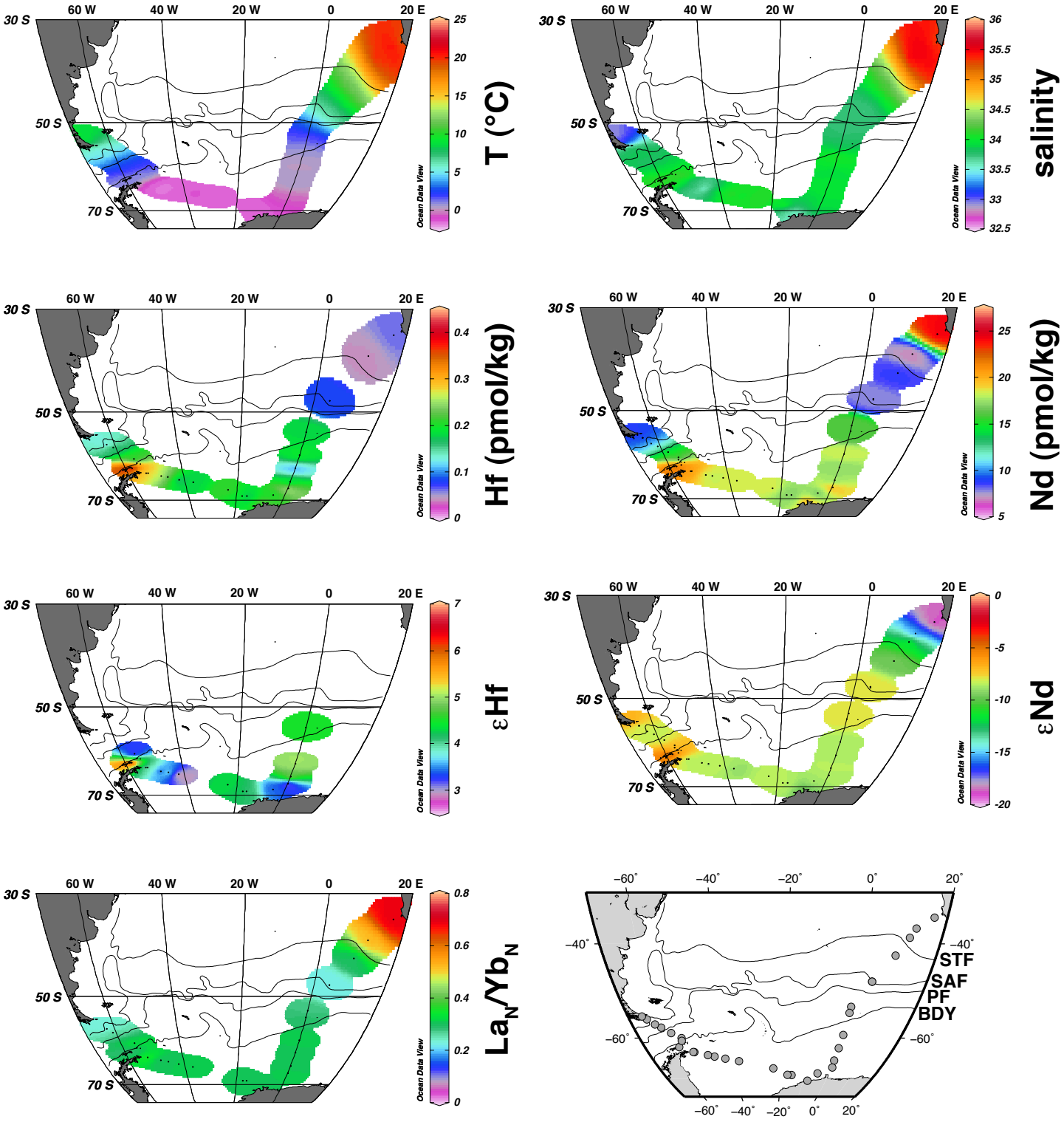

Figure A1: Geographical distribution of the stations and the measured surface parameters.

Fe, ether purification

The following procedure is a manual to clean di-ethylether and/or $FeCl_3$.

Steps 1 to 4 are used to pre-clean the ether. It is recommended to clean a stock of ~1 L of ether, which can be stored away and used for later Fe-cleaning. Alternatively, you can immediately proceed to the Fe-cleaning below, after you have cleaned the first 150 ml of ether.

1. Purification of the ether: fill separator funnel by ~150 ml (caution: inflammable and low surface tension, switch off hotplates)

2. Add 100 ml H_2O M.Q., cap funnel, wrap Kimwipe around cap and shake forcefully; leave it for a few minutes (contaminations of the ether are in the water)

3. Lower part of the funnel is filled by water, let the water flow out carefully by opening the cap; rather let some ether flow out

4. Repeat that with water and then with 6 M dest. HCl, ether should be clean now

The following steps describe the cleaning procedure of $FeCl_3$:

- Dissolve ca. 65 g $FeCl_3$ in 500 ml 6 M dest. HCl; the amount is enough for 2 x 2 separator funnels or 4 (to 5) successive portions

- When Fe has dissolved, add ~100 ml to ether in the separator funnel, shake and leave it for a few minutes (Fe is dissolved in ether, trace metals in Fe dissolve in the acid), acid is in the lower part of the funnel, let the acid flow out as described above (maybe there are streaks of Fe near the interface); if the color of the acid is rather orange than yellow (not enough ether to gather Fe completely) add some purified ether
- Once again add 100 ml 6 M dest. HCl, shake, leave it and let the acid flow out

- Add 50 ml H_2O M.Q., shake, leave it shortly (Fe is dissolved in the water now “back extraction”), water with Fe is in the lower part of the funnel ether on top of it

- Let the water flow out carefully and collect it (! this time: stop before reaching the ether interface!)

- Evaporate Fe-solution in Teflon beakers (0.5 l) on a heater carefully (if you use too much heat it might happen that the solution splashes out), do not evaporate completely, stop when there is just a muddy residual left

- Dissolve Fe in 40-50 ml of 3M dest. HCl, put this on a heater or into an ultrasonic bath to dissolve it completely

Acknowledgements

First of all I would like to thank Martin for being one of the best supervisors one can imagine. Your office door is literally always open and you do not feel disturbed by us students going in and out to seek for advice. I am curious if it stays like this, even if avalanches of new students arrive in our working group.

Jörg, without your help and your remarkable knowledge in geochemistry, this work would have been much harder. I thank you very much for allowing me to come to Zürich to learn and to have a lot of fun! I wish you all the best and hopefully we can think about future collaboration.

Roland, Paddy, the Claudias, Ed and all the rest of you: I enjoyed working, coffee, drinking beer (and Glühwein) and just being with very much! You are a funny bunch of guys.

Brian Alexander Haley! You left a big gap when you went back to Oregon. But you taught me very well to take responsibility and make decisions (even if they were not always thought through well…). I hope to see you soon again in the U.S.

A big hug goes to Jutta and Ana! I will miss you two very much. You were extremely helpful during my entire time at IFM-GEOMAR. One thing to Ana: It is just exemplary how you bridge gaps between working groups.

Speaking of other groups, Toni thank you very much for writing reference letters for me and being co-chief of my project. The consequence for you is that you happened to be co-referee of this work. It is by the way somehow your "fault" that I am in the isotope geochemistry now, by attending you lecture in "Marine Isotope Systems" as an undergraduate. Jan Fietzke, you are the lacking soul of our instruments. Your have a great ability to solve any occurring problems, plus you do not give up until the problems are solved.

During my expedition terrible things happened. Such accidents make clear that there are way more important matters than science. Thank you Eberhard and Hein for doing such a magnificent job as chief scientists during ANTXXIV/3. Captain Schwarze and his crew did very well in maneuvering Polarstern through the ice. I want to thank Celia very much for the great teamwork, which was crucial to gather this number of samples.

Luisa you are the center of my life. I am very grateful that you are who you are. You pushed me through this thesis with your lovely iron fist.

I want to thank my family. Ihr seid immer für mich da, habt mich unterstützt wo es nur geht. Auch wenn ihr mich manchmal mehr gebraucht hättet als ich Zeit für euch hatte, habt ihr immer Verständnis für mich gehabt. Ihr seid die besten!

Mahalo!